

NATIONAL AERONAUTICS AND SPACE ADMINISTRATION

Space Programs Summary No. 37-35, Volume III

for the period July 1, 1965 to August 31, 1965

The Deep Space Network

FACILITY FORM 602

N 66-10422

(ACCESSION NUMBER)

(THRU)

80

(CODE)

(PAGES)

CR 67728

(CATEGORY)

(NASA CR OR TMX OR AD NUMBER)

GPO PRICE \$ _____

CFSTI PRICE(S) \$ _____

Hard copy (HC) 3.00

Microfiche (MF) .75

ff 653 July 65

jpl

JET PROPULSION LABORATORY
CALIFORNIA INSTITUTE OF TECHNOLOGY
PASADENA, CALIFORNIA

September 30, 1965

NATIONAL AERONAUTICS AND SPACE ADMINISTRATION

Space Programs Summary No. 37-35, Volume III

for the period July 1, 1965 to August 31, 1965

The Deep Space Network

JET PROPULSION LABORATORY
CALIFORNIA INSTITUTE OF TECHNOLOGY
PASADENA, CALIFORNIA

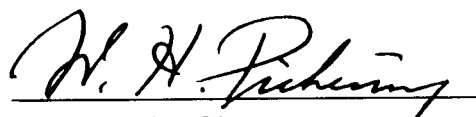
September 30, 1965

Preface

The *Space Programs Summary* is a six-volume, bimonthly publication that documents the current project activities and supporting research and advanced development efforts conducted or managed by JPL for the NASA space exploration programs. The titles of all volumes of the *Space Programs Summary* are:

- Vol. I. The Lunar Program (Confidential)
- Vol. II. The Planetary-Interplanetary Program (Confidential)
- Vol. III. The Deep Space Network (Unclassified)
- Vol. IV. Supporting Research and Advanced Development (Unclassified)
- Vol. V. Supporting Research and Advanced Development (Confidential)
- Vol. VI. Space Exploration Programs and Space Sciences (Unclassified)

The *Space Programs Summary*, Vol. VI consists of an unclassified digest of appropriate material from Vols. I, II, and III; an original presentation of technical supporting activities, including engineering development of environmental-test facilities, and quality assurance and reliability; and a reprint of the space science instrumentation studies of Vols. I and II.



W. H. Pickering, Director
Jet Propulsion Laboratory

Space Programs Summary No. 37-35, Volume III

Copyright © 1965, Jet Propulsion Laboratory, California Institute of Technology

Prepared under Contract No. NAS 7-100, National Aeronautics & Space Administration

Contents

I. Introduction	1
II. Tracking Stations Engineering and Operations	3
A. Systems Engineering and Integration	3
B. Systems Analysis	4
C. Antenna Engineering	12
D. Goldstone Operations	14
E. Advanced Antenna System	18
F. Goldstone Computer Facility	25
G. Spacecraft Visibility Program With Plotter Output	27
Reference	30
III. Space Flight Operations Facility	31
A. Simulation Data Conversion Center	31
B. <i>Mariner</i> Master Data Library	34
IV. Communications Engineering Development	38
A. S-Band Implementation for DSIF	38
B. Ground Instrumentation for <i>Mariner IV</i> Occultation Experiment	39
C. Venus Station <i>Mariner IV</i> Encounter Receiver and X-Band Lunar Radar	42
D. S-Band Receiver-Exciter System	45
E. DSIF Test Signal Control Assembly (TSCA)	47
F. 498-kc Phase Modulator	50
G. Amplitude Stabilized Signal Source	52
V. Communications Research and Development	54
A. Experimental Closed Cycle Refrigerators (CCR) for Masers	54
B. Experimental X-Band Lunar Planetary Radar Project: X-Band Radar Feed Installation	55
C. 22 Gc/sec Gain Calibration	55
D. CW Signal Power Calibration With Thermal Noise Standards	58
E. Venus Station Operations	62
F. Lunar Radar X-Band Transmitter	65
G. 100-kw S-Band Final Amplifier	65
H. Frequency Generation and Control	68
I. Efficient Data Systems	71
References	76

I. Introduction

1. General

The Deep Space Network (DSN) is a precision communication system which is designed to communicate with, and permit control of, spacecraft designed for deep space exploration. The DSN consists of the Deep Space Instrumentation Facility (DSIF), the Space Flight Operations Facility (SFOF), and the DSN Ground Communication System (GCS).

The DSN is a NASA facility, managed by JPL through a contract between NASA and the California Institute of Technology. The Office of Tracking and Data Acquisition is the cognizant NASA office.

It is the policy of the DSN to continuously conduct research and development of new components and systems and to engineer them into the DSN to maintain a state-of-the-art capability.

The DSN has facilities for simultaneously controlling a newly launched spacecraft and a second one already in flight. Within a few months, it will be able to control simultaneously either two newly launched spacecraft plus two in flight or the operations of four spacecraft in flight at the same time. The DSIF is equipped with 85-ft antennas having gains of 53 db at 2300 Mc and a system

temperature of 55°K, making it possible to receive significant data rates at distances as far as the planet Mars. To improve the data rate and distance capability, a 210-ft antenna is under construction at the Goldstone Mars station and two additional antennas of this size are planned for installation at overseas stations.

The DSIF utilizes large antennas, low-noise phase-lock receiving systems, and high-power transmitters located at stations positioned around the Earth to track, command, and receive data from deep space probes. Overseas stations are generally operated by personnel of the respective countries. The DSIF stations are:

I.D. No.	Name	Location
11	Goldstone, Pioneer	Goldstone, California
12	Goldstone, Echo	Goldstone, California
13	Goldstone, Venus (R&D)	Goldstone, California
14	Goldstone, Mars (under construction)	Goldstone, California
41	Woomera	Island Lagoon, Australia
42	Tidbinbilla	Canberra, Australia
51	Johannesburg	Johannesburg, South Africa
61	Madrid (under construction)	Madrid, Spain
71	Spacecraft Monitoring	Cape Kennedy, Florida
72	Spacecraft Guidance and Com- mand (under construction)	Ascension Island

The SFOF is located in a three-story building at the Jet Propulsion Laboratory in Pasadena, California, and utilizes operations control consoles, status and operations displays, computers, data processing equipment for analysis of spacecraft performance and space science experiments, and communication facilities to control space flight operations. This control is accomplished by generating trajectories and orbits, and command and control data, from tracking and telemetry data received from the DSIF in near real-time. The SFOF also reduces the telemetry, tracking, command and station performance data

recorded by the DSIF into engineering and scientific information for analysis and use by the scientific experimenters and spacecraft engineers.

The DSN Ground Communication System consists of voice, normal and high data rate teletype circuits provided by the NASA World-Wide Communications Network between each overseas station and the SFOF; teletype and voice circuits between the SFOF, Goldstone Stations, and Cape Kennedy; and a microwave link between the SFOF and Goldstone, provided by the DSN.

II. Tracking Stations Engineering and Operations

A. Systems Engineering and Integration

1. Ascension Island Equipment¹

Subsystems have been assembled at Goldstone Pioneer Station for system integration and initial test of the Ascension Island Station, DSIF-72, which will provide additional tracking and data acquisition support for spacecraft using direct ascent launching from Cape Kennedy. The station also will provide unique guidance and command functions when utilizing two-way communications.

DSIF-72 will use an Az-El tracking antenna with a 30-ft-diameter paraboloidal reflector as the main antenna, and additional acquisition antennas to facilitate early spacecraft acquisition (SPS 37-33, Vol. III, p. 26). A mock-up of the 30-ft Az-El antenna has been erected at the Pioneer Station for purposes of mechanical design development and initial component integration of the antenna microwave subsystem on the antenna structure and within the antenna-mounted electronics room. The

mock-up also serves as an aid in the design and development of the cable wrap-up mechanism. The primary antenna mechanical structure has been shipped to Ascension Island for erection and installation.

The Ascension Island equipment at Goldstone is scheduled for disassembly, packing, and shipment in September. Following completion of the installation and system integration at Ascension Island, scheduled system tests of the complete station will begin early in 1966.

2. Suitcase Telemetry Receiver

A modified suitcase telemetry receiving system (SPS 37-31, Vol. III, p. 8 and JPL Engineering Planning Document 235) was integrated with the L-S Tracking System at DSIF-51, Johannesburg, South Africa, to provide wide band telemetry capability for the *Surveyor* Mission A. As shown in Fig. 1, the suitcase receiver is connected via a directional coupler to the existing 85-ft antenna and traveling wave maser (TWM) in parallel with the existing L-S-band receiver. To compensate for line loss, a tunnel diode amplifier is located in the suitcase receiver channel. In this configuration the estimated system temperature with the suitcase receiver is 46.2°K.

¹For additional information, see Sections C (p. 12) and D (p. 18).

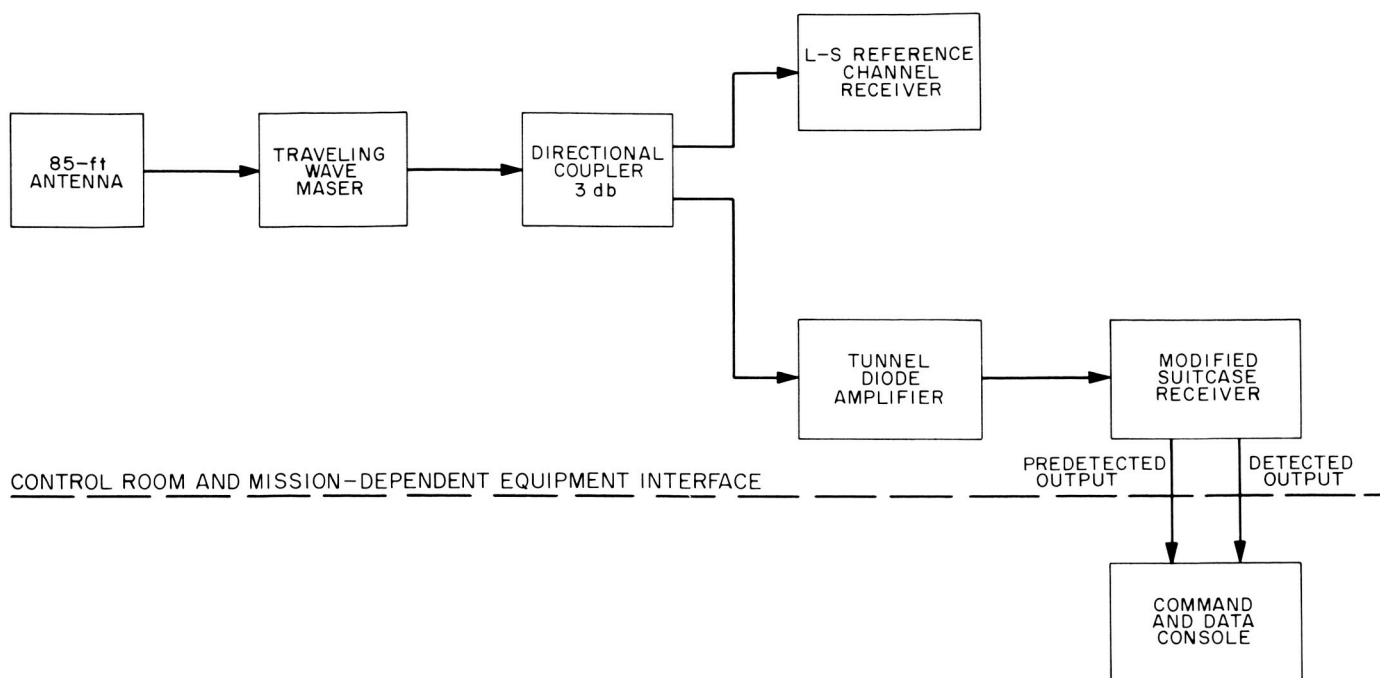


Fig. 1. L-S receiver and suitcase telemetry receiver

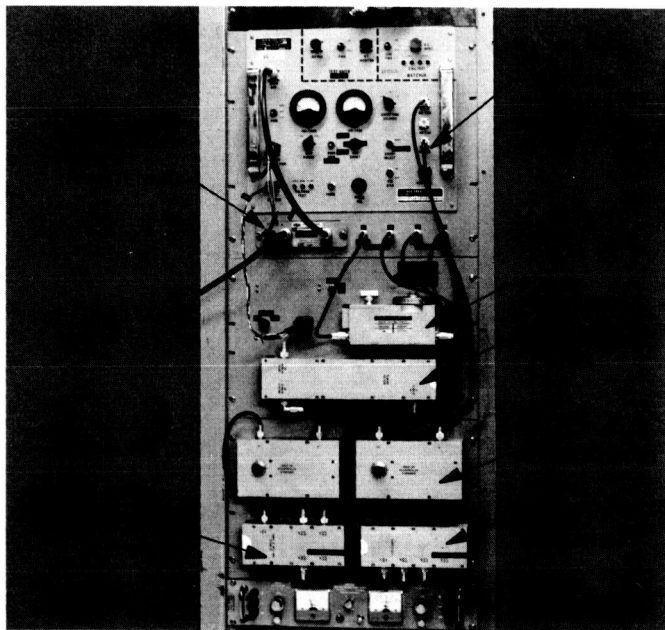


Fig. 2. Suitcase telemetry receiver

To provide the necessary telemetry outputs and levels, the suitcase receiver was modified using Goldstone duplicate standard (GSDS) S-band receiver components. These are: a four-channel band-pass filter, phase shifter, 10-Mc IF amplifier, video amplifier, and two variable attenuators. Since the receiver is to remain in use for an ex-

tended period of time, the battery power supplies were replaced with a commercial electronic power supply and the receiver with added components mounted in a rack (Fig. 2).

With the added components, the receiver has three standard bandwidths: 4.5, 20, and 420 kc. It also has a predetected 10-Mc output for FM telemetry of gyro speed data. In its present configuration, the receiver is not intended for TV reception.

When a complete GSDS S-band receiver is installed at DSIF-51, the suitcase telemetry receiver will be restored to its original condition as a portable receiver.

B. Systems Analysis

1. Y-Factor Technique for Automatic Gain Control (AGC) Calibration

An investigation was conducted to determine the feasibility of implementing the Y-factor technique (SPS 37-33, Vol. III, p. 81) for establishing an accurate signal level for calibrating the DSIF S-band receivers as a received-signal power detector. The technique is normally used in

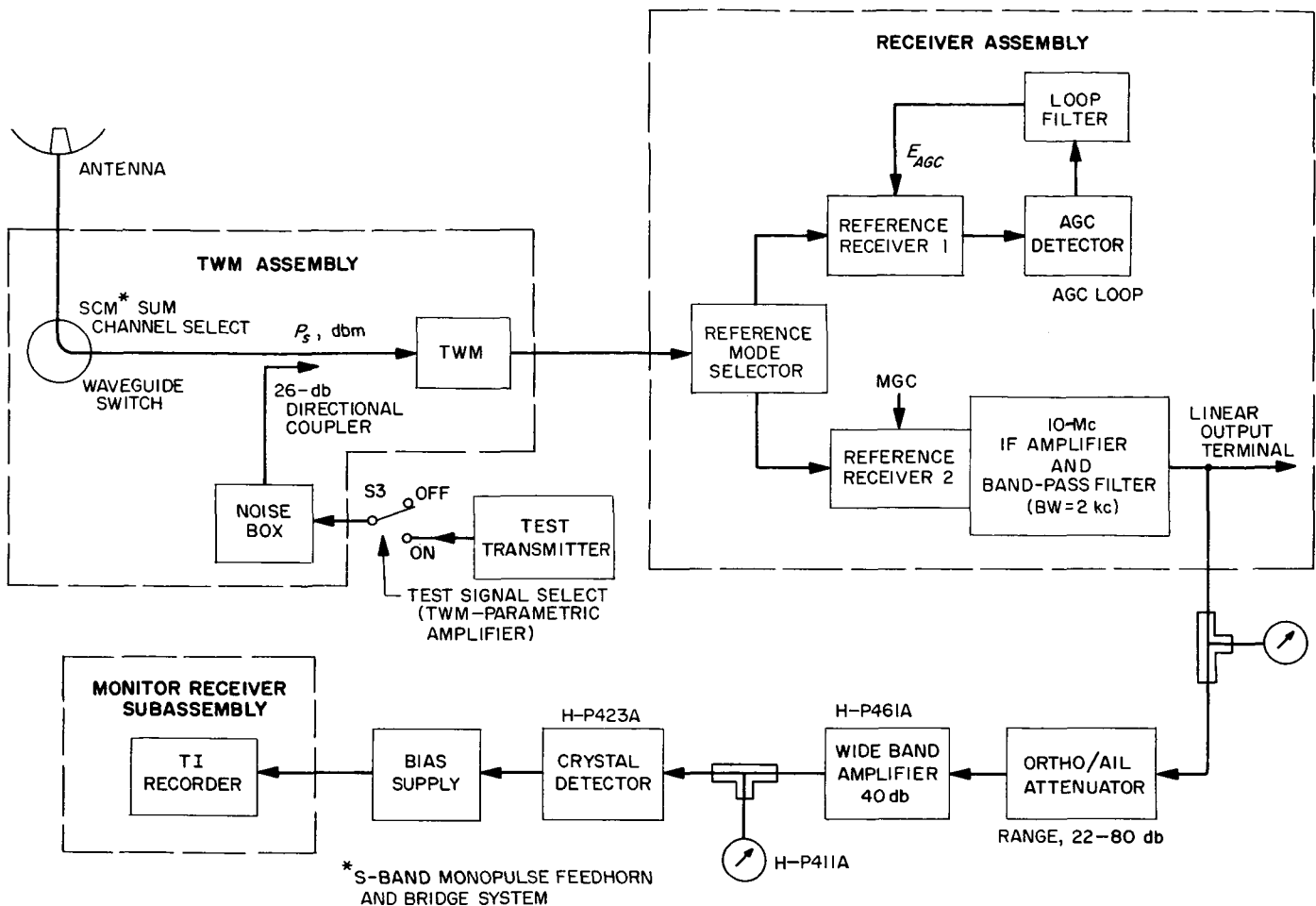


Fig. 3. Y-factor method

the DSIF for measuring the S-band system noise temperature. However, the basic principle can be applied in calibrating, at the input to the TWM (thus not requiring accurate cable loss calibration between the test transmitter and TWM input), a signal level from the test transmitter used for the AGC calibration. The procedure compares the signal power with accurately known noise power at the output of a filter whose noise bandwidth can be accurately established.

For the test configuration in Fig. 3, the range of calibration was -120 to -150 dbm (used at DSIF-11 and -12). Reference Receiver 1 was used as the AGC voltage monitor while Receiver 2 was used as the Y-factor receiving system [manual gain control (MGC) mode]; however, both systems were phase locked to the test transmitter's continuous wave (CW) output signal. The strong signal limitation resulted from the low sensitivity of the crystal detector, 0.4 mv/ μ w. The weak signal limit was set by

the 2-kc band-pass filter (10-Mc IF) used by the reference receiver.

Initially, an accurate gain frequency response measurement was made of the 2 kc-band-pass filter; and a trapezoidal rule computer program computed the noise bandwidth from the tabulated data. The relationship, which yields the signal power injected into the maser input from the test transmitter, is

$$P_s = kT_s (Y - 1) \frac{\int_0^\infty G(f) df}{G(f_s)} \quad (1)$$

where

$$k = \text{Boltzmann's constant, } 1.38 \times 10^{-23} \text{ joules/}^\circ\text{K or } 10 \log k = -198.6 \text{ dbm/}^\circ\text{K}$$

$$T_s = \text{system noise temperature, } ^\circ\text{K}$$

Y = difference in the precision attenuator setting for equal power levels with the CW signal on and off

$$\int_0^{\infty} G(f) df = \text{noise bandwidth of 2-kc band-pass filter}$$

$G(f_s)$ = filter gain at the signal frequency f_s

Thus, for the specific test at DSIF-11, it was found that

$$P_s = -148.4 \text{ dbm} + (Y - 1) \text{ db.}$$

The test procedure consisted of adjusting the Airborne Instruments Laboratory, New York, precision attenuator for equal power levels with the test transmitter switched on and off by switch S3 (shown in Fig. 3) on the test signal controls assembly. This procedure was followed for various settings of nominal signal levels from -120 to -150 dbm as indicated in Fig. 4, which

illustrates the results of the Y -factor measurement at DSIF-11 compared to the AGC calibration utilizing the present operational procedure.

A cursory error analysis of the basic Y -factor equation

$$Y = \frac{P_s + kT_s B}{kT_s B}, \quad (2)$$

where

$$B = \int_0^{\infty} G(f) df = \text{effective noise bandwidth,}$$

yields the following error equation which can give the percent of error in signal power as

$$\frac{\Delta P_s}{P_s} = \left\{ \left[\left(\frac{P_s + kT_s B}{P_s} \right) \frac{\Delta Y}{Y} \right]^2 + \left(\frac{\Delta T_s}{T_s} \right)^2 + \left(\frac{\Delta B}{B} \right)^2 \right\}^{1/2} \quad (3)$$

Using this relationship, the accuracy for the test conducted at DSIF-11, of the calibrated test signal at $P_s = -150$ dbm (point of marginal accuracy), is computed by substituting the following values for the equation parameters:

$$P_s = -150 \text{ dbm or } 10^{-18}$$

$$B = 2288 \text{ cps}$$

$$T_s = 44.2^\circ \text{K}$$

$$k = 1.38 \times 10^{-23} \text{ joules/}^\circ \text{K}$$

$$\frac{\Delta B}{B} = 1.0\% \text{ or } \Delta B = \pm 22.3 \text{ cps}$$

$$\frac{\Delta Y}{Y} = 1.5\% \text{ or } \Delta Y \cong \pm 0.05 \text{ db}$$

$$\frac{\Delta T_s}{T_s} = 4.5\% \text{ or } \Delta T_s = \pm 2.0^\circ \text{K}$$

The percent error in measuring the injected signal power into the maser input by the Y -factor technique becomes

$$\frac{\Delta P_s}{P_s} = 5.7\% \text{ or } \pm 0.24 \text{ db.}$$

Y -factor measurements were taken at other DSIF stations using the basic Y -factor principle; however, other methods of power detection had to be innovated because of nonavailable identical equipment used in the DSIF-11 test. An over-all summary of the test results is given in Table 1.

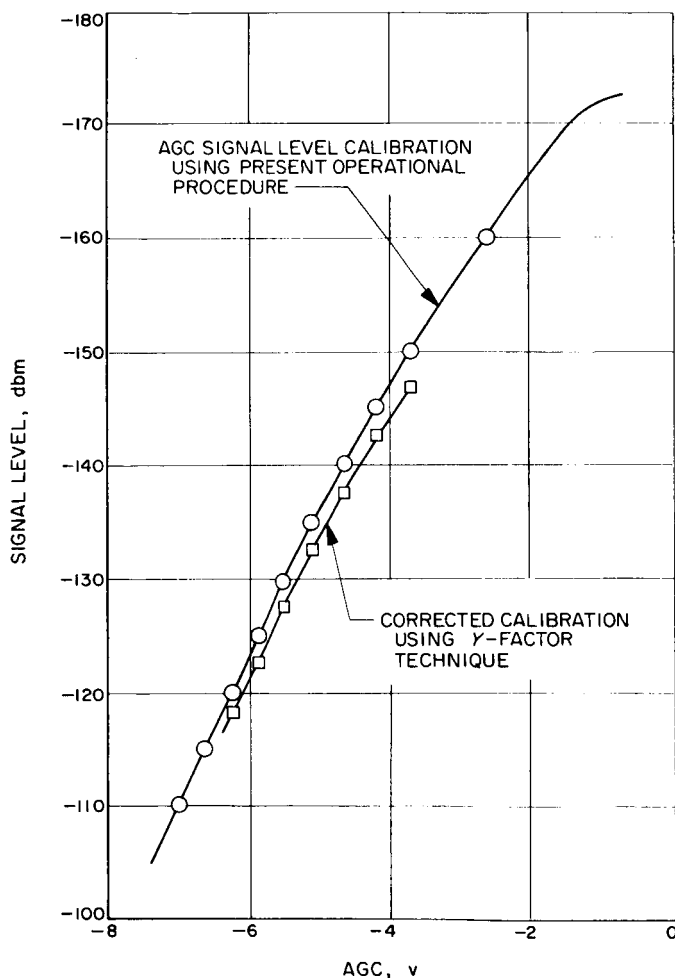


Fig. 4. Results of Y -factor measurement

Table 1. Test results using Y-factor technique

DSIF Station	Indicated Y-factor error, db	Error found in recalibration, db
11	2.4	2.2
12	-2.0	-1.0
41	No significant error	—
42	1.8	1.0
51	0.7	Not available
61	No significant error	—

2. Determination of DSIF Tracking Antenna Frequency Response

The 85-ft antenna RMS angular jitter resulting from the receiver input noise spectral density, and the optimum adjustments of the servo loop time constants to permit the tracking of signals approaching threshold have been of concern in the analysis of the angle tracking system. Recent analysis has been performed to verify and improve the derived data and to provide a firm basis for correlating field data with theoretical information. Some of these system tests performed on the Pioneer 85-ft antenna are reported here.

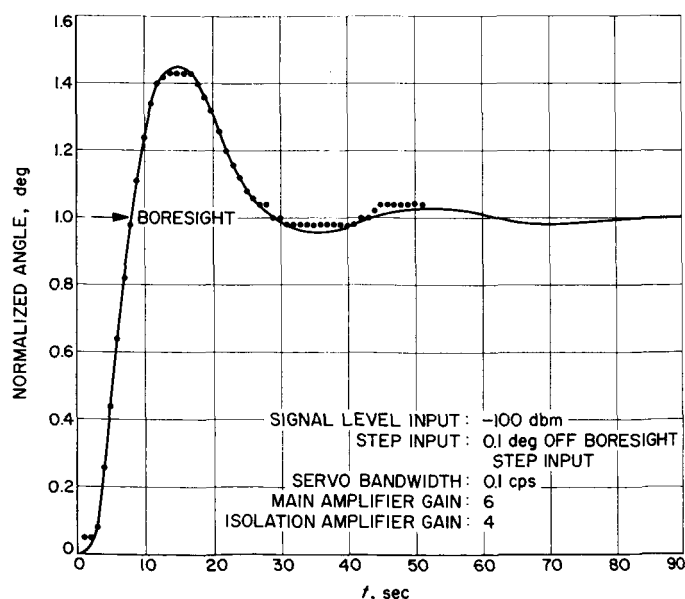


Fig. 5. Time response for step function input, hour angle low-speed case

The derivation of a transfer function for each axis (hour angle and declination) has been accomplished recently and used as a basis for analytical studies of DSIF performance.²

²Interoffice Memo, JPL Section 332, March 8, 1965.

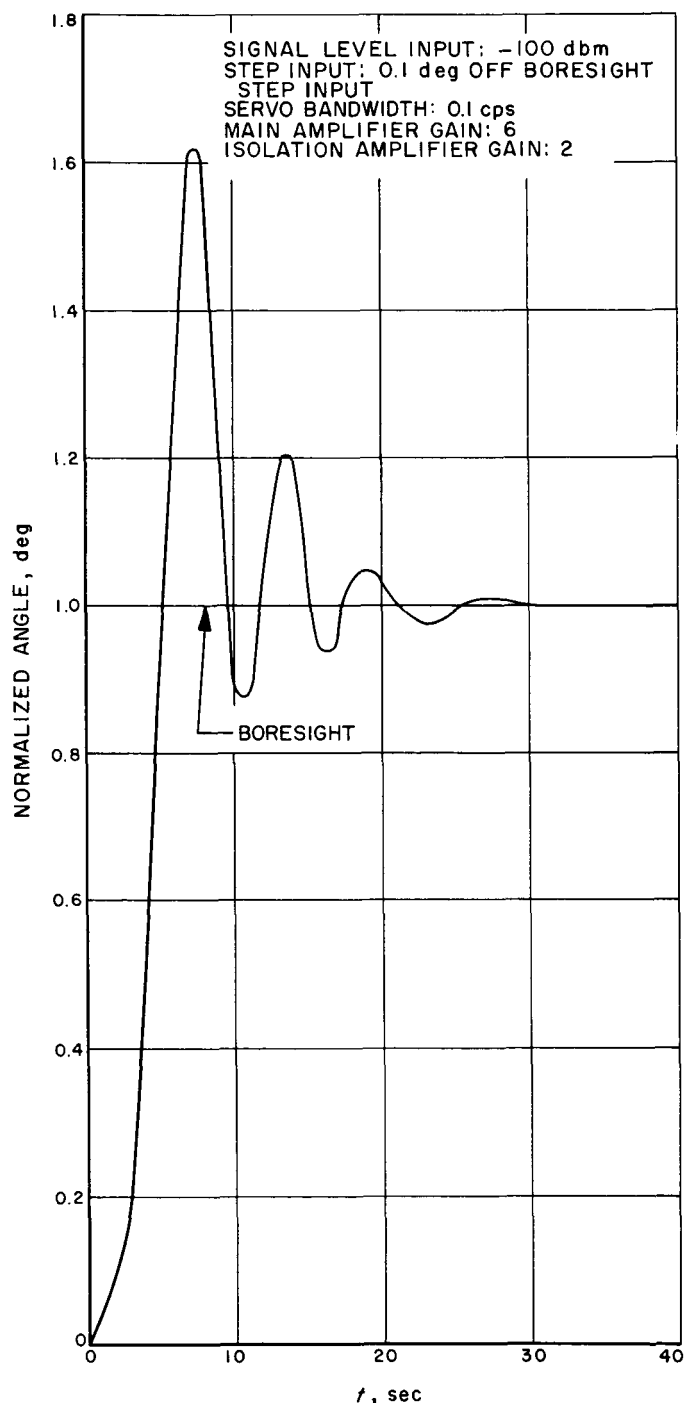


Fig. 6. Time response for step function input, declination angle low-speed case

More recently, servo snap-on tests have been performed on the angle tracking system with the aid of a test transmitter in the collimation tower. These tests involved moving the antenna a small angular displacement from the boresight alignment to the collimation tower and then closing the servo loop. The resultant step-input time response was then recorded from the Datex digital angle system for both the hour angle and the declination axes. These normalized response curves as a function of time are shown in Figs. 5 and 6. The curves were smoothed to eliminate nonlinear gear "hitching" and "sticktion" so that linear response information could become evident.

By utilizing the modern approach of functional transformation, a complete description of a function in the

time domain will provide a complete description of the function in the frequency domain. The principle of the Laplace transform was employed in a finite summation to obtain a satisfactory frequency response function. The hour angle and declination time domain step function response curves were sampled every half sec. These small individual steps were then summed with an exponential term and thereby Laplace-transformed into the frequency domain as shown by

$$G(\omega_i) = \sum_{n=0}^N A_n e^{-j\omega_i n\tau}$$

where N is the number of points sampled in the domain curve, τ is the sampling interval, and A_n is the amplitude of each step in the time domain.

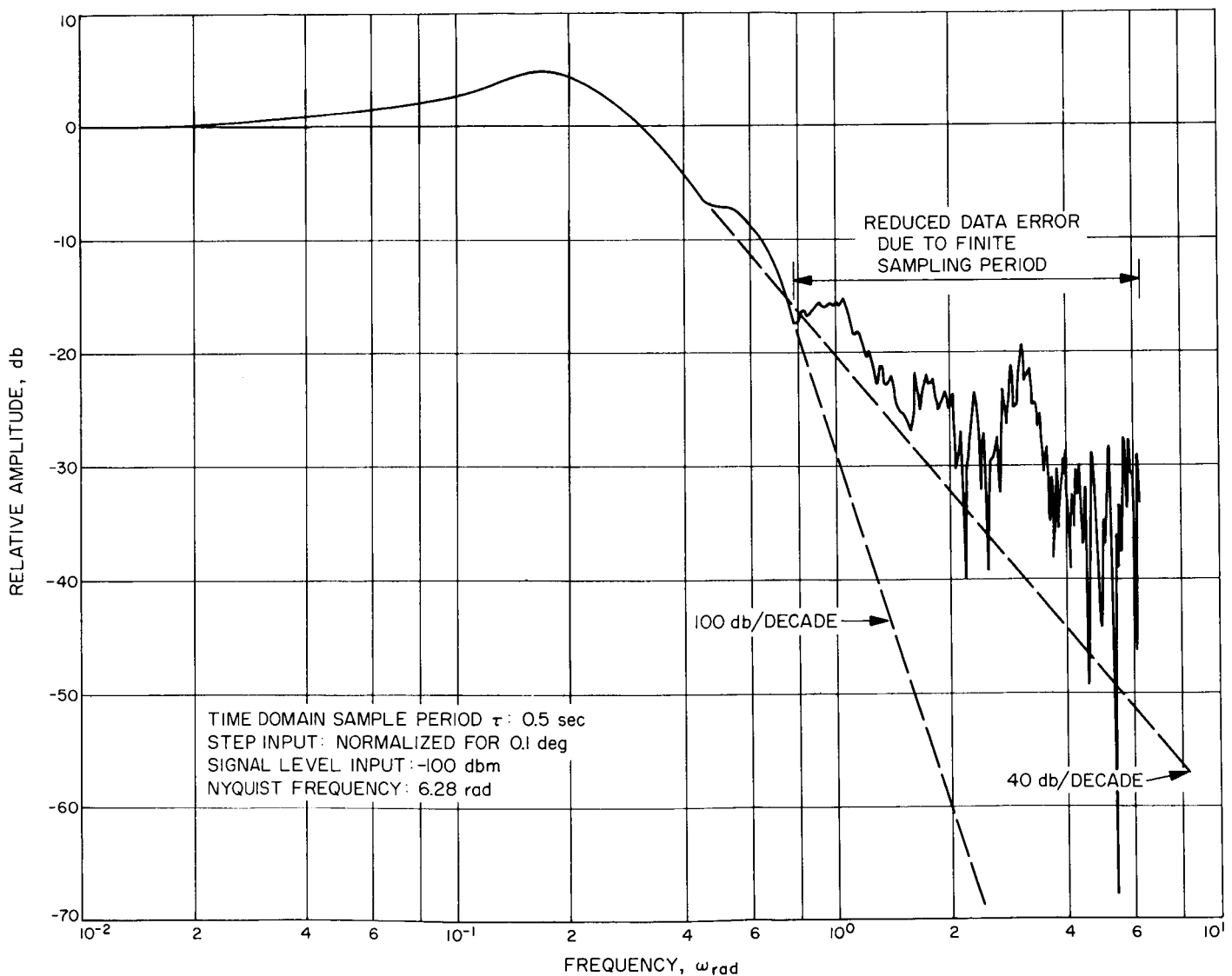


Fig. 7. Computer plot of frequency response, hour angle low-speed case

This process must be repeated on the computer for each ω_i frequency point in the frequency response plot.

H. A. Samulon (Ref. 1) has shown that a correction term, β , may be applied to the higher frequency terms to reduce errors due to sampling close to the cutoff frequency. This term is given as the reciprocal of

$$\frac{\sin\left(\frac{\pi}{2} \frac{\omega}{\omega_{co}}\right)}{\left(\frac{\pi}{2} \frac{\omega}{\omega_{co}}\right)} = \frac{1}{\beta}$$

multiplied by $e^{j\omega(\tau/2)}$, which can be given as $\beta e^{j\omega(\tau/2)}$.

One caution must be observed: The cutoff frequency must be noted or intuitively assumed. The sample spacing in the time domain must then be smaller than half the period of the cutoff frequency (e.g.: $\tau < 1/2f_{co}$) as a consequence of Nyquist's sampling theorem. The cutoff frequency will become evident after a preliminary com-

puter run and frequency plot have been made. The hour angle and declination normalized response curves were sampled and the computer run on each is plotted in Figs. 7 and 8, respectively. The effects of a finite sampling period as the higher frequencies are recorded can be noted above 0.8 rad in the Fig. 7 hour angle plot and above 2.5 rad in the Fig. 8 declination plot.

Figs. 9 and 10 give the comparison between the plots of the derived transfer functions² and the transfer functions computed from measured step-function response.

The hour angle plot of Fig. 9 shows the damped resonant frequency of the actual response to be somewhat higher than that of the derived function; however, the correspondence between the derived and actual response in the declination case of Fig. 10 is remarkably good. In both cases there is a small antenna resonance mode that is illustrated in the computed response and not indicated by the derived response.

²Interoffice Memo, JPL Section 332, March 8, 1965.

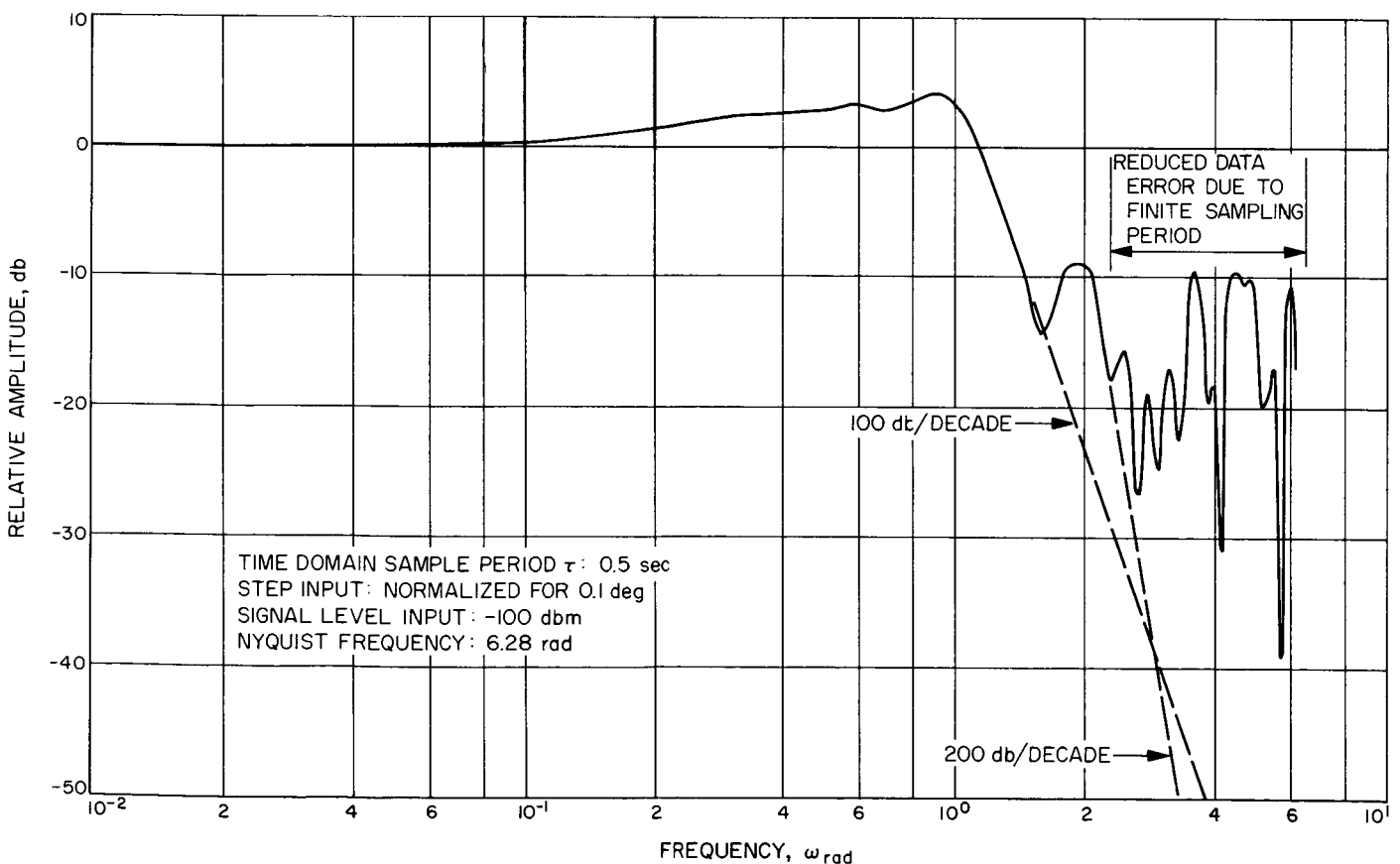


Fig. 8. Computer plot of frequency response, declination angle low-speed case

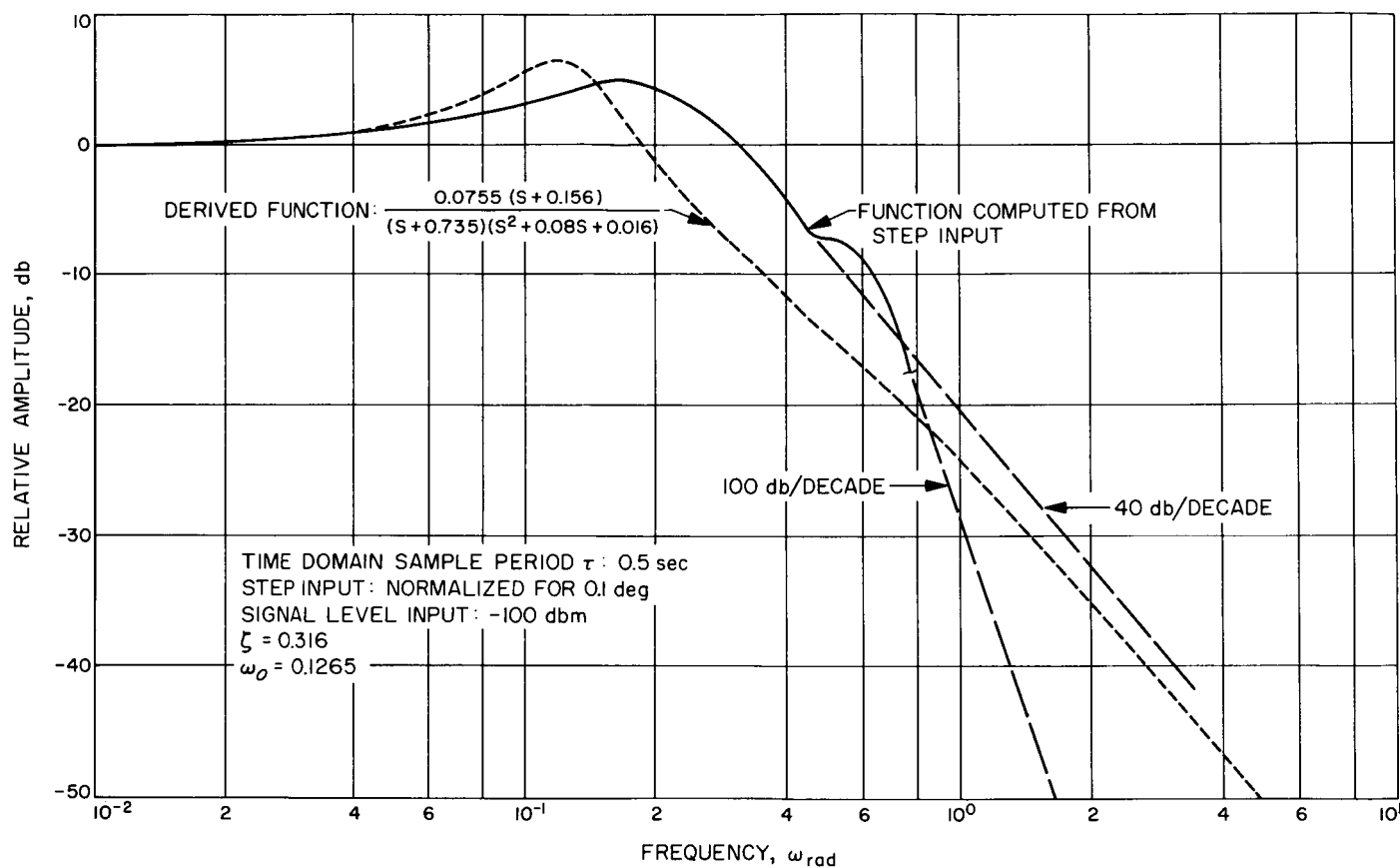


Fig. 9. Computed frequency response compared with derived frequency response, hour angle low-speed case

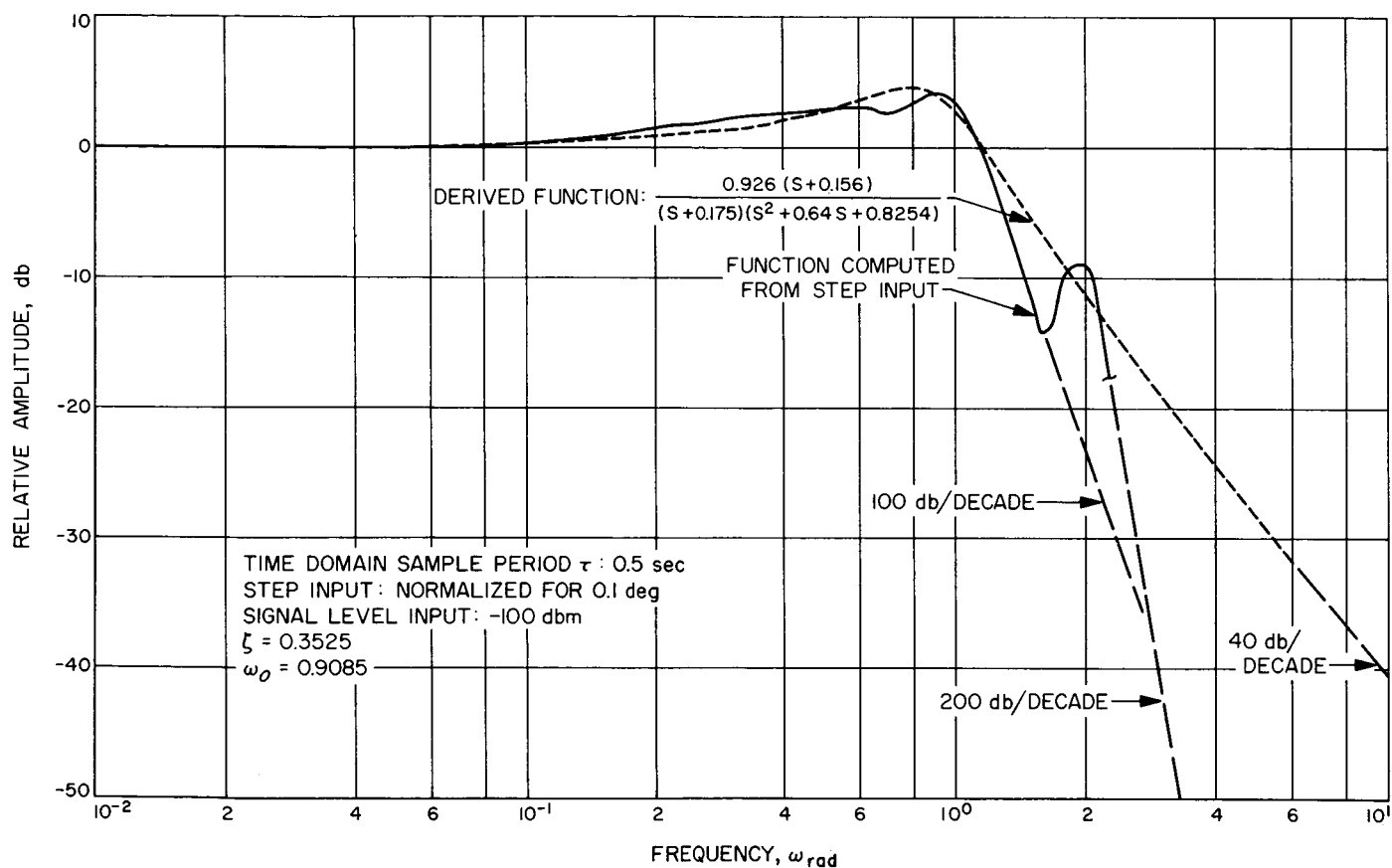


Fig. 10. Computer frequency response compared with derived frequency response, declination angle low-speed case

A comparison of the respective noise bandwidths normalized for both $H^2(0)$ and $H_m^2(S)$ is given below.

	Derived function, rad/sec	Computed function, rad/sec
Hour angle	$H_m^2(S) : 0.116$ $H^2(0) : 0.476$	0.180 0.558
Declination angle	$H_m^2(S) : 0.859$ $H^2(0) : 2.459$	0.872 2.252

The use of step-function time response data, reduced in a computer program, has proved useful. The original derived transfer functions were verified and higher-order resonance modes were detected. An important result is the determination of more accurate noise power bandwidths which will provide a sound basis for theoretical investigations of RMS tracking jitter and minimum acquisition signal levels.

C. Antenna Engineering

During this reporting period, the antenna engineering activities described in this article were completed.

1. Interim S-Band Retrofit

To enable the Echo Station to be operational during the *Mariner IV* encounter, an interim S-band system transmitter mounting, an electronics cage, and HA-Dec counterweight cages were installed on the 85-ft antenna.

Figs. 11 and 12 show a bottom and side view, respectively, of the interim electronics cage and S-band transmitter mounting.

2. Antenna Dish Surface Reskinning

The dish surface at the Woomera Station was reskinned with perforated plate, replacing the torn, deformed, and reduced-performance aluminum diamond mesh skins. The new skins improve the surface tolerance by a factor of two, afford a medium level (up to 1-in. hailstones) of impact survivability, reduce noise temperature, and will allow personnel to walk over the surface without inflicting damage.



Fig. 11. Interim electronics cage and S-band transmitter mounting, bottom view

The implication of the level of improvement afforded by the interpretation of JPL graphical data is about $\frac{1}{4}$ to $\frac{1}{2}$ db in gain and 1 to 3°K reduction in noise temperature at S-band frequencies.

3. Ascension Island 30-ft Antenna Mock-up³

The Pioneer Station's 30-ft mock-up of the Ascension Island Az-El tracking antenna has been completed for the purpose of solving, at Goldstone, difficult and critical mechanical and RF plumbing interface and mechanization problems.

Fig. 13 shows construction and forming of the foundation and Fig. 14 shows the completed foundation.

The mock-up was fabricated in modular sections to expedite its erection. Fig. 15 depicts the installation of the antenna dish and Fig. 16 shows the completed mock-up and installation of the SAA transmitting horn.

³For additional information, see Sections A (p. 3) and D (p. 18).

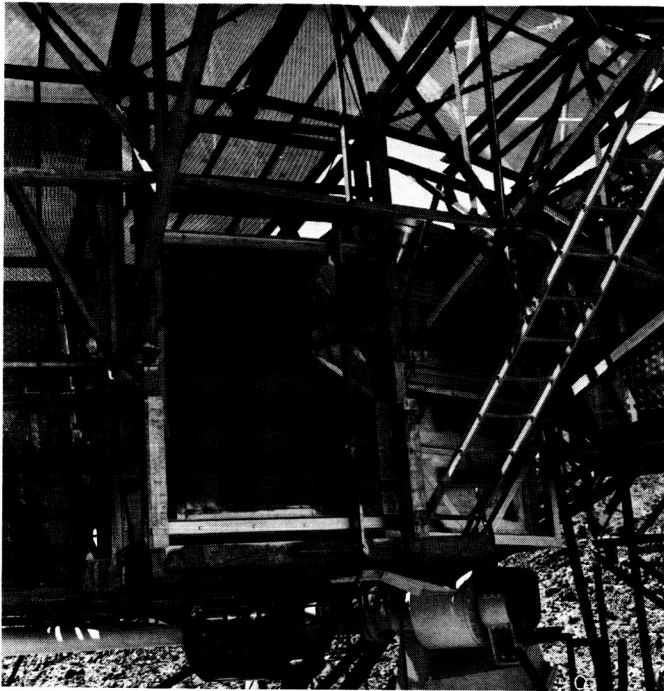


Fig. 12. Interim electronics cage and S-band transmitter mounting, side view

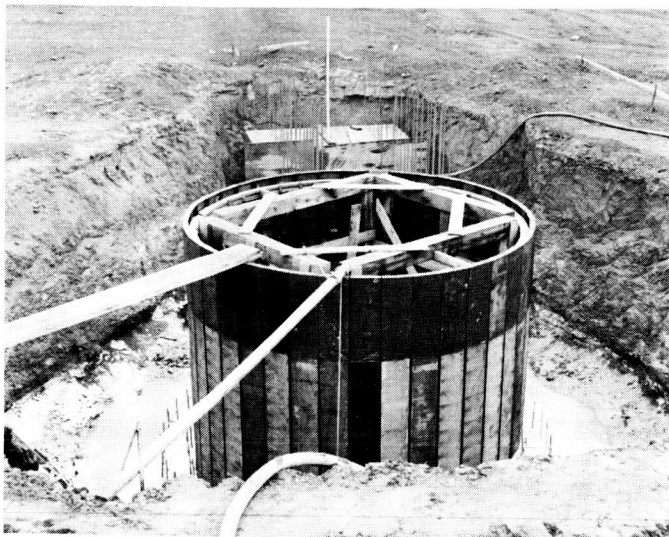


Fig. 13. Forming the mock-up foundation

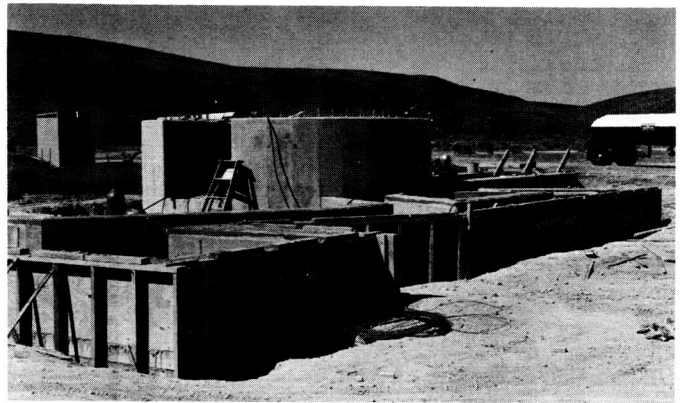


Fig. 14. Completed foundation



Fig. 15. Installation of antenna dish



Fig. 16. Completed mock-up with SAA transmitting horn installed

As shown in Fig. 16, the mock-up was positioned so that it lies under the horizon mask of the Pioneer Station 85-ft antenna, so that the 85-ft antenna lies under the mock-up horizon mask, and so that the 100-ft collimation tower is visible.

D. Goldstone Operations

The *Mariner IV* flyby of Mars on July 15, 1965 (GMT), during the 229th day of the mission, was recorded by the Pioneer and Echo Stations. The Venus Station was in a standby status to provide command transmission with a 100-kw transmitter if needed. Both the photography of Mars' surface and the occultation experiments were completed successfully. During the post-encounter period, the TV picture data were transmitted twice. The second recording of the pictures was completed by the Echo Station, which then continued to track the spacecraft.

Currently, the Pioneer Station is preparing for the *Surveyor* Mission, and Echo Station is preparing for the *Pioneer* Mission.

1. *Mariner IV*

a. Pioneer Station. Prior to the Mars flyby, successive tests were conducted as training for operations personnel and for command system capability determination at planetary distances. Practice command loop lockup tests with the spacecraft, using the 100-kw capability of the Venus Station, also were performed. The results indicated that all systems were functioning well, with no apparent degradation of spacecraft response to commands because of distance.

The occultation experiment equipment was operationally tested, including a backup installation at the Echo Station.

A duplicate read-write-verify command console and a mission-dependent equipment console were installed for backup support.

b. Echo Station. *Mariner IV* was acquired by the Echo Station for the first time on the night of June 15, 1965 (GMT). Installation of the S-band system began immediately after completion of the *Ranger* Program (SPS 37-33, Vol. III, pp. 5-9), March 24, 1965. Acquisition of the *Mariner* spacecraft culminated 10 wk of installation effort which included removing the L-band equipment from the 85-ft antenna and the control building. Except for certain modified L-band modules, and compatible test equipment and power supplies, the S-band system was essentially a completely new installation.

Late in June, the Echo Station tracked the spacecraft in a series of tests to determine operational characteristics and to make all final adjustments to the S-band system. Beginning July 5, the Echo Station began daily backup tracking to the Pioneer Station from 30 min prior to the tracking transfer from Johannesburg to Pioneer until 30 min after Tidbinbilla had acquired.

Subsystem installation continued with temporary cables being replaced with permanent ones as they arrived. Also, minor assemblies of the various subsystems were installed, tested, and integrated into the operation. Two-way lock had not been attempted because of the uncalibrated transmitter; Echo was tracking in one-way lock, and the Venus Station could provide the up-link lock if

needed. By the week of the Mars flyby, the Echo Station was ready to provide full support to the Pioneer Station.

With the conclusion of the first TV data transmission from the spacecraft, the Echo Station stopped tracking to perform a series of peaking adjustments to the system in preparation for assuming full tracking as the prime station. Complete subsystem-system countdowns were performed daily; the station was on a 15-min standby status for the Pioneer Station. Tracking resumed July 29, and the following day Echo assumed prime station status.

A two-way lock with the spacecraft was established July 30. Until August 20, the Echo Station tracked intermittently in the two-way mode as a test of the system's capability to perform this function at planetary distances. The command loop was locked up August 20, for the first time by Echo Station as a test of the 10-kw transmitter's capability to place commands into the spacecraft. Commands were sent to the spacecraft from the Echo Station August 21.

During the week of August 23, a variety of command experiments were performed, and August 26, commands were placed in the spacecraft to inhibit its performing a midcourse maneuver. The Canopus sensor was updated August 27.

The TV actuating commands were transmitted August 30; reception of the first picture began at Echo Station at 02:06:01 (GMT) August 31.

c. Venus Station. Continuing in the *Mariner* Mars 1964 transmit configuration, the Venus Station will remain as command transmit station for the DSIF until October 1965.

During the Mars encounter, the Venus Station 100-kw transmitter provided the up-link signal enabling the *Mariner IV* spacecraft to successfully establish the exit occultation spacecraft up-link lock.

August 2, Venus Station transmitted commands DC-28, DC-26, and DC-2, which effectively turned off the transmission of the TV data and resumed the transmission of engineering and science data.

2. Surveyor Project

At the Pioneer Station, preparations for the *Surveyor* Project have been progressing concurrently with the

Mariner tracking. The ground control equipment for *Surveyor* is located in the control building (SPS 37-27, Vol. III, and subsequent issues). Since their arrival in the Summer of 1964, Hughes *Surveyor* personnel have been engaged in installation and testing of the equipment.

Numerous tests, conducted on a time-share basis when the system was available, have included most of the interface tests and a series involving the use of *Surveyor* equipment located in the screen room at the Microwave Test Facility. The latter tests used a microwave antenna link between the screen room and the Pioneer Station.

An enlarged screen room was constructed at the Microwave Test Facility, using parts of the former smaller room (SPS 37-34, Vol. III, p. 5). This building, 28 × 28 × 20 ft inside, is capable of housing the full-sized spacecraft. Arrival of the *Surveyor* T-21 spacecraft (Fig. 17) August 3, signaled the start of the final *Surveyor* testing.

Through July, crew training tests were conducted on the ground equipment using tapes simulating the spacecraft action. In August, crew training tests were started using the spacecraft located in the screen room. Via microwave, simulated tracking was conducted which included sending commands and receiving spacecraft telemetry. Tests were performed using the full system interfaces between the *Surveyor* ground equipment and the Pioneer S-band system. Received information was sent to the Space Flight Operations Facility at JPL, simulating normal tracking conditions. The tests covered simulated flight, landing, and postlanding operations. Spacecraft TV equipment was tested by taking pictures of targets inside the screen room and views of the desert through a window in the outer wall. Testing is expected to continue until time of mission.

3. Pioneer Project

The display and recording equipment at Echo Station has been installed in the *Pioneer* Mission control room. The complete installation (Fig. 18) comprises five racks. Interfaces with the Echo S-band system are completed, and tests are being conducted by *Pioneer* Project personnel assisted by Echo personnel operating the S-band equipment. Because of the full tracking of *Mariner IV*, system compatibility tests are being performed on a time-share basis between postcalibrations and the pretrack countdowns.

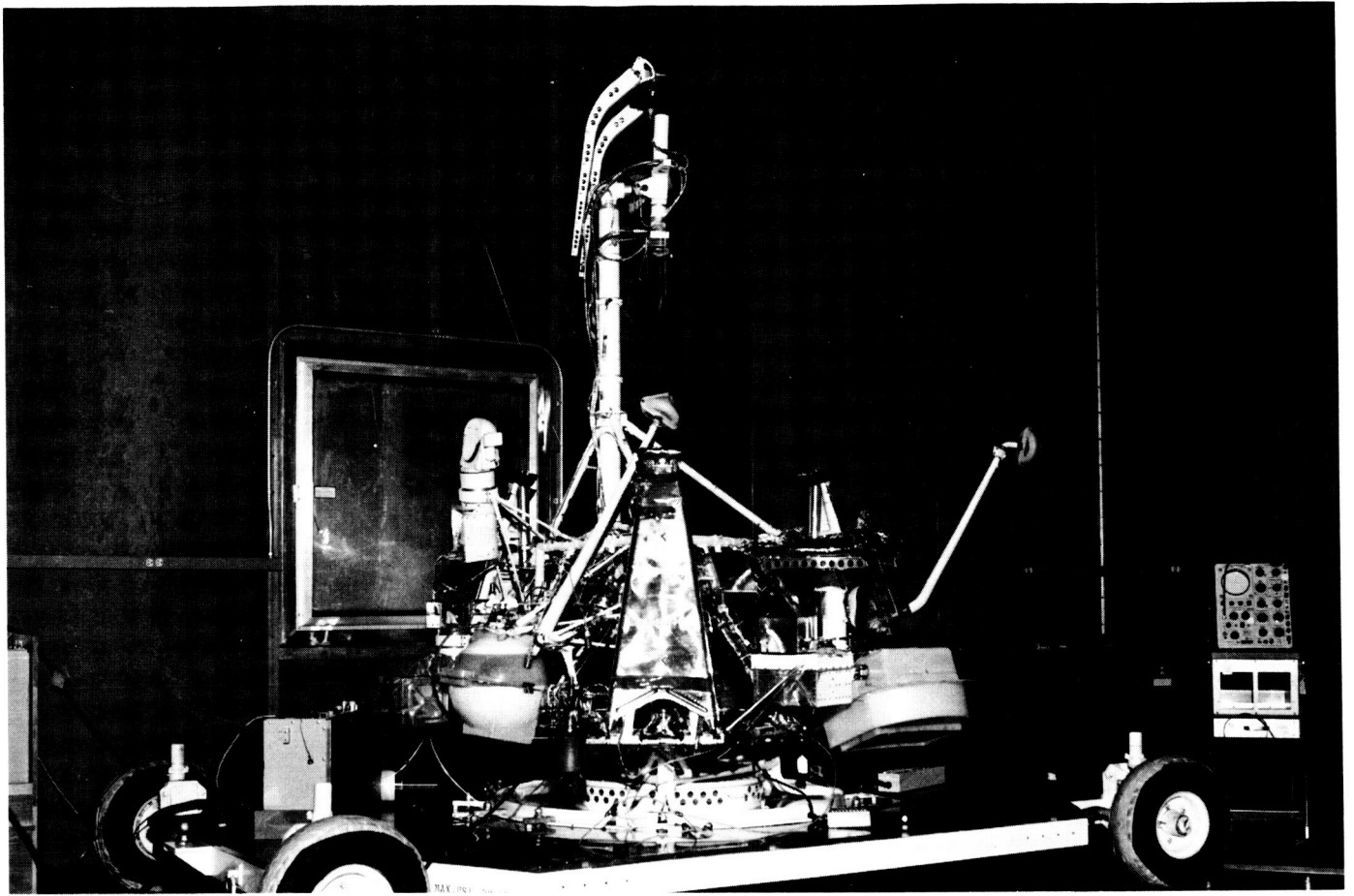


Fig. 17. Surveyor T-21 model in Microwave Test Facility screen room

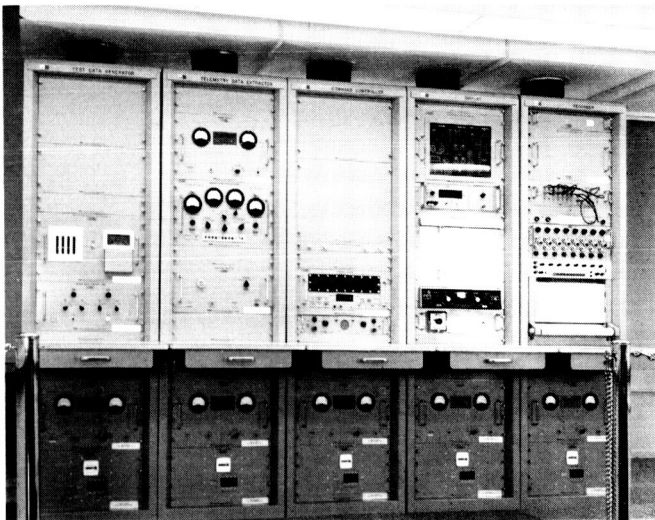


Fig. 18. Complete rack assembly of Pioneer Mission ground equipment

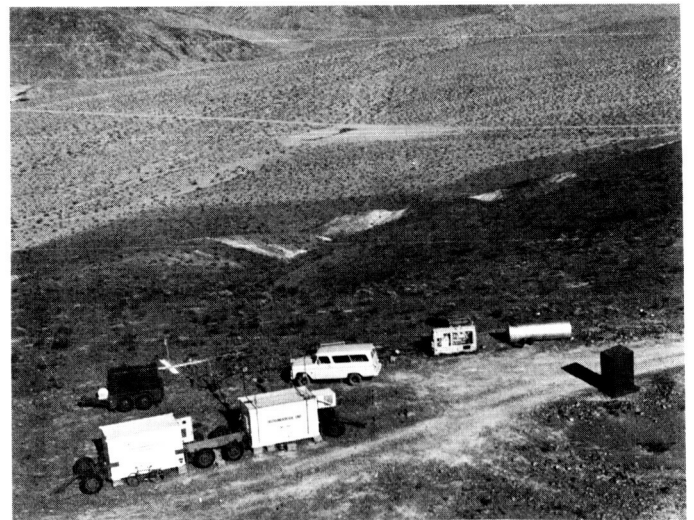


Fig. 19. U.S. Navy mobile tracking station at Echo Station

4. Lunar Orbiter Project

Advance personnel from this project have visited the Echo Station for initial survey of the control building space reserved for installation of *Lunar Orbiter* equipment.

5. Atlas-Centaur (AC-6) Track

Launch of the AC-6 *Surveyor* Project test August 11 was tracked by DSIF Stations. The Pioneer Station acquired the spacecraft at 02:00 GMT, August 12, and tracked for approximately 5 hr. Recorded tracking data were forwarded to JPL for processing.

6. Geodetic Satellite Tracking Project

From July 1 to August 12, a mobile survey tracking station from the Physical Science Laboratory of the New Mexico State University, Las Cruces, established operations at the Goldstone Echo Station (Fig. 19). Associated with the NASA/TRANET Project under a U. S. Navy contract, this station tracked a geodetic satellite.

7. Antenna Cable Installation Project

The normal cable installation used on the 85-ft antenna at Echo Station consisted of long-hanging loops of cable to allow for antenna movement. Because the cables were subject to excessive wear, abrasion, and damage when caught on a moving element of the antenna, a re-design was initiated to remount the S-band cabling in a manner which would permit full antenna movement while maintaining full support to the cables. Using an operating model of the antenna, cable runs were simulated with cord passing over the rotating assemblies of the hour angle and declination shafts in order to determine the desired mounting.

Fig. 20 illustrates the cable wrap-up around the south end of the hour angle shaft, and Fig. 21 shows the cable wrap-up around the east bearing of the declination shaft. Since its installation prior to the Echo Station's tracking of *Mariner IV*, and during the subsequent tracking, the cable wrap-up assembly has been performing well. Cable pulling, abrasion, or snagging on the moving antenna appear to be eliminated completely.

8. S-Band System Testing

a. *Pioneer Station-Woomera*. Located in the east wing of the control building, the Woomera Station S-band test

installation is receiving a continuing operational performance evaluation. Installed in essentially the same location as it will be in Woomera, each subsystem is operationally interfaced with associated subsystems and is performance-tested. Personnel from Australia who made the installation, and who will also make it at Woomera, are receiving

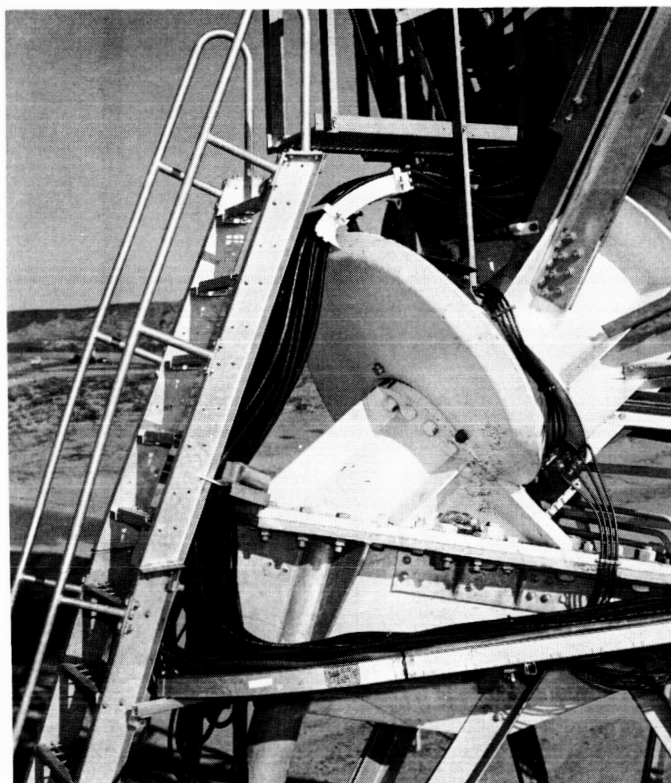


Fig. 20. Echo 85-ft hour angle shaft cable mounting



Fig. 21. Echo 85-ft declination shaft cable mounting

training in its operation and maintenance. All necessary documentation and procedures are being prepared to accompany the transfer of the system to its final location. During the week preceding and including the Mars flyby, Woomera personnel assisted in tracking operations at the Pioneer and Echo Stations.

b. Pioneer Station–Ascension Island.⁴ Located in the Manned Space Flight Network annex building, the Ascension Island Station S-band system assembly and testing is in progress (SPS 37-34, Vol. III, p. 4). Personnel who will make the installation on Ascension Island are receiving instruction on the receiver, the analog instrumentation, microwave equipment, and ranging subsystem at the Pioneer Station. Subsystems are being operationally tested as they arrive, and interface tests are being conducted as the system assembly continues.

E. Advanced Antenna System

1. Mars Station 210-ft Antenna

Located 14 mi northwest of the Echo Station, the Mars Station (DSIF-14) 210-ft antenna (Fig. 22) is nearing completion. Designated as the Advanced Antenna System (AAS), construction began with site clearing in October 1963. Excavation for the pedestal started in December 1963, and the first concrete was placed in January 1964. Placement of the first steel on the pedestal was in August 1964, and has continued on schedule until the current near-completion status.

The Mars 210-ft antenna is the azimuth–elevation type, capable of approximately 570 deg rotation in azimuth and 85 deg in elevation. Contained within the pedestal on the first floor are: power distribution and air conditioning equipment, offices, and workshop areas. The antenna drive and S-band equipment control room are on the second floor. Structurally isolated from the pedestal and the rotating alidade is the central instrumentation tower on top of which is the master equatorial equipment for pointing and steering the antenna. Within the outer wall of this tower, enclosed in a central circular room, is the cable wrap-up which provides for all power, signal, air conditioning, and hydraulic cables, permitting rotation of the antenna about the azimuth axis.

⁴For additional information, see Sections A (p. 3) and C (p. 12).

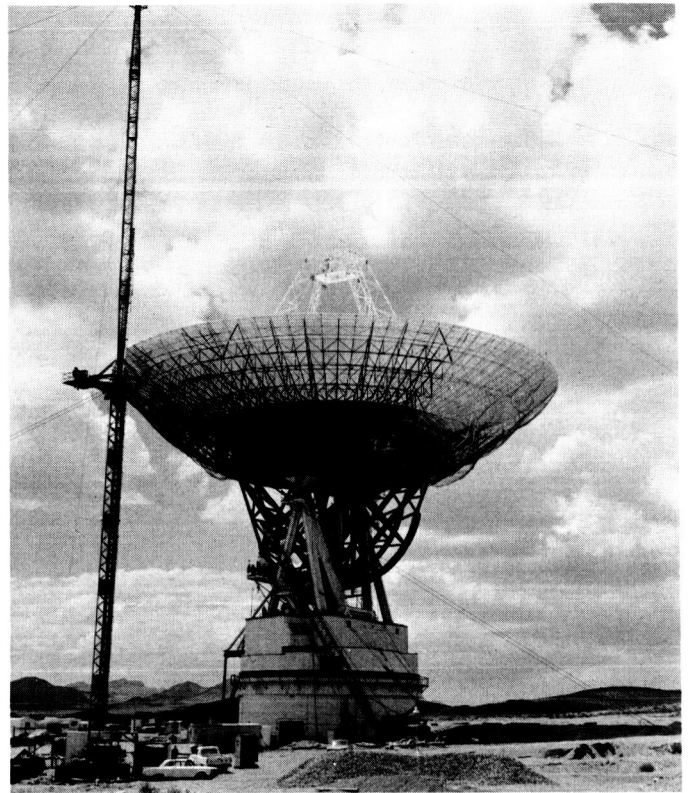


Fig. 22. Mars Station 210-ft antenna structure

In August 1964, the DSIF station manager's office was moved from the Pioneer Station to a trailer at the site of the Mars Station. In March 1965, the office was moved to its present location on the first floor of the pedestal. Currently, ten men are assigned to the station, in addition to the JPL manager.

Since the antenna is still under construction, the present crew has been procuring test and S-band system equipment. Rohr Corp. engineers have been conducting special training in the servoelectronics, servohydraulics, and the antenna mechanical systems.

The DSIF assumed responsibility for operation and maintenance of the power building and generators in November 1964; the pedestal, air conditioning equipment, and the cooling tower in March 1965. In early Spring, 1965, the three 500-kw generators were rotated through the manufacturer's facility for updating modifications. A treating system has been installed in the cooling tower to minimize water scale buildup.

Currently being installed in the control room on the second floor of the pedestal is the servoelectronics subsystem (Fig. 23). In storage at the Echo Station are the

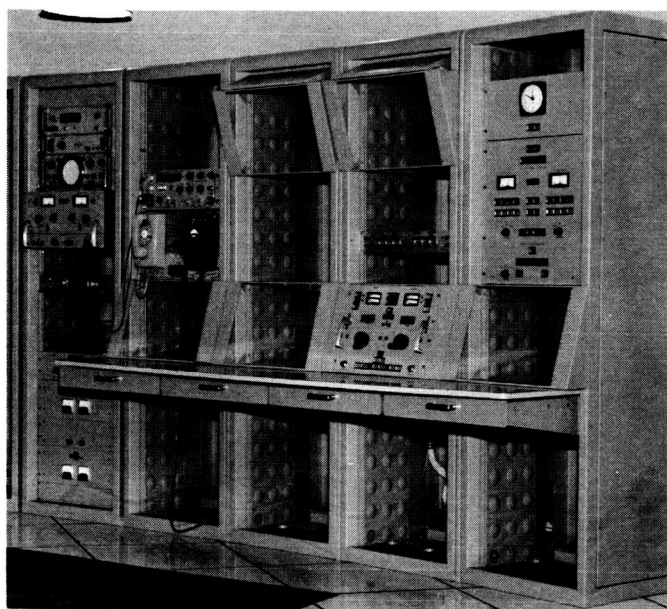


Fig. 23. Antenna servo rack installation at Mars Station

frequency and timing subsystem, the system junction modules, and the surveillance television equipment. After arrival, additional equipment is being held at Echo Station for later installation in the pedestal control room.

2. Construction Progress

All major components of the AAS structure have been fabricated and are now at the Mars Station. Erection of the components has been accomplished except for the subreflector and the feed cone assembly.

Installation of the servo and control system was essentially completed July 29, 1965. Azimuth and elevation rotation, under servo power, have been accomplished. Initial elevation rotation was made August 6, when the reflector structure was rotated from the zenith to the 20-deg-above-horizon position. Adjustment of the gears and drives is in progress.

Fig. 24 shows the broad expanse of the 210-ft diameter primary reflector during installation of the 552 aluminum surface panels.

Fabrication of the precision angle data subsystem (master equatorial) is in progress at various locations. Installation of electronic components is scheduled to begin in late November 1965, upon completion of the AAS structure and drives.

3. Scale Model RF Tests

The Venus Station 30-ft reflector has been modified to provide an accurate $\frac{1}{4}$ -scale model of the 210-ft AAS. Most important among the modifications, from the standpoint of RF performance, are the model quadripod installation and adjustment of the individual surface panels to yield a true paraboloid at the horizon look attitude. This report will show recent far-field radiation patterns of the modified reflector at the scaled DSIF frequency of 16330 Mc.

a. Recent radiation pattern test results. Previous issues of SPS have shown earlier 30-ft reflector secondary radiation patterns at the scaled frequency, using the nonscaled quadripod (SPS 37-30, Vol. III, pp. 110-115). Based on those data, surveys to determine the exact shape of the reflector were conducted and reported (SPS 37-33, Vol. III, pp. 14-18). The surveys proved the horizon look surface to be sufficiently astigmatic to produce, at $D/\lambda \simeq 500$, a nonsymmetrical secondary beam. In order to obtain low elevation angle far-field collimation tower gain and pattern data representative of a near-perfect paraboloid, the decision to change the nominally true paraboloid at zenith to a nominally true paraboloid at horizon was made. The results obtained (Figs. 25-28) are to be considered an extremely close representation of the 210-ft AAS performance near 45-deg elevation angle; this is because the AAS panels are optically aligned in this attitude and the panel manufacturing tolerances for the model and the prototype, with due regard for scaling, are estimated to be within a factor of 1.5. This factor cannot be reduced since the 30-ft reflector panel manufacturing tolerance is not well known (SPS 37-33, Vol. III, pp. 14-18 and 69-81).

Figs. 25 and 26 show azimuth and elevation secondary patterns using the high efficiency low noise dual mode horn feed. Subreflector scattered primary illumination patterns for this feed have been shown (SPS 37-32, Vol. III, p. 77); the patterns are essentially figures of revolution. Small differences between the E- and H-planes in Figs. 25 and 26 are felt to be caused by the 30-60-deg quadripod geometry and/or slight perturbations of the parabolic surface between measurements caused by different thermal and wind environments.

Figs. 27 and 28 show the E- and H-plane monopulse error channels using the tracking feed. Because the H-plane channel produces higher edge illumination of the paraboloid than the E-plane channel, Fig. 28 exhibits the generally higher sidelobe level produced.

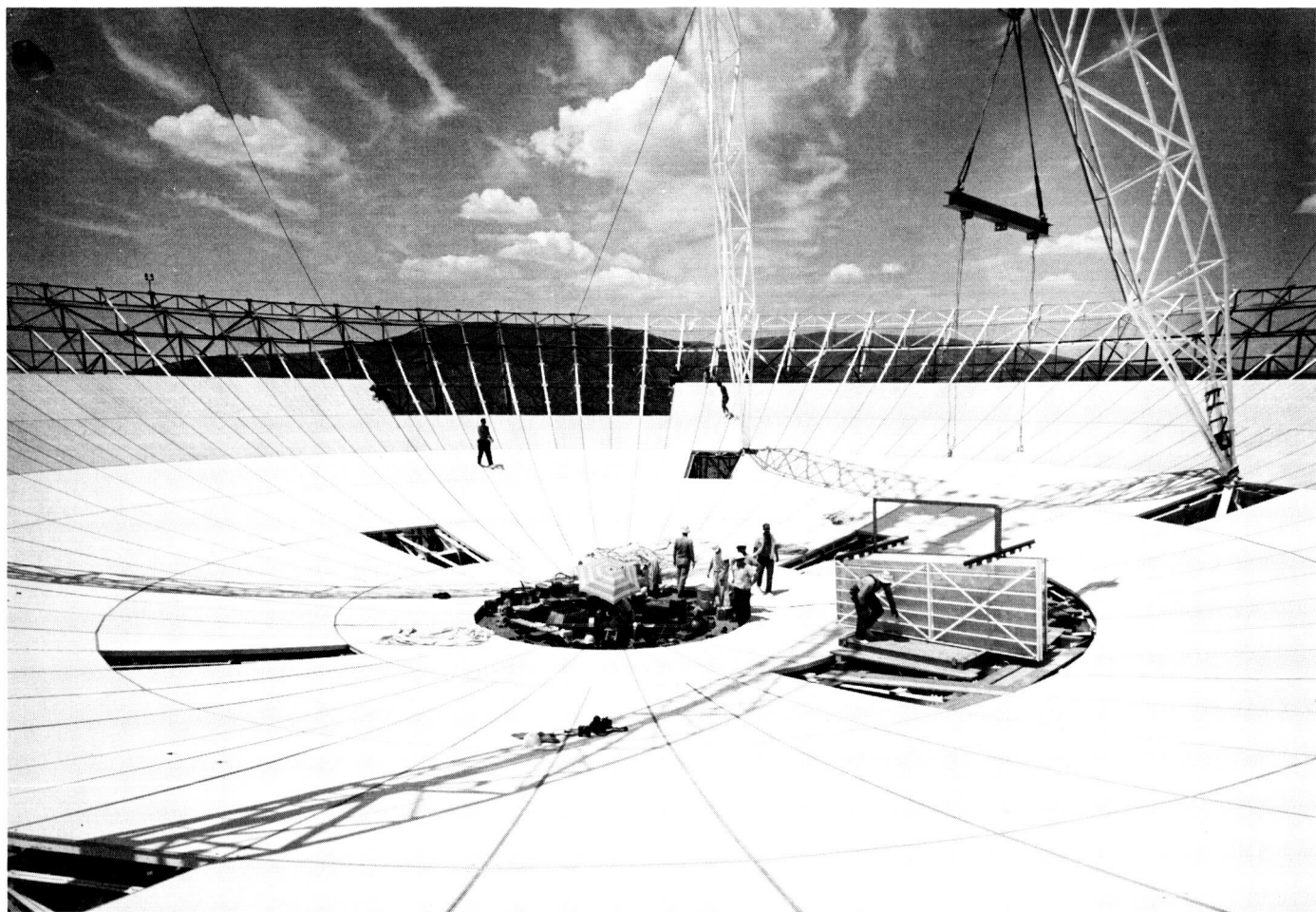


Fig. 24. AAS reflector surface panel installation

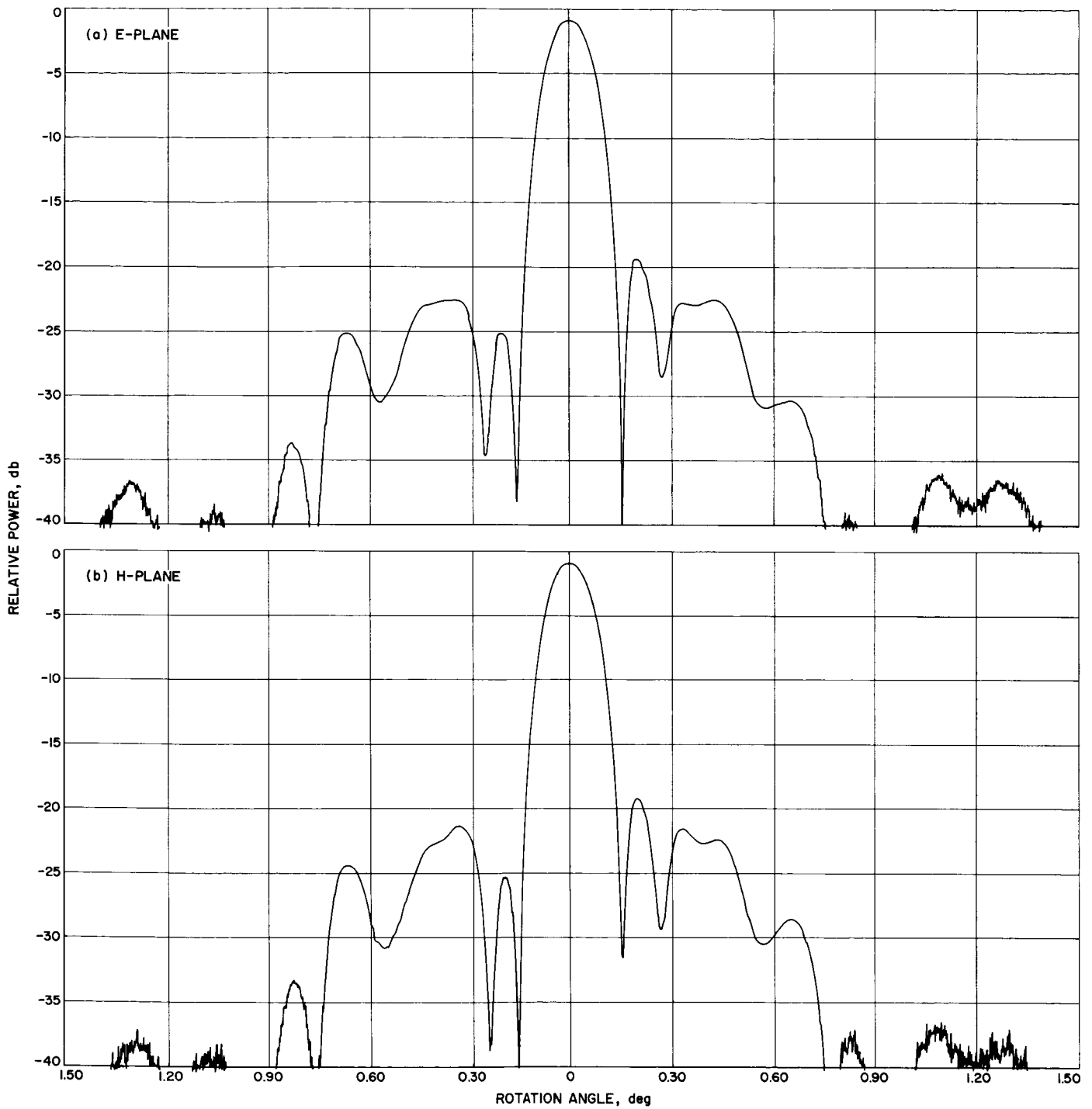


Fig. 25. AAS model, listening feed, azimuth E- and H-plane patterns

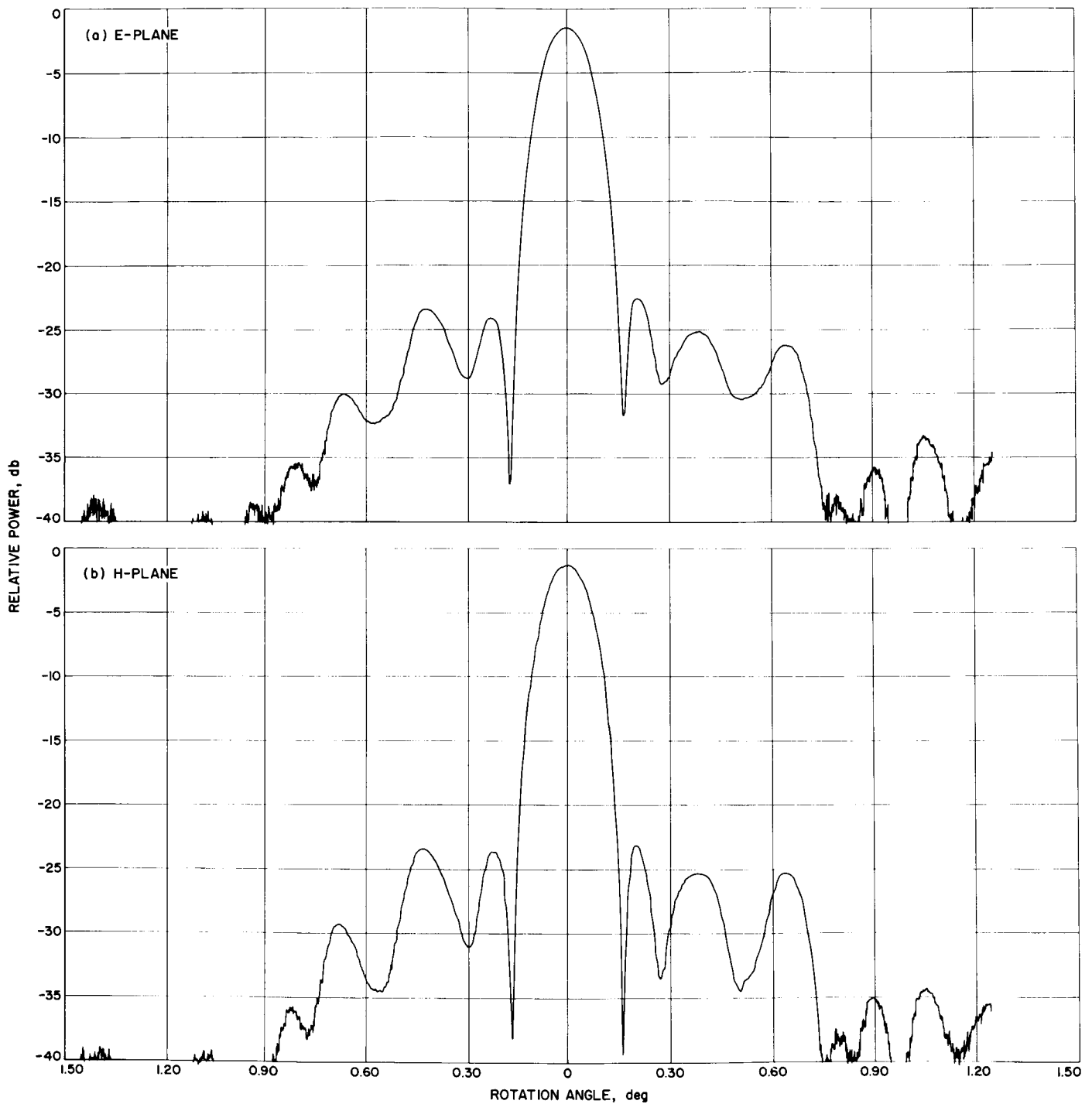


Fig. 26. AAS model, listening feed, elevation E- and H-plane patterns

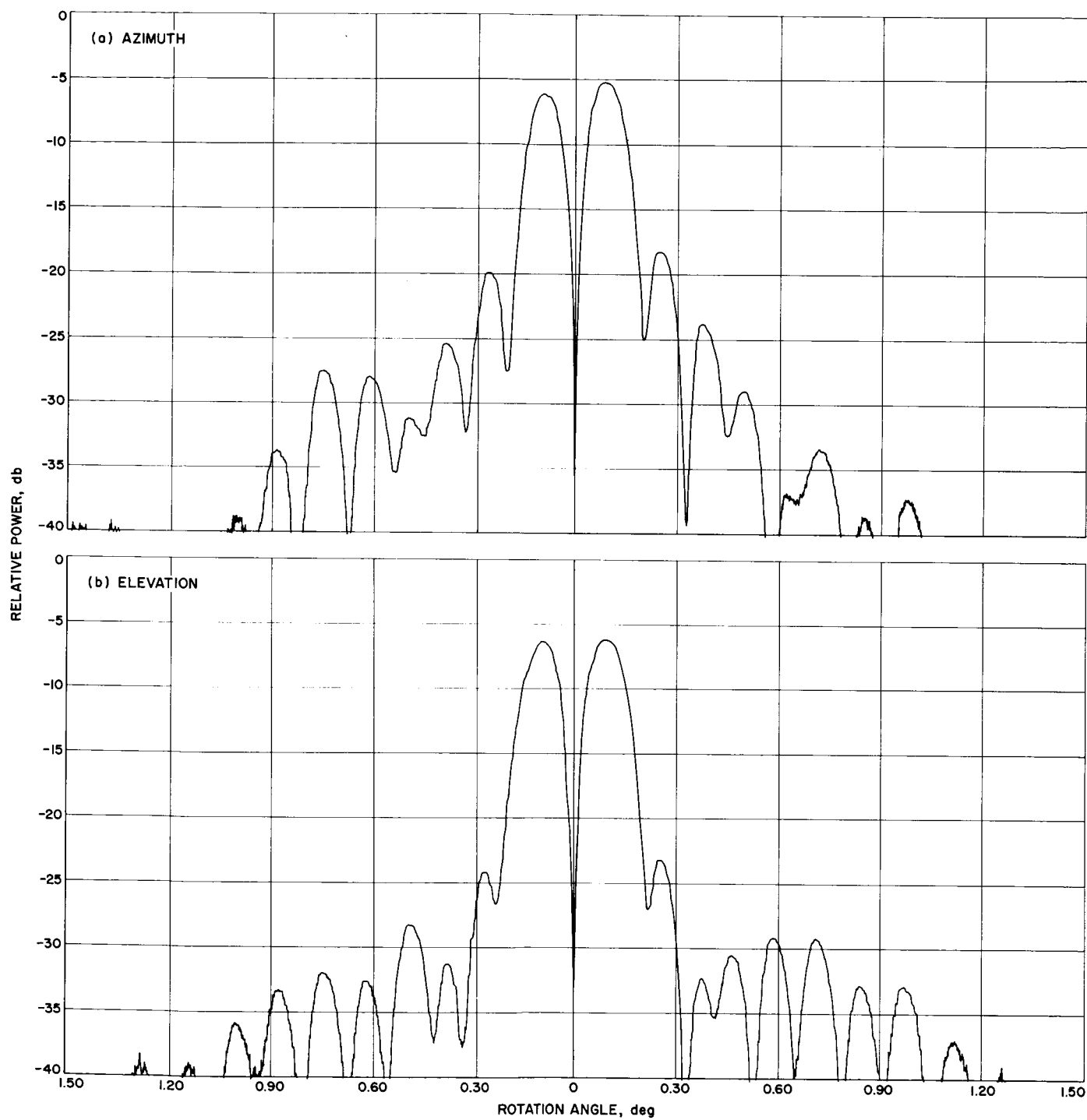


Fig. 27. AAS model, tracking feed, E-plane error channel azimuth and elevation patterns

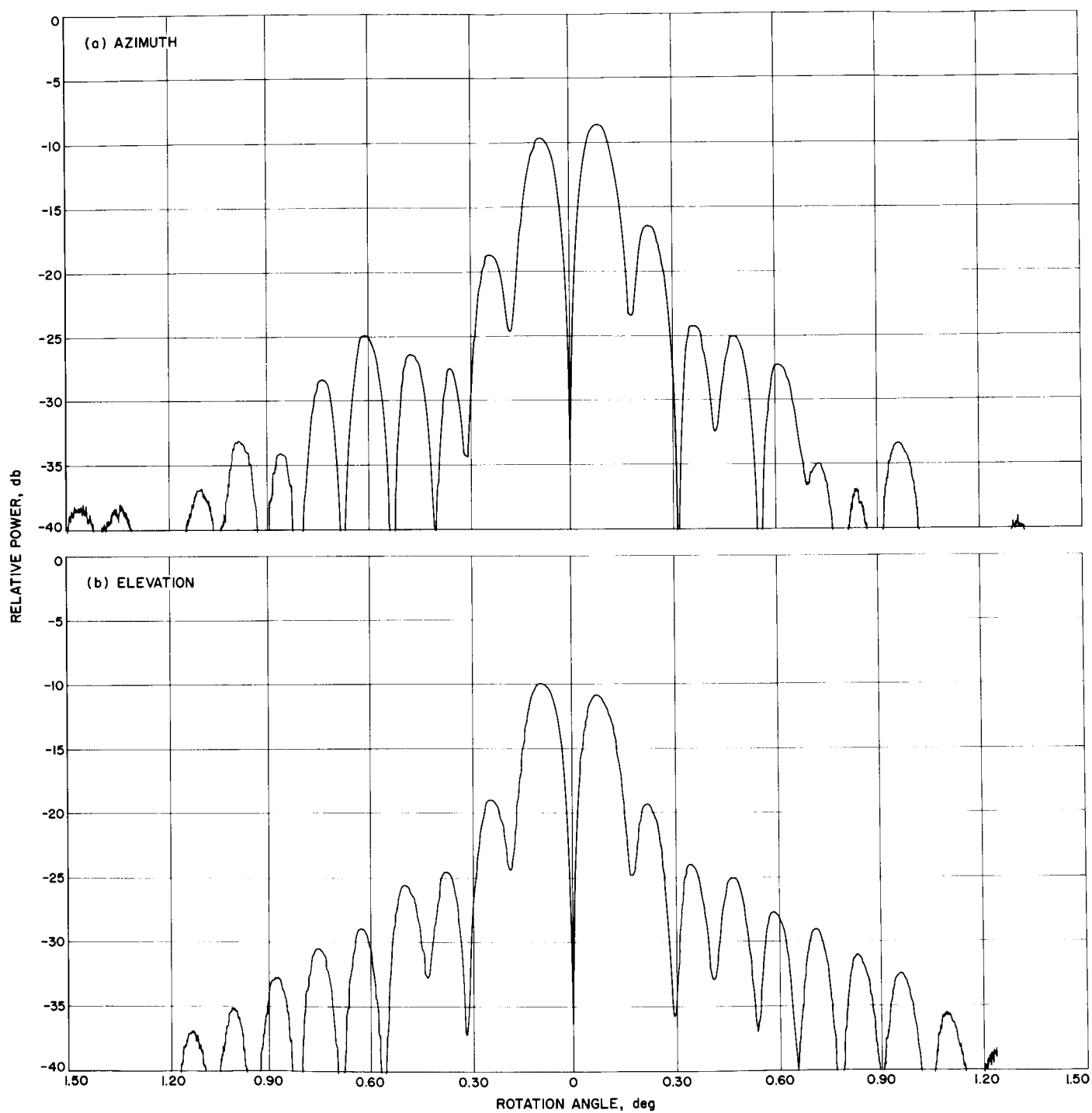


Fig. 28. AAS model, tracking feed H-plane error channel azimuth and elevation patterns



Fig. 29. Tiefert Mountain 48-in. paraboloid and gain standard

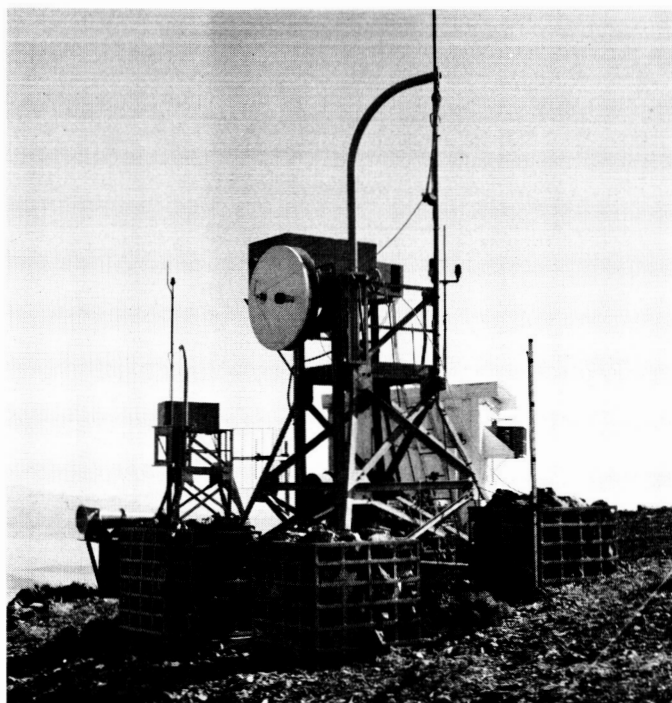


Fig. 30. Tiefert Mountain 48-in. paraboloid tower

All patterns presented were obtained using a tuned bolometer mount with an on-axis power level of -8 dbm. Frequent checks of bolometer linearity were made using a precision rotary vane attenuator at the Tiefert Mountain collimation tower. Peak nonlinearities for the entire system were less than 0.5 db. The Tiefert Mountain equipment has been described (*SPS 37-34*, Vol. III, p. 9); Figs. 29 and 30 show the 48-in. diameter illuminator paraboloid used. Also shown in Fig. 29 is the dual mode reference horn used during the previously reported gain calibration.

F. Goldstone Computer Facility

The Goldstone Computer Facility is a digital data processing center located at the Goldstone Space Communications Station. The basic functions of the facility (*SPS 37-30*, Vol. III, p. 17) are: reduction and analysis of tracking data; the making of pre- and post-flight calibrations; and the conducting of performance studies on improved tracking data monitoring techniques. To meet the growing work load in these areas, the Scientific Data System (SDS) 920 digital computer was replaced recently with a more advanced SDS 930 computer.

The SDS 930 computer is a high-speed, general-purpose digital computer. The main frame consists of 5 racks which contain 8192 24-bit words of core storage, 16 priority interrupts, power supplies, and time-multiplexed communication channels. The memory cycle time is $1.75 \mu\text{sec}$. Fig. 31 shows the basic SDS 930 computer with some of its peripheral equipment; Fig. 32 shows the control panel.

Basic peripheral equipment (Figs. 33 and 34) includes a 60-character/sec paper tape punch, a 300-character/sec paper tape reader, and a 10-character/sec teleprinter. These devices are common to most medium-sized computer systems and provide a means for loading and controlling the operating programs.

Additional peripheral equipment provided on this computer system for bulk input and output (Figs. 31, 35, and 36) are four magnetic tape transports, a line printer, and an IBM card reader-punch. The magnetic tape units are IBM compatible and will operate at 15, 41, or 60 kc. This corresponds to packing densities of 200, 556, or 800 bits/in. The line printer operates at 300 lines/min with



Fig. 31. SDS 930 computer with peripheral equipment

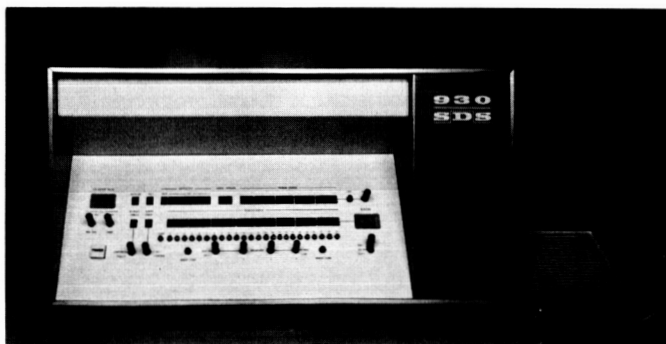


Fig. 32. SDS 930 control panel

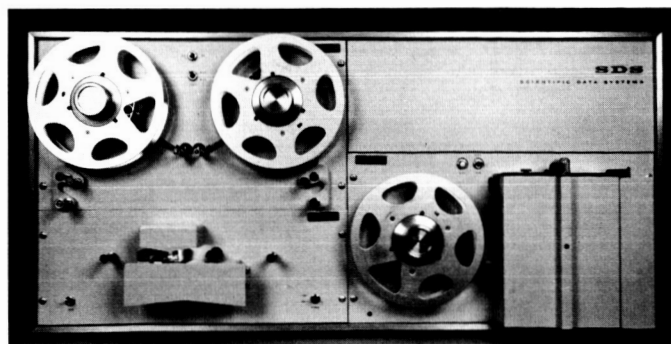


Fig. 33. Paper tape reader and punch

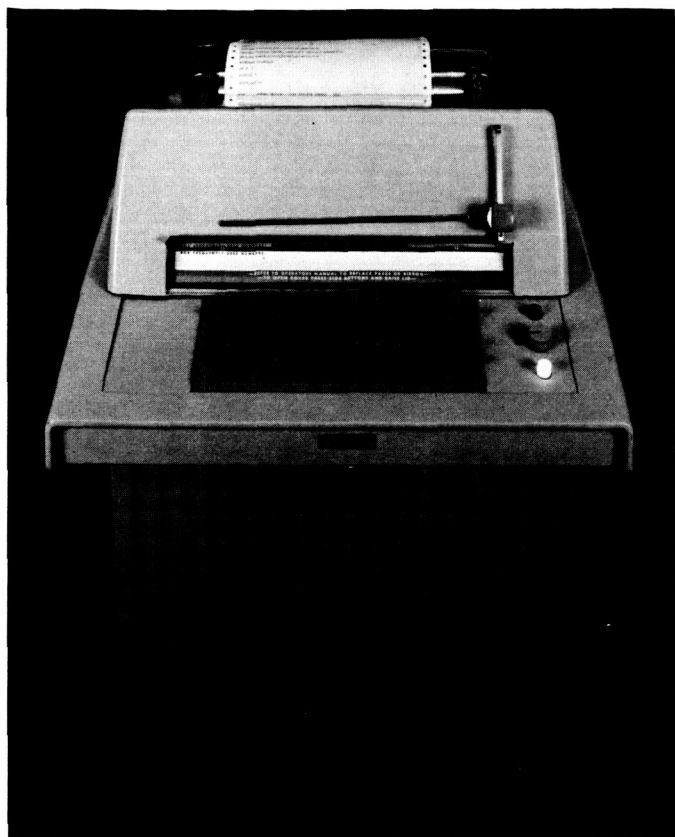


Fig. 34. Teleprinter

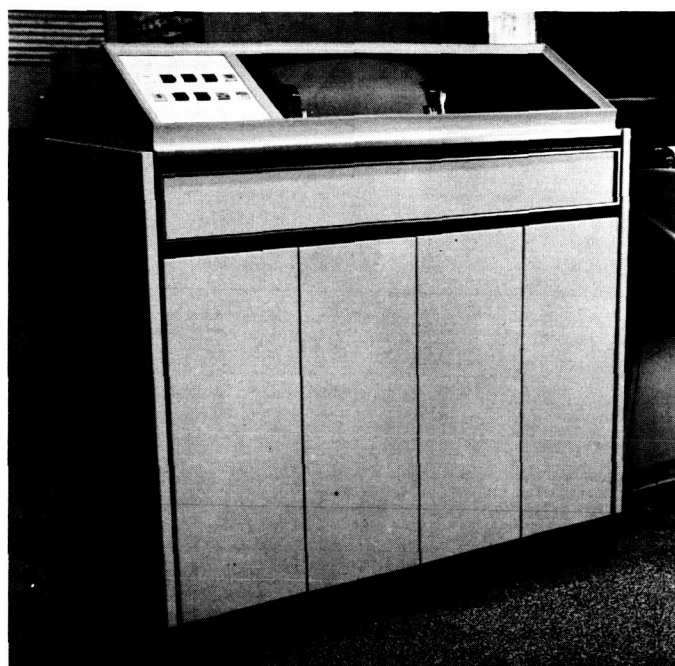


Fig. 35. Line printer



Fig. 36. IBM 1622 card reader-punch

a line width of 132 characters. The IBM card reader-punch will read IBM cards at 250/min and will punch at 125/min. Two channels for special input-output are provided, allowing direct input of teletype information and direct output of plotter data to a Benson-Lehner point plotter.

G. Spacecraft Visibility Program With Plotter Output

A program which will calculate and plot the range of visibility of DSIF antennas has been developed by the Systems Data Analysis group at JPL. When the location, type of antenna, and spacecraft altitude are known, a plot made on a Mercator map of the world will show how far away the spacecraft can be seen. The program is capable of calculating for any existing antenna at any location and, in addition, can handle any theoretical antenna and location.

The necessary input parameters are the type of antenna, the location of the antenna (longitude and latitude), the horizon mask, the antenna limits, and the altitude of the spacecraft.

In the DSIF there are two types of antennas utilizing two different coordinate systems: Az-El and HA-Dec. Az-El is azimuth and elevation, or local coordinates.

Azimuth is the angle from local north in a plane parallel to the Earth's surface to the antenna position. Elevation is the angle measured up from the local plane. HA-Dec is hour angle and declination with one axis of the antenna pointing true north (parallel to the Earth's axis). Hour angle is the angle measured in a plane parallel with the Earth's equator, and declination is measured from this plane. HA-Dec coordinates have the advantage of being

easily converted to Earth coordinates, greatly simplifying relations between coordinates of stations at different locations, but have the disadvantage of imposing structural limitations on the visibility of the antenna.

At Goldstone the 85-ft Echo and Pioneer antennas are HA-Dec, whereas the 85-ft Venus and the new 210-ft Mars antennas are Az-El. A stereographic projection

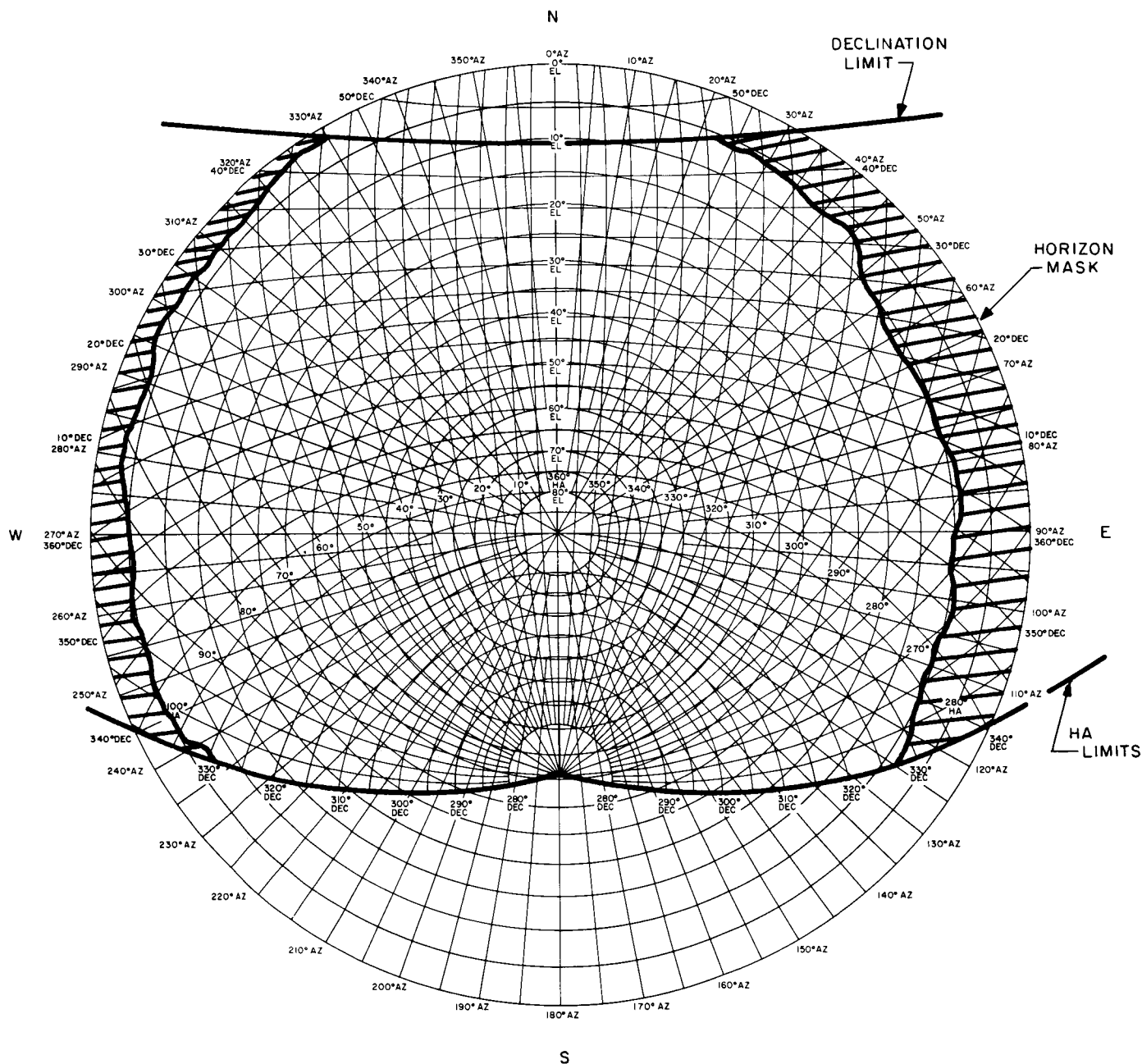


Fig. 37. Stereographic projection of Az-El and HA-Dec coordinates

(Fig. 37) of these coordinates (which is different for each location) aids in visualization of these coordinate systems.

The horizon mask is the configuration of the local horizon which blocks the view of the antenna. This mask is shown on the stereographic projection. There are usually gaps in the horizon mask data, and to fill these gaps and to work for an antenna where the mask is unknown or nonexistent, the program can generate its own theoretical horizon.

The antenna limits are mechanical restrictions on the antenna. In HA-Dec antennas there is a major hour angle and a major declination limit. The HA limit is most often at 90 and 270 deg. The HA and Dec limits are both visible on the stereographic projection.

The Spacecraft Visibility Program is written in FORTRAN II for the SDS 930 computer at Goldstone. Input is by punched card. Digital output is on a line printer and visual output is on a Benson-Lehner, Model J electroplotter which has been converted by Systems Data Analysis personnel to on-line usage.

To operate the program, a minimum of four cards is input. The first card contains the number and the longitude and latitude of the station. The second card contains three indicators. The first indicator tells the program whether the antenna is Az-El or HA-Dec. The second tells whether a horizon mask will be given or whether the program should generate a theoretical horizon. The last indicator tells whether the antenna has the usual HA limit or whether the HA limit will be an input. The third

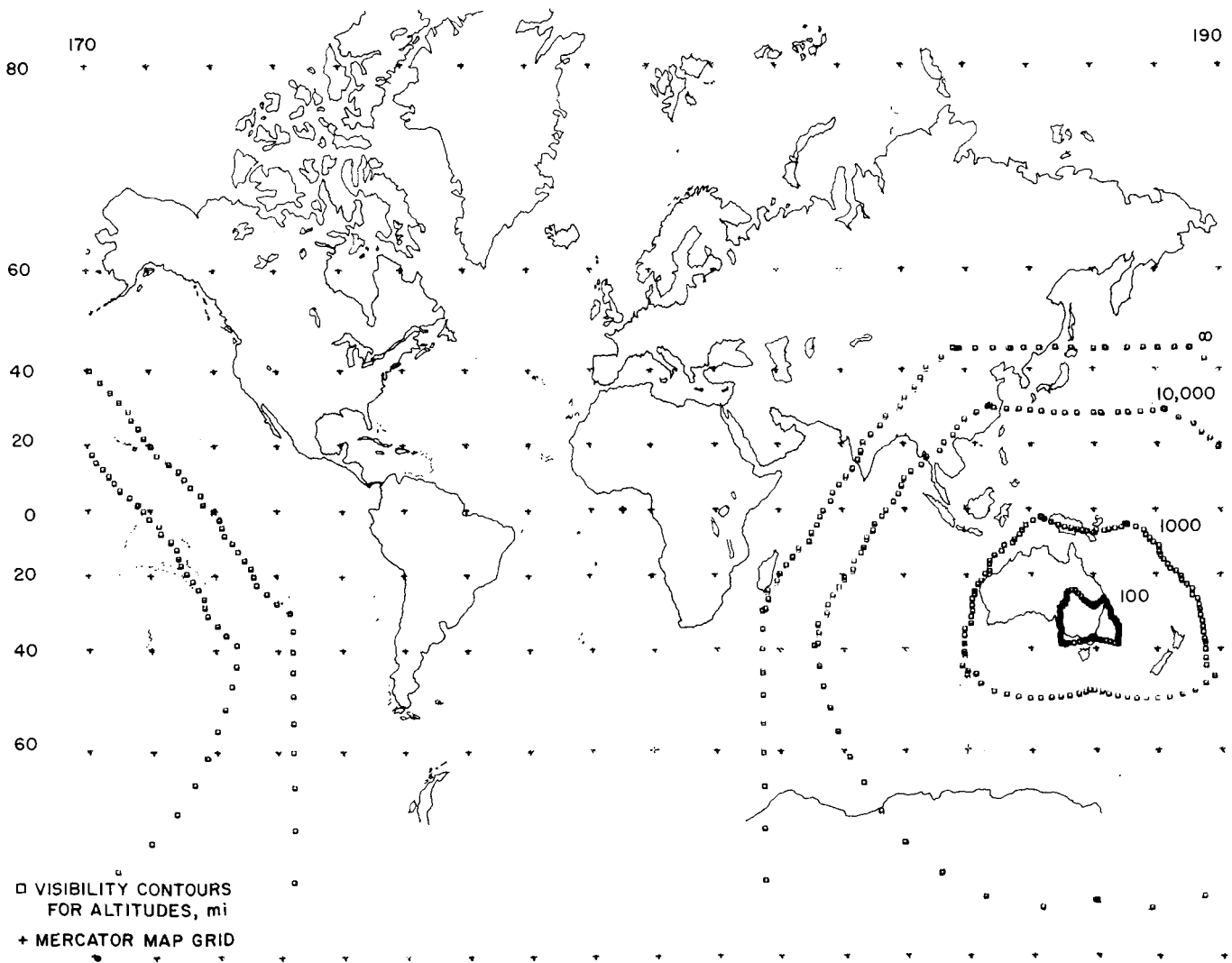


Fig. 38. Plot of antenna visibility at Tidbinbilla Station

card contains the spacecraft altitude. If called for, the next card is the HA limit, and the last card is the Dec limit. If a horizon mask is indicated, then a deck of the mask data follows the Dec limit card.

From this information, the program calculates local x, y, z coordinates from the internally generated (theoretical horizon) or externally given (horizon mask) Az-El or HA-Dec angles (which are the lowest possible viewing positions of the antenna). It then transforms these local x, y, z coordinates to an Earth-centered x, y, z system and from this calculates the longitude and latitude of the viewed spacecraft. Finally, the longitude and latitude are projected onto a Mercator world map of any scale, and plotted. Fig. 38 is an actual plot for the same station as the stereographic projection (Fig. 37).

On the plot, the squares are the visibility contours and the crosses are a Mercator map grid generated by the program. The result is converted easily to a reproducible

form eliminating long and tedious manual conversion of the data.

Plans for the program include producing separate overlays for each existing DSIF station. The overlays can be placed over readily available Mercator world maps and may be gathered for the stations which are to be used in a particular mission; total visibility is thus quickly pictured.

The flexibility of the program will allow visibility plots to be drawn to aid in evaluation of proposed antenna configurations and locations.

The program may be used with a preexisting program that plots satellite paths on a Mercator map to give quick indications of when a particular satellite will be in and out of view.

A simple internal change of one constant would allow the program to produce visibility plots for such antenna sites as a tracking station on the Moon.

Reference

1. Samulon, H. A., "Spectrum Analysis of Transient Response Curves," *Proceedings of the IRE*, Vol. 39, pp. 175-186, 1951.

III. Space Flight Operations Facility

A. Simulation Data Conversion Center

The Simulation Data Conversion Center (SDCC) of the Space Flight Operations Facility (SFOF) was developed to satisfy continuing DSN requirements for a means of realistically exercising the data handling elements of the space flight operations complex in support of lunar and planetary projects. The center is designed to expedite the implementation of an evolutionary testing philosophy whereby testing may proceed from the verification of individual computer programs and hardware subsystems and the training of operationally oriented analysis teams, through the interfacing of these various elements and the evaluation of resulting interactions, to the integration of the operation into a contiguous whole. Present capabilities include the pretest preparation of simulated spacecraft tracking and telemetry data, the playback of data during tests, and the coordination of test activities to enhance realism and ensure adherence to the test plan.

1. Phase I Development

Development of the center is proceeding in stages or phases, with Phase I being completed in August 1965. The Phase I SDCC is located on the second floor of the

SFOF and consists of: a small general purpose digital computer, the PDP-1, having special input-output capabilities; three FR 600 analog tape transports with record and playback electronics; a voice communications system interconnected to that of the SFOF; and facilities for preparation, reception, and transmission of data by teletype. In addition, special communications lines are provided to permit the insertion of data at points within the SFOF.

The PDP-1 digital computer is a parallel, binary arithmetic, general purpose machine having 8,192 18-bit words of addressable storage and a flexible 16-channel priority interrupt input-output system. Input-output devices currently installed include:

Combined input-output devices:

Automatic magnetic tape control with four Potter tape transports

Console typewriter

Input devices:

Burroughs card reader

60-word/min single-channel teletype input

300-character/sec paper tape reader

External incremental clock

Output devices:

8-channel, 60-word/min teletype

High-speed 300-line/min line printer

BRPE-11, paper tape punch at 60 character/sec

Parallel-to-serial output shift register with variable word length and bit rate, modulating selected VCOs

The priority interrupt, or sequence break, system expedites use of the PDP-1 computer in real-time applications by permitting input-output operations to take place concurrently with computing activities.

Input-output devices have been chosen which are suitable for directly driving the outgoing lines to the Communication Center or the Telemetry Processing Station in real-time, or in nonreal-time for the production of test data packages in the form of magnetic or punched paper tapes.

Analog magnetic tape recording and playback capabilities consist of three Ampex FR-600 tape transports with seven channel recording heads and electronics for processing recordings made in direct record or frequency modulation modes. The recorders are compatible with similar devices installed at the DSIF stations and are normally used in the generation of test tapes for remote playback.

Communication facilities consist of ten full duplex teletype circuits to the JPL Communications Center, linkage to the Goldstone wide-band microwave link, analog circuits to the Telemetry Processing Station, and interconnection to the SFOF operational voice communication system. Teletype hardware installed in the SDCC includes seven transmit-distributors, two receive-only page printers, a keyboard send-receive unit, and a tape reperfector. Timing of teletype transmission may be controlled by a programmable timer to simulate the periodic transmission of tracking data. There is considerable flexibility in the patching of the above equipment to any outgoing and incoming lines.

Additional peripheral equipment consists of an IBM 047/063 combination card punch-tape-to-card converter, time code generators, and selected Inter-Range Instrumentation Group standard frequency VCOs for the conversion of telemetry data to analog form.

The Phase I SDCC has been used extensively by the *Surveyor* Project in preparation for early missions. Ex-

perience gained in this use is currently being applied toward the development of a more advanced capability, designated SDCC Phase II.

2. Phase II Development

Phase II of the simulation data conversion is being designed to permit a more realistic real-time response, during mission tests, than is feasible in the Phase I center. Phase II will also incorporate a two-mission simulation capability. The latter feature will not only permit the concurrent control of two simultaneous mission tests, but will provide for testing and debugging of new simulation programs and the generation of data packages for remote station use.

To expedite the real-time response capability, the Phase II system will be organized into (1) an operations area containing the data handling hardware and operators, and (2) control areas from which the operation of mission tests may be controlled. Within a control area are consoles for monitoring and talking on the SFOF operational voice communications system and the closed circuit television system, and for monitoring and controlling operation of the SDCC operations area. Linkage between the operations area and the controllers will be accomplished using an automated system which permits the formatting and transmission of data from the operations area to be controlled remotely from consoles located in the control areas. Functionally, the system will be divided into subsystems which simulate activities within a space flight operation. Specifically, these systems are: spacecraft simulator, DSIF simulator, and NASCOM simulator.

3. Spacecraft Simulator System

The spacecraft simulator system will simulate data normally telemetered by a spacecraft during a mission; it is composed of four subsystems:

- (1) Telemetry data profile
- (2) Spacecraft commutator
- (3) Signal generator
- (4) Command perturbation

The telemetry data profile subsystem provides a source of data simulating the engineering and scientific measurements on board a spacecraft which are telemetered to Earth. Normally, this will consist of an off-line generated digital magnetic tape containing time-data pairs for all

telemetry measurements, and will thus reflect a pre-planned mission profile. Real-time control of the profile tape is afforded by monitoring and control sections on the control area consoles. These devices provide the operator with a real-time indication of the input data content, and with the option of either stopping the profile tape or seeking other locations on it. In addition, capability is provided for preempting selected telemetry values and substituting new ones of the operator's choosing.

The spacecraft commutator subsystem will simulate the function performed by the spacecraft on-board data encoder by sampling the input tape values at appropriate intervals and releasing the telemetry data in a commutated form peculiar to the spacecraft being simulated. Data mode and rate controls will provide the option of changing these parameters in real-time as required.

The signal generator subsystem will simulate the functions performed by the spacecraft signal conditioning and communications system. This system will accept the digital output of the spacecraft commutator subsystem.

The command and perturbation subsystem will simulate telemetry data reflecting the spacecraft's response to real-time commands transmitted by the DSIF. This subsystem will permit, through requests entered from the control consoles, measurement values to be generated other than those initially canned on the profile tape. Additionally, it will permit real-time spacecraft failure modes to be initiated which were not previously programmed.

4. DSIF Simulator System

The DSIF simulator system will simulate the functions performed by the DSIF stations, during a mission, that are reflected within the SFOF operation. To accomplish this, the simulator system is composed of eight major subsystems:

- (1) Receiver
- (2) Telemetry data recovery
- (3) On-site data processing
- (4) Telemetry data recording
- (5) Trajectory data profile
- (6) Tracking data handling
- (7) Transmitter
- (8) Administrative data generation

The receiving simulator subsystem provides operator control over the receiver lock status, signal strength, frequency and mode of operation.

The telemetry data recovery subsystem simulates the functions performed by the telemetry recovery equipment at the DSIF stations, i.e., discriminators, demodulators, and decommutators. The reason for simulating these functions is to provide data degradation due to faulty equipment performance.

The on-site data processing subsystem will simulate the functions performed by the DSIF SDS 910 and 920 computers. This subsystem will accept the output of the telemetry data recovery subsystem, decommutate and identify the data, and output selected data formats for teletype or high speed data line transmission to the SFOF. In addition, this subsystem will be capable of accepting teletype format command messages generated by the SFOF and generating command verification messages in return.

The telemetry data recording subsystem will record the output of the telemetry data recovery subsystem in a manner consistent with DSIF station playback capabilities.

The trajectory data profile will be similar to the telemetry data profile, i.e., it will be an off-line prepared digital tape containing tracking data which reflects a preplanned trajectory for the spacecraft.

The tracking data handling subsystem will permit control over the following characteristics of the tracking data:

- (1) Sample interval and averaging time
- (2) Data condition codes
- (3) Data quality
- (4) Doppler type
- (5) Two-way lock status
- (6) Data format

The transmitter simulator subsystem will allow control of the simulation of transmitter power level and reference frequency.

The administrative data generation subsystem will simulate the DSIF stations' facilities which are used to

communicate with the SFOF during a mission. This subsystem will be capable of accepting prepunched paper tape and generating teletype messages in real-time from keyboard entry. It also will accept voice inputs and route them through the NASCOM simulator system to the SFOF Communications Center.

5. NASCOM Simulator System

The NASCOM simulator system will simulate the functions performed by the worldwide NASCOM communications network during a space flight operation. It will consist functionally of two subsystems:

- (1) Circuit routing
- (2) Communications perturbation

The circuit routing subsystem will provide the capability to patch any output from the DSIF simulator system to any of the incoming circuits to the Communications Center. Operator control of the circuit routing subsystem will be provided by a patch board located on the operator's control panel. Output signals from the SDCC may be patched to any appropriate line at the discretion of the operator.

The communications perturbation subsystem will provide the capability to selectively degrade any output of the circuit routing subsystem in a manner simulating noise, character errors, fading, or ARQ (assured radio quality) action.

The Phase II SDCC is planned to be operational in late 1966, and is an integral part of the over-all DSN mission simulation system.

B. Mariner Master Data Library

Since August 1964, an active program has been under way for designing, developing, and implementing a system to produce a master library of all data received and recorded during the *Mariner* Mars 1964 mission. This master data library (MDL) will provide the best source of telemetry and tracking data received and recorded by the DSIF during the *Mariner* mission, as well as discrete DSIF instrumentation performance parameters.

The primary purpose of the MDL is to produce a history of the *Mariner* mission from which postflight analysis may be accomplished on the spacecraft's subsystems, the scientific payload, the spacecraft's trajectory, and the performance of the DSIF.

1. System Description

The over-all flow of telemetry and tracking data from the DSIF to the SFOF and its internal processing of this data are depicted in Figs. 1 and 2. To afford a more flexible and expedient access to data comprising the MDL, the system is categorized into three data groups: telemetry, tracking, and comment.

a. Telemetry data. The MDL telemetry data are a series of two types of digital recorded magnetic tapes which are generated by IBM 7094 computer programs: station master merge tapes, and composite master merge tapes.

Station master merge tapes. The station merge tapes are generated by the merge program for each Deep Space Station (DSS) and contain the "best" telemetry data and ground instrumentation performance parameters recorded during each station's pass. The best telemetry data available is derived from the three data sources processed: the demodulator input, the demodulator output, and the teletype encoder output. The selection of the data source is made by the merge program, based upon the data quality and continuity of each of the data streams within a recorded source.

Composite master merge tapes. The composite merge tapes which are also generated by the merge program contain a continuous and sequential stream of the best telemetry data derived from the composite of DSIF stations receiving and recording telemetry data (station master merge tapes) during each day of the *Mariner IV* mission. The overlap of telemetry data between DSIF stations is eliminated by data source selection based upon data quality and continuity of each recorded source. The ground instrumentation performance parameters are not contained on these tapes.

b. Tracking data. The MDL tracking data are developed from both real- and nonreal-time data. Real-time data (data sampled at low rates only) are received from the DSIF stations via teletype communications into the SFOF and processed through the data processing system (DPS) in real-time. Nonreal-time data (data sampled at

both low and high rates) are received from the DSIF stations and are also processed through the DPS. Both real- and nonreal-time tracking data are maintained on digital recorded magnetic tapes in formats compatible with the tracking data processor (TDP) program and orbit data generator (ODG) program, which are in themselves user programs. The raw tracking data as recorded on teletype paper tapes are maintained as part of the MDL.

duplicates become the real-time tracking data input to the MDL.

c. Comment data. To explain peculiarities and/or anomalies which occur in both the telemetry and tracking data tables, the supporting flight operations logs and MDL processing logs are maintained in the comment data table which is recorded on microfilm. The flight operations logs consist of the space flight operations log

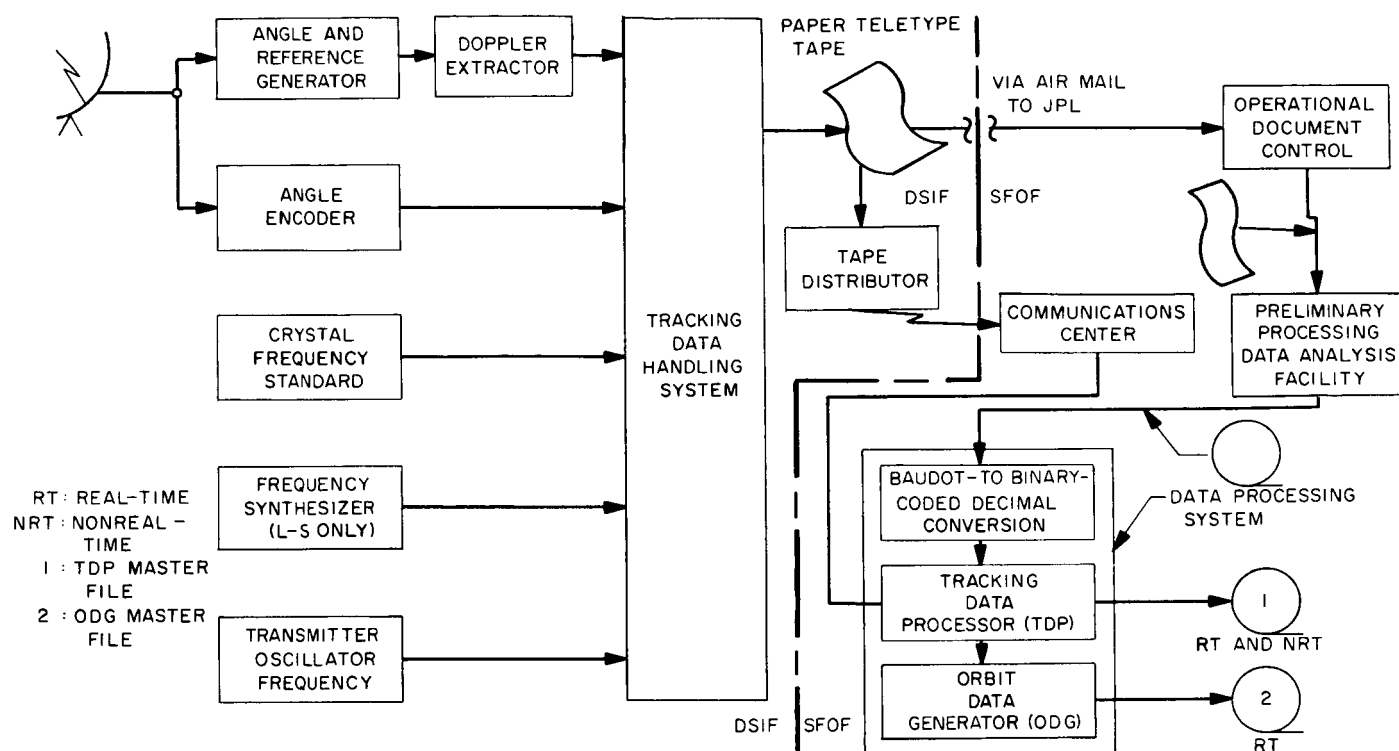


Fig. 2. Tracking data flow for real-time operations and master data library

and the DSIF operations log from each DSS. The history of the MDL processing is contained in the MDL data processing logs and the actual telemetry and tracking data which are printed in tabular outputs. Each type of operations log, MDL data processing log, or tabulated output is maintained on separate positive microfilm records providing convenient reproduction and access by users.

2. Facilities

The areas-facilities and their related functions required to develop and produce the MDL are described here.

a. Deep Space Instrumentation Facility (DSIF). The DSIF performs the following functions:

- (1) Recording-telemetry (magnetic recording and teletype) and tracking (teletype only)
- (2) Quality control (magnetic tape recording verification)

b. Space Flight Operations Facility (SFOF). The following facilities and functions within the SFOF are utilized to produce the MDL.

Operational document control (ODC). All data packages from each DSS are received by ODC, checked, and logged in. Telemetry magnetic and paper tapes are forwarded to the telemetry processing station (TPS) for processing; tracking data is forwarded to the Data Analysis Facility; and comment data is processed by ODC which maintains data files of all raw data, including DSIF recorded magnetic and telemetry paper tapes (telemetry and tracking) received from each DSS. The MDL master files for the three data groups are maintained in this area.

Telemetry processing station (TPS). The TPS provides a controlled environment for the postflight retrieval of telemetry data from magnetic and telemetry tapes which have been received from ODC. The magnetic tapes are processed by the analog tapes stack program which time-tags and reformats the data to be IBM-compatible and the teletype tapes are processed by the teletype tape stack program which also reformats the data to be IBM-compatible. In general, the TPS performs these primary functions:

- (1) Converts telemetry data received in analog, digital, and composite subcarrier form to a 36-bit word format that is time-identified and compatible with IBM system requirements.

- (2) Converts telemetry data on paper tape to magnetic digital tapes in a 36-bit format compatible with IBM system requirements.

Data processing system (DPS). The DPS provides the 7094 computer processing support required to develop the MDL in eight principal operations and/or programs: five are required for processing and evaluation of telemetry data, and three are required for processing tracking data. The 7094 computer programs used in preparing the MDL are:

TM EDIT	}	Telemetry data
TM REEDIT		
TM MERG		
Science lister		
Engineering lister		
TELPRT	}	Tracking data
TDP (tracking data processor program)		
ODG (orbit data generator program)		

TM EDIT

TM EDIT receives TPS stack tapes for each data source (i.e., predemodulation, postdemodulation, and teletype) and processes them into an edit tape. The data stream is grouped by spacecraft data frames and synchronized by pseudonoise sequence and frame count. Concurrently with the editing function, all data which cannot be successfully synchronized are formatted and printed on a bad data listing for off-line evaluation of the edit processing. The editor quality-flags each data frame and the summary of quality information is printed also on the bad data listing.

TM REEDIT

This program provides the capability to manually correct and reprocess the edited data to remove any data or processing anomalies. The program also provides for time-correcting each spacecraft data frame. The outputs of this program are the same as for the editor above.

TM MERG

This program receives TM EDIT, TM REEDIT, or TM MERG output tapes as inputs, and selects the best data from these tapes and merges these sources into a single telemetry master tape (either station or composite). The data source priority is predemodulation, postdemod-

ulation, and then teletype data. The level at which the merge is accomplished is at the data frame which is tagged as to its time, source, and quality. An on-line log is produced that provides summary and directory information for both the MDL station and composite telemetry master tapes.

Science lister and engineering lister programs

The science and engineering listers are production and quality monitoring programs used to produce complete tabular listings of science and engineering data for evaluation and for microfilm tabular records of all the MDL telemetry data which is recorded on magnetic tape in the telemetry data group.

Science lister

Data processed by the science lister, a TM EDIT and TM MERG option program, constructs a time-sequential record of all science data retrieved by MDL processing. The data is then decommutated and converted into science units and printed on a two-page tabular format.

Engineering lister

The engineering data concerning spacecraft performance is processed by this program which is a TM EDIT, TM REEDIT, and TM MERG option program. The data is decommutated to the engineering high-deck sync and converted into decimal number (DN) and printed in a tabular format.

TELPRT

The purpose of the TELPRT program is to convert Baudot-coded magnetic tapes to BCD-coded magnetic tapes.

Tracking data processor (TDP). The purpose of the TDP is to generate a master file of tracking data (data sampled at low and high rates) on magnetic tape which is format-compatible to the input requirements of the orbit data generator ODG program. In nonreal-time, BCD magnetic tapes from the TELPRT program are used as the input requirements to the TDP. The TDP outputs of a TDP master file and a tabular log printout listing the contents of the master file constitute the MDL tracking data file.

Orbit data generator (ODG). This program receives the TDP master file as its input and is used to process the tracking data pertinent to the orbit of the *Mariner IV* trajectory during real-time support of the mission operations.

IV. Communications Engineering Development

A. S-Band Implementation for DSIF

1. *Traveling Wave Maser (TWM) for DSIF*

Successful operation of all TWMs was achieved during the *Mariner* Mars 1964 encounter. A weekly reporting from the daily log of the pertinent pressures and temperatures in the closed cycle refrigerator (CCR) to JPL was required to optimize reliability and performance. During the encounter "vigil" the reports were received on a daily basis, and, whenever necessary, telephone conferences were established with the various station operators.

Graphs of the important data were plotted for each station on a continuing basis. These graphs proved to be surprisingly effective in diagnosing troubles and warning of impending failures. In addition to indicating such routine troubles as leaks in the gas system, the graphs were used to discern more subtle difficulties such as the cause of contamination in the Joule-Thompson (J-T) circuit.

Fig. 1 shows the flow diagram for the J-T expansion circuit. Important variables monitored were (1) the sup-

ply pressure, (2) J-T pressure, and (3) J-T flow rate. These three interdependent variables made it possible to determine whether oil or gas contaminants caused the J-T pressure to drop. A slow, gradual drop in this pressure usually indicated oil contamination in the J-T supply line; an abrupt drop in the J-T pressure indicated air contamination. The latter condition was remedied by warming the machine to 90–100°K and allowing the air to pass through the J-T valve. The system was then re-started with a liquid nitrogen trap in the helium supply line to remove the contaminants.

An interesting phenomenon noted in one system was a relaxation type of oscillation at the 4.4°K station. The temperature was observed to increase very slowly from 4.4 to 15°K; subsequently, the machine quickly cooled itself to 4.4°K and repeated the cycle. A plausible explanation for this phenomenon was that hydrogen gas contaminants froze at the J-T valve and blocked the gas flow. This caused the J-T stage to stop refrigerating until at 15°K the hydrogen was able to flow through and unblock the J-T valve. The problem was solved by replacing the gas cylinder and purging the system.

There have been no known failures in the electronic equipment associated with the maser subsystem.

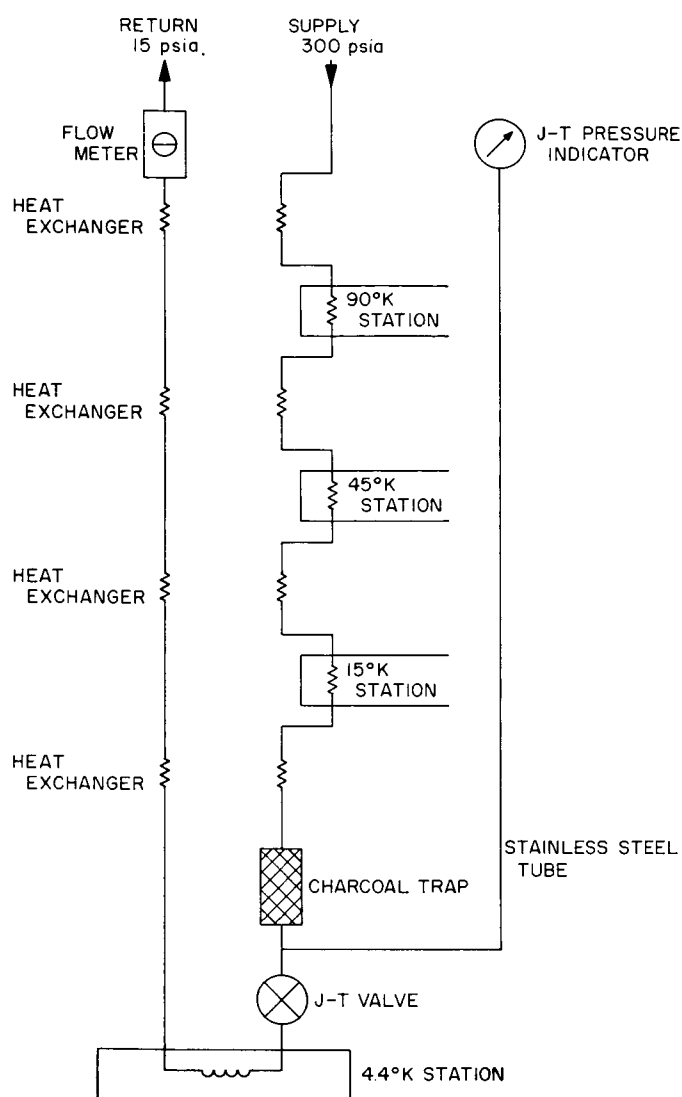


Fig. 1. Schematic flow diagram of J-T circuit in CCR

B. Ground Instrumentation for Mariner IV Occultation Experiment

The passage of the RF communication signal through the Martian atmosphere on July 15 produced a maximum perturbation on the received doppler frequency of approximately 6 cps in a total frequency of 2.3×10^9 cps. The duration of residuals in excess of 1 cps was less than 15 sec. Normally the DSIF tracking system can use long integration times to smooth and average data. However,

since the effects were small and the duration was short, normal operating equipment and procedures would not have given the results desired; therefore, special instrumentation was implemented.

By determining the difference between the measured frequency and the frequency computed on the basis of an orbit in free space (refractive index of unity), it is in principle possible to determine the refractive index profile of the Martian atmosphere. In addition to the required measurement of carrier frequency perturbation, received power as a function of time was also desired, so that Mars-induced Fresnel diffraction effects could be observed.

Fig. 2 is an over-all block diagram of the communication system used in the experiment.

The ground station used a rubidium frequency standard to drive a frequency synthesizer, which produced a signal of 23.411222 Mc. This signal was then modulated, multiplied 96 times in frequency, amplified, and transmitted to the spacecraft. The spacecraft radio system coherently translated the frequency and phase of the 2.11-Gc received signal by the ratio of 240:221, yielding a carrier frequency of approximately 2.297 Gc. When the spacecraft receiver was in lock with the uplink signal, the 2.297-Gc frequency was derived from the receiver's voltage controlled oscillator (VCO), which was phase-locked with the received signal. However, when no uplink signal was received, the signal was then derived from a free-running crystal oscillator in the spacecraft. The RF signal was amplified and transmitted from a high-gain spacecraft antenna.

The ground transmitter and receiver system employed an 85-ft parabolic antenna with a Cassegrainian simultaneous-lobing feed. The front end employed a TWM cooled by a closed cycle helium refrigerator operating at about 4.2°K. After amplification by the maser, the signal was split into two separate receiver channels. The first channel consisted of a triple-conversion phase-locked superheterodyne receiver which operated in the standard DSIF receiver configuration. This receiver's VCO was kept in phase synchronism with the received signal. By a series of frequency multiplications, divisions, and additions, the transmitter exciter frequency was coherently compared to the receiver VCO to obtain an output of the RF doppler frequency plus a 1-Mc bias. In order to reduce quantization errors, this resultant doppler frequency was multiplied by 8 before counting. The receiver automatic gain control (AGC), which is a received-signal

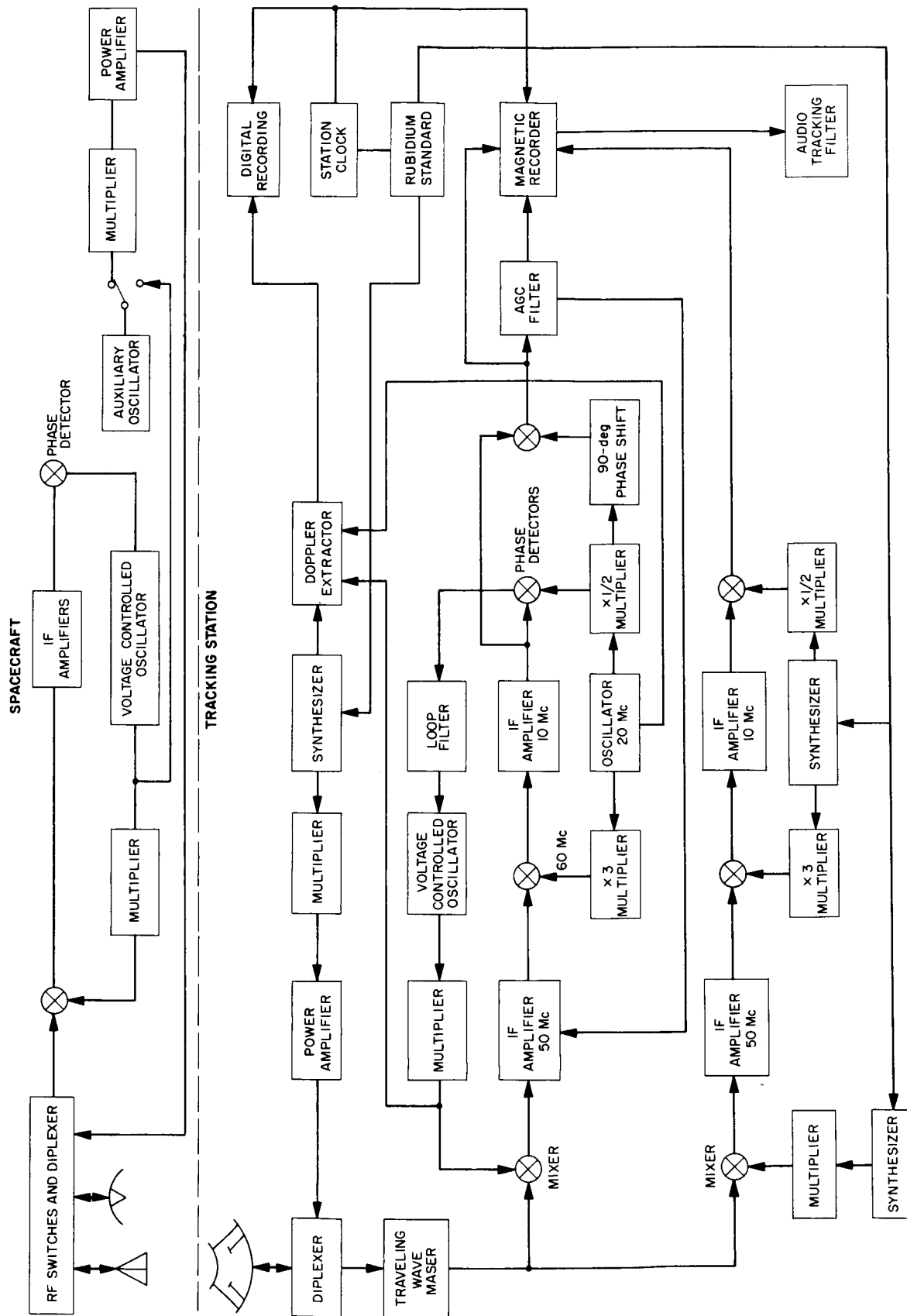


Fig. 2. Communications system for Mariner IV occultation experiment

power-level tracking servo, was used to determine received power level. Normally the static AGC voltage is used to determine received signal level. However, since the time constants in the static AGC were too great to measure the rapid power fluctuations expected, it was necessary to filter and record the dynamic AGC (SPS 37-30, Vol. III, pp. 34-35; SPS 37-33, Vol. III, pp. 32-37; SPS 37-34, Vol. III, pp. 41-44). The multiplied doppler output was counted and digitized in real time, and the AGC voltages were recorded on magnetic tape. This channel was also used as the sum channel of the pointing system for the simultaneous-lobing antenna.

The second receiver channel was a manually tuned constant gain, triple-conversion superheterodyne which operated in a nonstandard configuration. It simply amplified and frequency-translated the S-band input signal to the audio-frequency region of the spectrum and then recorded it on magnetic tape. The local oscillator (LO) signals for this receiver were derived from the rubidium frequency standard, which drove a pair of synthesizers. The first synthesizer produced a signal of 23.411222 Mc. This was multiplied by 96 to produce the first LO signal at approximately 2.245 Gc. This LO frequency was stepped to keep the signal in the receiver's pass band. The second and third LO signals were derived from the second synthesizer, operating at 19.996 Mc. The output of the third mixer had a pass band of 1-3 kc, which was recorded on magnetic tape. Since the frequency of the signal recorded on the tape was used to derive the doppler residuals, it was necessary to keep wow and flutter perturbations to a small fraction of a cycle. This was done by FM-recording a zero voltage on Track 2, FM-recording the signal voltage on Track 4, and direct-recording a 100-kc standard signal on Track 6. In reducing the data, Track 2 could be used as a voltage compensating correction, and Track 6 could be used as a time base correction for wow and flutter effect.

The data were reduced by digitizing the discriminated output of Track 4 while counting down the signal from Track 6 in a scaler and using it to trigger the analog-to-digital converter every 10^{-4} sec (referred to the tape time base). Track 1 used a subcarrier technique to record static and dynamic phase error and static and dynamic AGC. Track 3 was used to direct-record the output of the open loop receiver. Track 5 had the NASA 36-bit time code and Track 7 had voice labeling. The digitized signal information was first processed by running through a wide-band spectral analysis to roughly determine the frequency as a function of time. A narrow-band digital filtering technique was then employed to improve the

SNR and to reduce the number of points that were to be processed. These filtered data were analyzed using narrow-band power spectral density programs and a nonlinear sinusoidal least-squares fit.

Prior to occultation the spacecraft was in the two-way lock with the Pioneer Station. At 02:11:00 GMT July 15 the 1-sec cumulative count started, and the open loop receiver recorders were turned on. At 02:31:11 the signal was lost as *Mariner IV* was occulted by Mars. An additional 5 min of noise was obtained for later power calibrations. At 03:20 the recording was resumed and the signal level was detectable at 03:25:09 at the one-way crystal oscillator frequency. At 03:25:16 the received signal decreased by approximately 1 kc, indicating that the spacecraft receiver had acquired the signal transmitted from the Venus Station and had switched to its phase-locked VCO rather than the free-running auxiliary oscillator as a frequency source.

Fig. 3 shows a power spectral density plot of the open loop recorder for the time interval of 03:25:16 to 03:25:17. During this time the one-way signal (frequency translated to approximately 2.9 kc) stopped and two-way transmission started (1.19 kc). The telemetry sideband offset, ± 150 cps from the carrier, can clearly be seen.

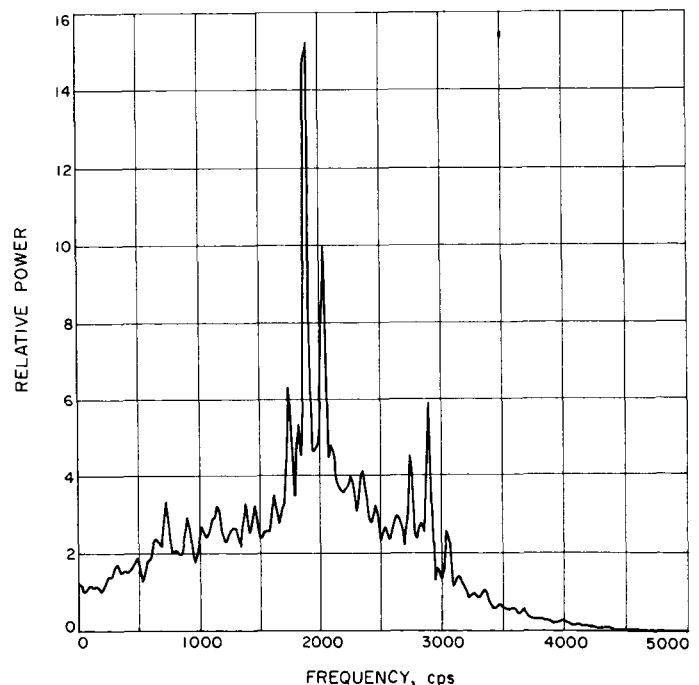


Fig. 3. Power spectrum of open loop received signal during one- to two-way signal switching

The reduction of the occultation data will be discussed further in SPS 37-35, Vol. IV.

C. Venus Station Mariner IV Encounter Receiver and X-Band Lunar Radar

1. Introduction

The *Mariner IV* project receiving capability at the Venus Station (SPS 37-33, Vol. III, pp. 58-62) has been

implemented to support the spacecraft telemetry reception and the occultation experiment during the Mars encounter. The X-band planetary radar receiver was adapted to provide simultaneous operation at this time to afford continuous support of the lunar mapping experiment during and after the *Mariner* project.

2. Instrumentation

The X-band system consists of an antenna-mounted X-band to 30-Mc converter (SPS 37-33, Vol. III, pp. 58-62), an X-band signal generator (SPS 37-34, Vol. III, p. 59), and control room portions of the Mod IV S- and X-band planetary radar receivers. Originally, the S- and X-band receivers shared operator controls, control room

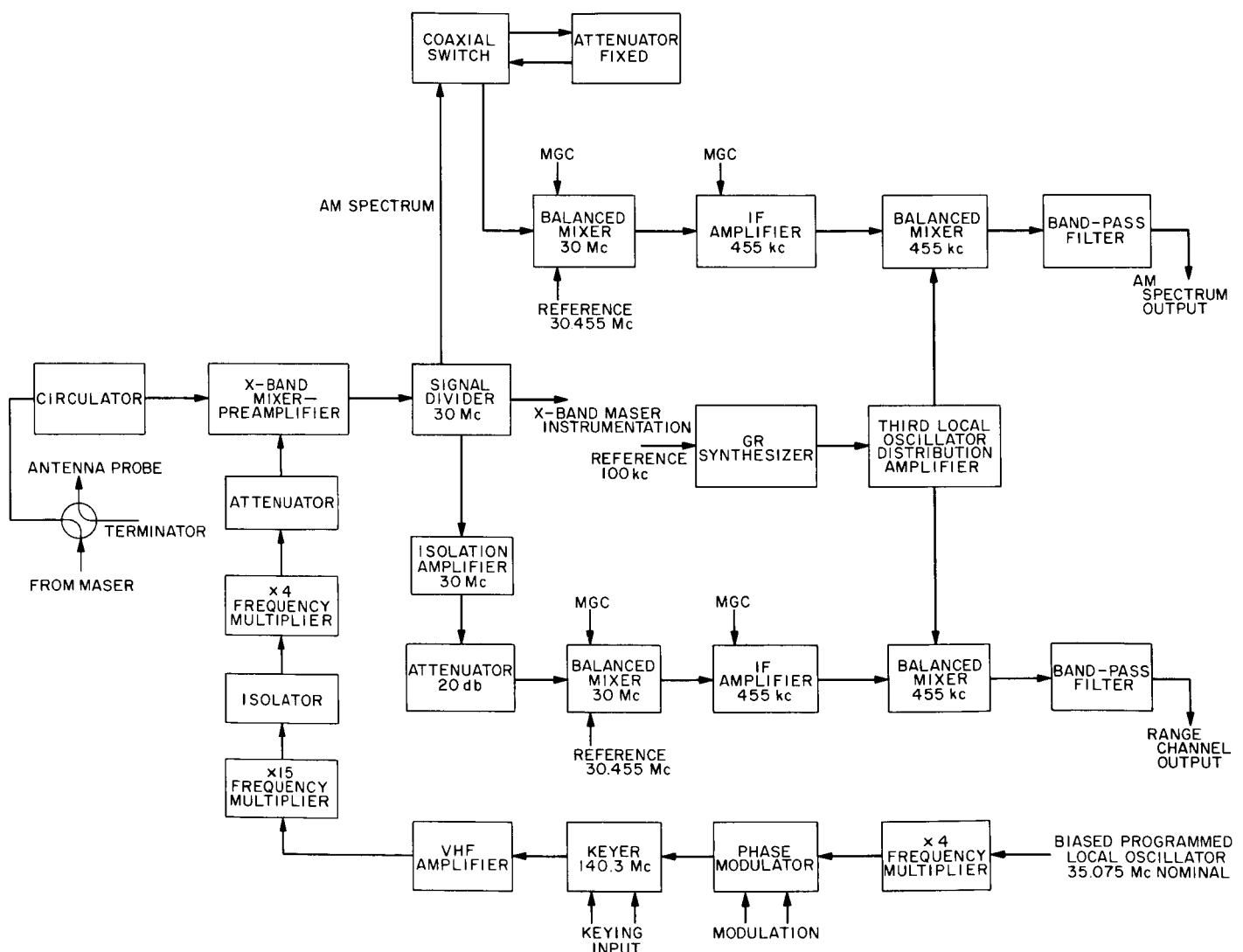


Fig. 4. X-band receiver

systems, and remote monitoring of antenna equipment. To completely separate operation of the X-band receiver from that of the S-band receiver, additional controls and monitoring were provided. The X-band modules were also regrouped so that all would be located in one cabinet. A General Radio (GR) frequency synthesizer was installed in the X-band system, replacing the free-running oscillator previously used as the third LO, in order to afford the experimenter greater system flexibility. (For example, long lead time is no longer needed for crystal procurement when the experiment calls for a change in frequency.) The GR synthesizer also increased stability and reduced the amount of time needed for precalibration, assuring more time for the actual experiment. (A com-

plete block diagram of the X-band system is shown in Fig. 4.)

Since it was necessary to provide a high degree of reliability as well as experiment flexibility needed to return quickly to R&D experiments, the *Mariner IV* encounter receiver required the addition of a one-bay rack to the Mod IV radar receiver (Fig. 5). Two vertical thermal stabilizing panels were installed in the lower portion of the cabinet to which all the RF modules were mounted (Fig. 6). The center of the cabinet contains all operator controls, including the Hewlett-Packard (H-P) frequency synthesizer. The upper half contains another aluminum thermal stabilizer, installed horizontally, to which the system DC power supplies are mounted.

The several modules that make up the receiver system dissipate a wide range of heat levels, and as radiated leakage (problems resulting from high-gain amplifiers

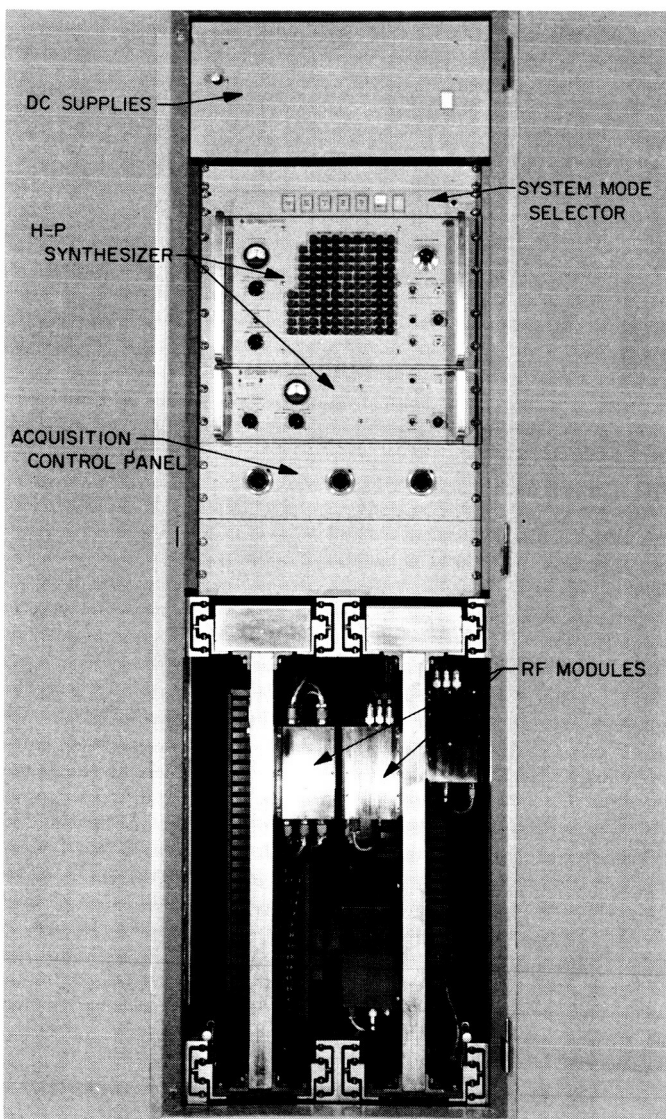


Fig. 5. *Mariner IV* encounter receiver subsystem

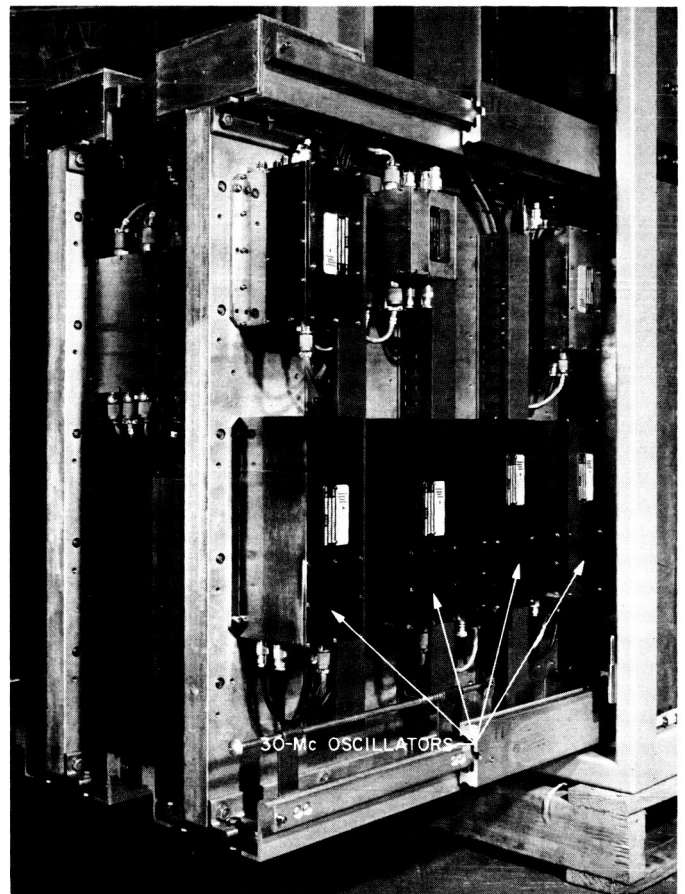


Fig. 6. *Mariner IV* encounter receiver subsystem (lower half)

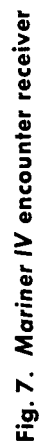


Fig. 7. Mariner IV encounter receiver

mounted near coherent high-level RF signals) dictates module layout, thermal stabilization is best obtained by flowing temperature-controlled water through the thermal stabilizers. This method of system temperature control completely eliminates internal system hot spots, and also improves system stability and reliability; e.g., equipment doors can be opened during operation with little effect on system temperature. Also, the removal of blowers used in conventional air cooling lowers the audio level in the control room, thus reducing operator fatigue during a mission.

The *Mariner* encounter receiver subsystem was assembled and tested at JPL using a special lab receiver which resembles the Venus Station Mod IV. The subsystem was then installed at the Venus Station and interconnected with Mod IV (Fig. 7).

3. Testing

The X-band system was subjected to a coherent leakage test by injecting a known amount of signal into the system and observing the spectrum on the amplitude modulated (AM) spectrum analysis channel. The signal was then removed, and the spectrum was observed again; the only leakage found was from the X-band signal generator mounted in the electronics cage of the 30-ft antenna. Since this signal generator had not yet been completely shielded, the test will be repeated upon completion of the generator.

The *Mariner IV* backup receiver was installed, and a previously calibrated signal generator in the *Mariner* cone was used to calibrate the AGC voltage. After a closed-loop check (involving the Pioneer Station), the *Mariner IV* backup receiver was locked to the spacecraft, and telemetry was sent to the Space Flight Operations Facility at JPL, completing on-site checkout of the receiver. Bendix operators were then provided with a short training course and necessary system documentation. Occultation support capabilities were not tested because of cancellation of Venus Station commitment.

4. Conclusion

With the exception of the work being done on the signal generator and the digital phase modulator development (SPS 37-31, Vol. III, pp. 54-56), the X-band system has met its requirements and is able to function without interference to or from the *Mariner* backup receiver. By successfully tracking *Mariner IV* for 3 days while the

Pioneer Station was undergoing maser maintenance, the *Mariner* backup receiver has proven its ability to perform its design function—that of receiving the spacecraft signals as backup to the DSN.

D. S-Band Receiver-Exciter System

1. Introduction

The functional description and preliminary characteristics of the DSN 1964 S-band RF receiver-exciter system were published in SPS 37-28, Vol. III, pp. 30-39. The

Table 1. Receiver-exciter System 17 test data

Item	Data	Specifications
Exciter:		
Power	35.3	35.5 \pm 1.5 dbm
RF bandwidth (-1 db)	13.5	10.0 Mc, minimum
Test output	5.4	7 \pm 3 dbm
Synthesizer loop response	(Fig. 8)	
Phase jitter (exciter and receiver in 2 B_{L_0} = 50 cps)	3-5 deg	7 deg RMS, maximum
Receiver:		
Threshold, cps 2 B_{L_0} = 50	-147 ^a -148 ^b	-146.8 \pm 0.0, -4.0 dbm
2 B_{L_0} = 200	-143 ^a -144 ^b	-140.8 \pm 0.0, -4.0 dbm
2 B_{L_0} = 700	-137 ^a -138 ^b	-134.5 \pm 0.0, -4.0 dbm
AGC characteristic response	(Fig. 9)	
RF loop response	(Fig. 10)	
CCTL response	(Fig. 11)	
Range receiver loop response	(Fig. 12)	
Detected phase modulated telemetry (wide band)	1.30	1.25 Mc, minimum (-1 db)
^a Receiver 1. ^b Receiver 2.		

first ten systems, called the Block I design, were fabricated as described. Performance data of a typical system of this design have been reported in SPS 37-32, Vol. III, pp. 10-13.

Beginning with System 11, the requirements of the Manned Space Flight Network (MSFN) were incorporated in the Block II design. The functional description and preliminary characteristics of this design are covered in SPS 37-33, Vol. III pp. 39-43. The Block II design includes not only the additional features required by the MSFN but also improvements in some of the marginal design areas which were discussed in SPS 37-32.

2. Receiver-Exciter Block II Performance

Some performance data from the final test of System 17 are included (Table 1 and Figs. 8-12) in order to show the results of the improved design and to present the Block II system data where the design differs from Block I. The primary design differences are loop noise bandwidths, thresholds, and telemetry bandwidths.

a. Exciter. With the cascade buffer amplifier, the output power is near the nominal level of 35.5 dbm, with a -1-db bandwidth greater than 10 Mc. The overshoot in the synthesizer loop has been eliminated (Fig. 8) by the removal of some of the RF filtering which affected

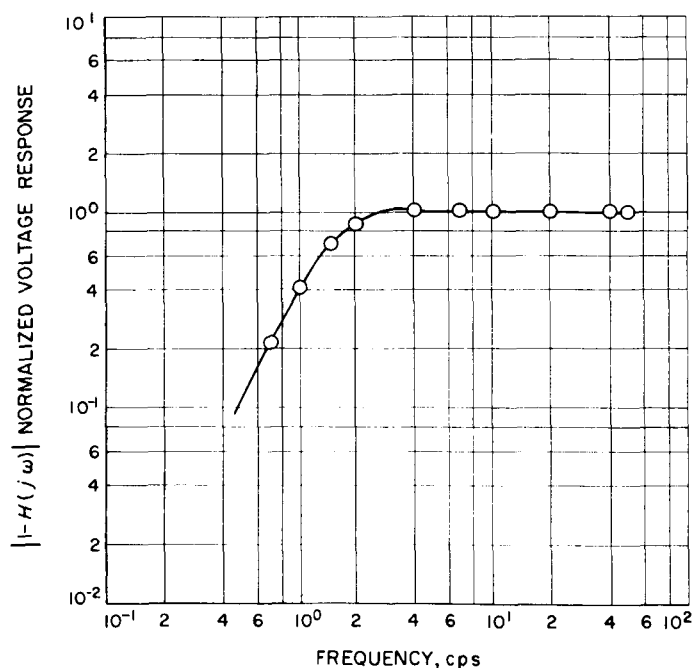


Fig. 8. Synthesizer loop frequency response

the loop filter time constants. The exciter phase jitter represents the high-gain wide-range VCO performance (SPS 37-34, Vol. III, pp. 48-54).

b. Receiver. The receiver response (Fig. 10) indicates some overshoot, particularly in the wide-band operation, which results from the phase characteristics of the predetection filter. The phase slope of this filter has been kept at a minimum value by using (1) the widest bandwidth filter compatible with the hardware design, and (2) a filter design with a minimum phase slope over the passband. Since the effect on system performance is negligible, no compensating network was added to counter the phase response of the predetection filter. In the range receiver, the overshoot is caused by an additional time constant in the VCO. Here again, the overshoot does not affect system performance. However, the VCO will be

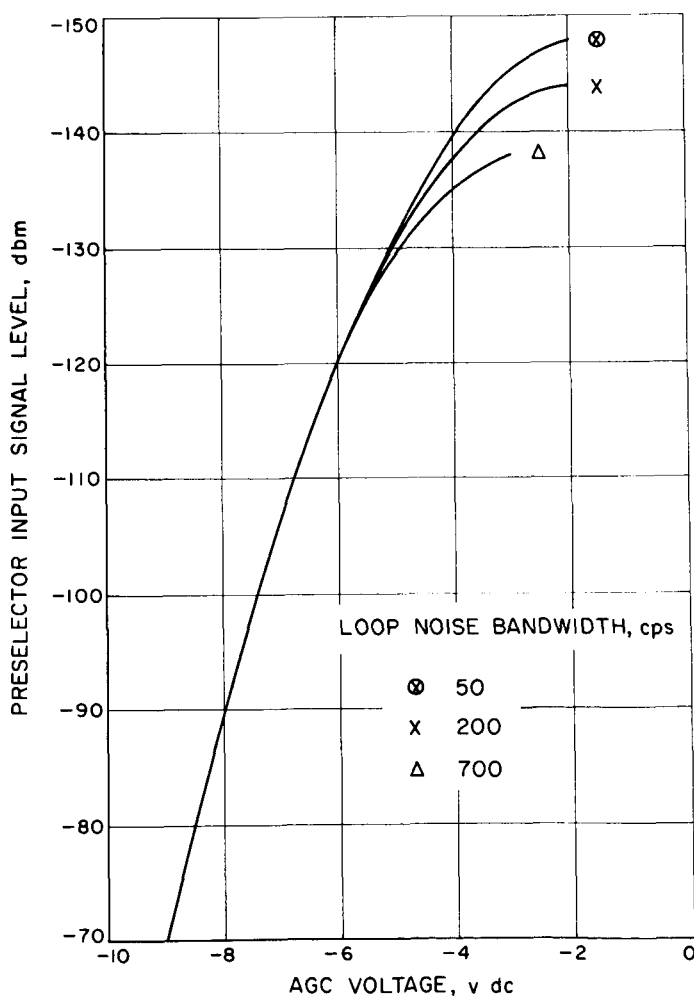


Fig. 9. AGC characteristics

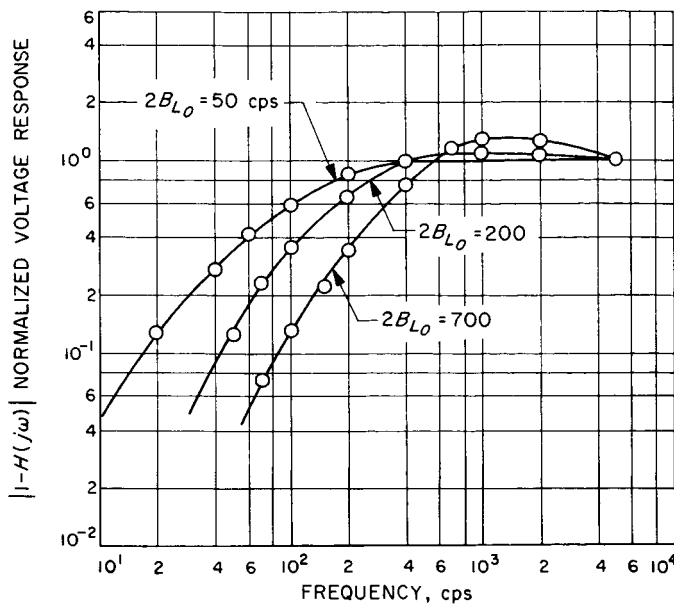


Fig. 10. RF loop frequency response

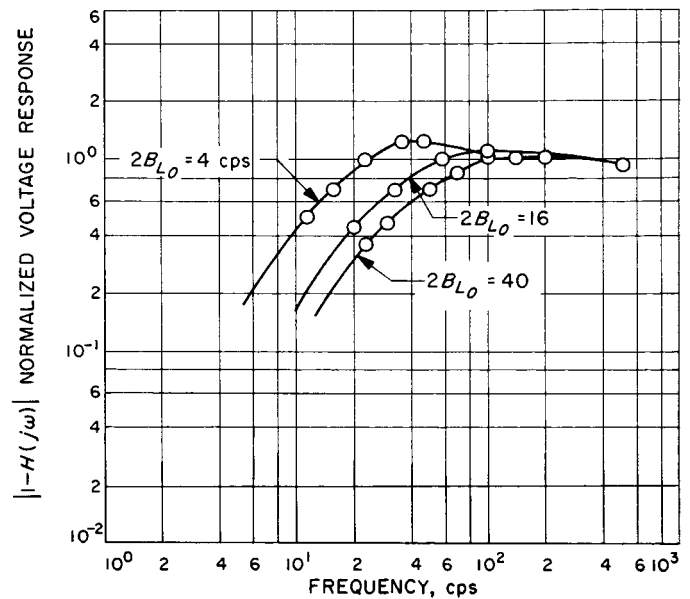
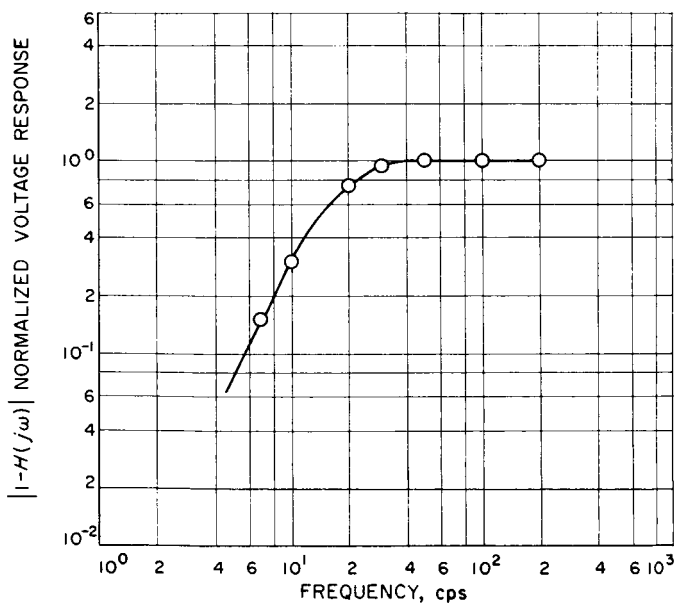


Fig. 12. Range receiver loop frequency response

Fig. 11. Code clock transfer loop (CCTL)
frequency response

modified at some time when it is convenient to incorporate this change in the network. The frequency response of the wide-band detected telemetry output has been increased to 1.25 Mc (-1 db) at the receiver output.

The Block II design, as now being produced, fulfills the MSFN requirements listed in SPS 37-33, Vol. III, pp. 39-43.

E. DSIF Test Signal Control Assembly (TSCA)

The complexity of the DSIF Tracking and Communication System necessitates integrated, accurate, reliable and convenient calibration and fault-finding instrumentation (SPS 37-28, Vol. III, pp. 29-39). To instrument such a program a number of provisions were designed into the basic RF circuitry to allow monitoring or injection of microwave test signals by means of the TSCA. The TSCA switching capabilities provide for remote selection of any of several microwave test signals and for application of the test signal to any of various test points within the receiver system. During a station countdown the TSCA becomes the control center for the reference RF and exciter signals. Calibration of the subsystems from the maser or parametric amplifier to the recording equipment is obtained by applying reference signals controlled by the TSCA.

The assembly is composed of a rack-mounted test signal control panel (TSCP), an antenna-mounted test signal control box (TSCB), and associated control cables. The TSCP is located in the parametric amplifier control rack 1043/UWV; the TSCB is located on the support structure of the high-gain antenna.

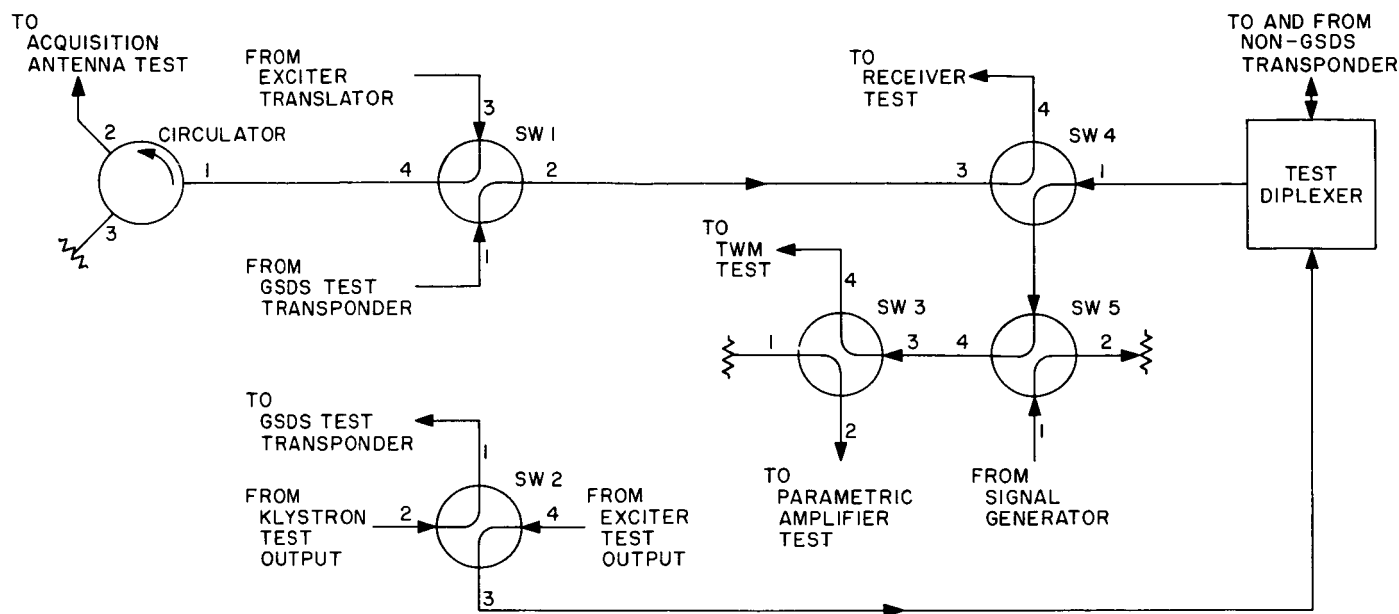


Fig. 13. Test signal control

The logic of the RF switching matrix (Fig. 13) was designed primarily to provide the following functional test conditions:

- (1) A path for connection of either the exciter translator or the GSDS transponder outputs to the input of the acquisition aid collimation tower, the receiver test, the parametric amplifier, or the maser.
- (2) A means of applying the output of the signal generator to the parametric amplifier or the maser inputs.
- (3) A diplexed connection of the non-GSDS transponder output with the input of the parametric amplifier, the maser, or the receiver test.
- (4) A connection of the klystron tests or the transmitter exciter outputs to the input of either the GSDS transponder or the non-GSDS transponder.

Test signal control box. The TSCB (Fig. 14) is a weather-sealed enclosure with 11 coaxial Type N jacks and three multiconductor plugs. The TSCB contains five remotely controlled Type N coaxial transfer switches, a circulator, a diplexer, three RF terminations, connecting coaxial cables, and a wiring harness. The RF characteristics are very broad band for all circuits except the acquisition aid collimation tower circuit which includes a circulator, and the non-GSDS transponder circuit which

includes a diplexer. Typical insertion losses and VSWRs at the receiver frequency, 2295 Mc, are:

Input	Output	Insertion, db	VSWR
Exciter translator	Acquisition aid	0.7	1.18
GSDS transponder	Receiver test	0.4	1.14
Signal generator	Parametric amplifier test	0.5	1.08
Non-GSDS transponder	Maser test	1.1	1.07

The electrical characteristics of the circuits designed for the transmitted frequency, 2113 Mc, are represented as:

Input	Output	Insertion, db	VSWR
Klystron test	GSDS transponder	0.30	1.04
Exciter test	Non-GSDS transponder	0.85	1.21

Throughout the TSCA, isolations between adjacent RF paths are at least 60 db. The transmitter frequency level is down 60 db at the receiver port of the diplexer. The

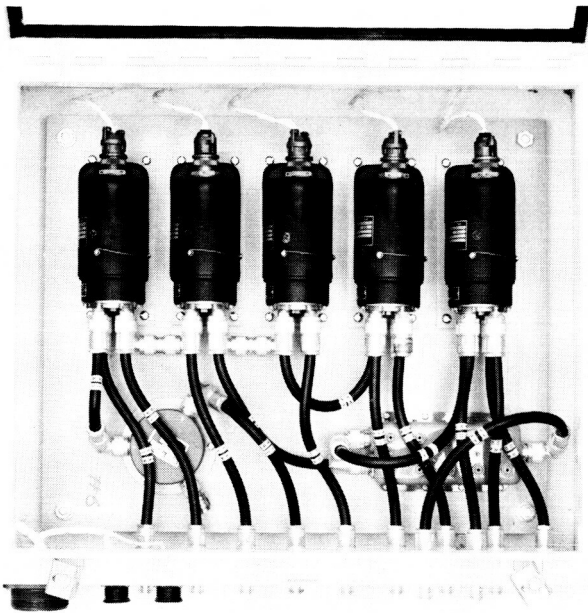


Fig. 14. TSCB interior

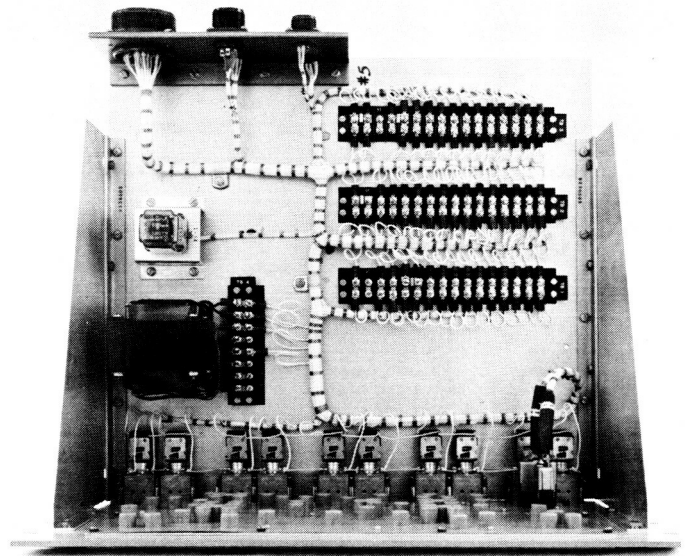


Fig. 16. TSCP top view

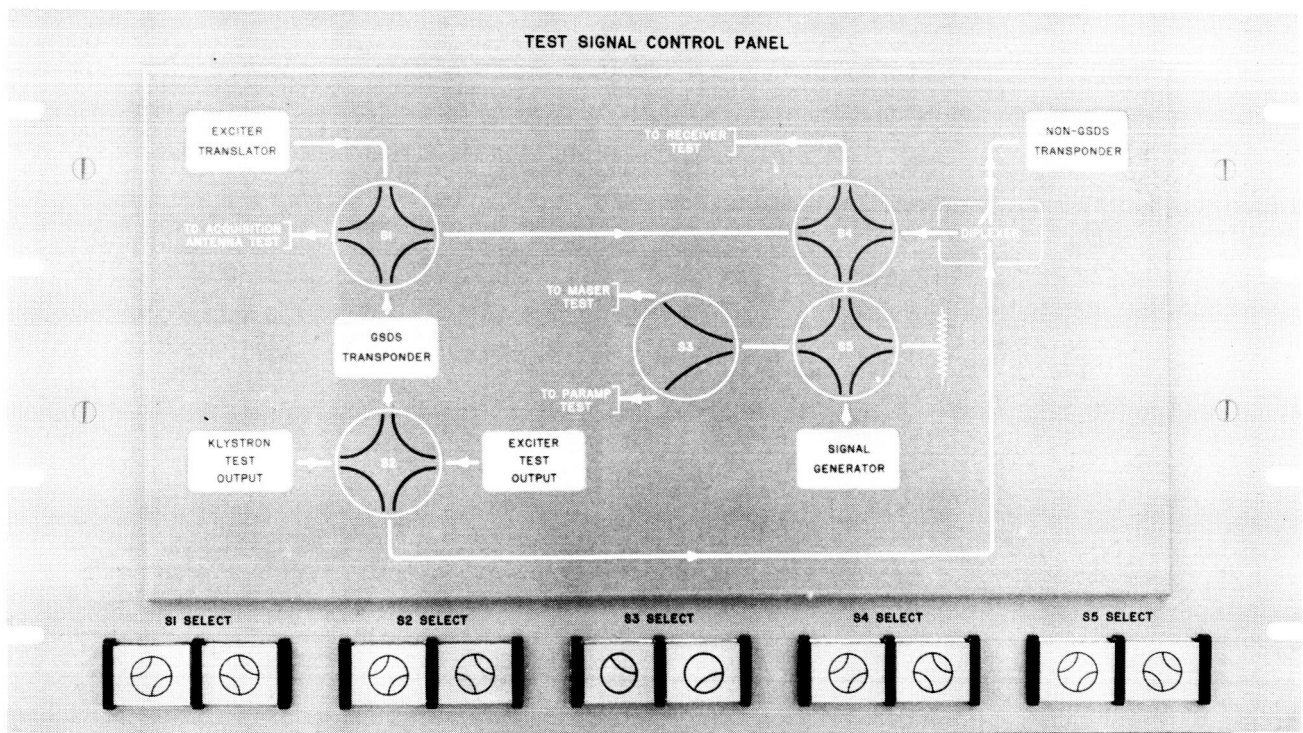


Fig. 15. TSCP front view

acquisition aid collimation tower circuit has a three-port circulator to furnish approximately 25-db isolation of any spurious signals received by the acquisition aid collimation tower antenna near the transmitter frequency.

Test signal control panel. The TSCP (Figs. 15 and 16) is a rack-mounted unit which provides remote control of the five coaxial transfer switches located in the TSCB. As a visual aid for the operator, the TSCP has a back-lighted panel identifying signal flow paths, microwave switches, the diplexer, and equipment directly connected to the TSCA. Flow lines, switch designators, the diplexer, and the subsystem location of the test signal injection points are continuously illuminated white. The six signal source indicators are designed to show operation-nonoperation status. The illumination of the flow lines of the microwave switches is controlled by the position-indicating switches of the microwave switches. The sources which might produce RF interference are illuminated red.

Although used primarily for station countdown during a tracking mission, the TSCA offers a readily available means of controlling RF signals for subsystem integration test, malfunction location detection, and familiarization exercises for station personnel.

F. 498-kc Phase Modulator

Both the DSN Block I and MSFN Block II receivers contain a range receiver loop and a transfer loop at the clock frequency of 498 kc. To measure the response of these loops, it is necessary to phase-modulate a signal at the clock frequency to an index of 0.5 rad and a modulating frequency of 500 cps. At present, the phase-modulated test signal at the clock frequency is derived with a VCO similar to that used in the loops. However, since this oscillator does not have the frequency range required, a wide-angle phase modulator at the clock frequency has been developed to facilitate making these measurements.

The schematic diagram of the modulator is shown in Fig. 17. The 498-kc clock signal is applied to J1. This is followed by a 50- Ω resistive attenuator to assure a proper impedance match to the clock signal source. At the attenuator output the signal divides into two paths: one path through the phase lag network (R1, C1), the other through a phase lead network (R2, C2). The phase lead

appearing across R2, relative to the input signal, is approximately equal to the phase delay appearing across C1. The delayed signal across C1 is applied to the base of amplifier Q3—an NPN transistor; the leading signal appearing across R2 is applied to the base of amplifier Q4—a PNP transistor. The collector circuits of the amplifier pair (Q3 and Q4) are in parallel signalwise; therefore the resultant signal appearing across the common collector load (L1, C5, C6) is the vector sum of the amplified inputs to the transistors.

To increase the modulation capability, the summed output is again split into two paths through a lag network (R3, C3) and a lead network (C4, R4). These signals are then amplified and summed across the common collector load of transistors Q5 and Q6.

Q1 and Q2 comprise a Compound Darlington amplifier for the modulation input. One of the characteristics of such an amplifier is that the output signal appearing on the emitter of Q2 is in phase with the input signal applied to the base of Q1. The resistive attenuator is connected between the modulation input terminal J2 and the base of Q1 to facilitate an impedance match for an external 600- Ω audio generator.

The modulation amplifier output is DC-coupled to the base circuits of transistor pairs Q3, Q4, and Q5, Q6. When a modulation voltage is applied to J2, the output of the modulation amplifier varies the base bias voltage on the transistor pairs. A modulation voltage of positive polarity increases the gains of Q3 and Q5 and decreases the gains of Q4 and Q6; conversely, a negative modulation voltage increases the gains of Q4 and Q6 and decreases the gains of Q3 and Q5. Therefore, the vector resultant of the clock signal across the common collector loads of the paired transistors varies proportionately in phase with the modulation voltage waveform. Fig. 18 shows the resultant phase shift through the modulator as a function of a DC modulation voltage. The measured half-power modulation response to a sinusoidal voltage is approximately 5.5 kc.

The diodes CR1 and CR2 across the common collector load for Q5 and Q6 act as an amplitude limiter on the modulated signal, reducing amplitude variations to less than 0.25 db. The modulated signal is amplified by Q7 which drives the signal output terminal J3.

The capabilities of the modulator are more than adequate for loop response measurements. The distortion contributed by the modulator is negligible at the comparatively low indices and frequencies normally used.

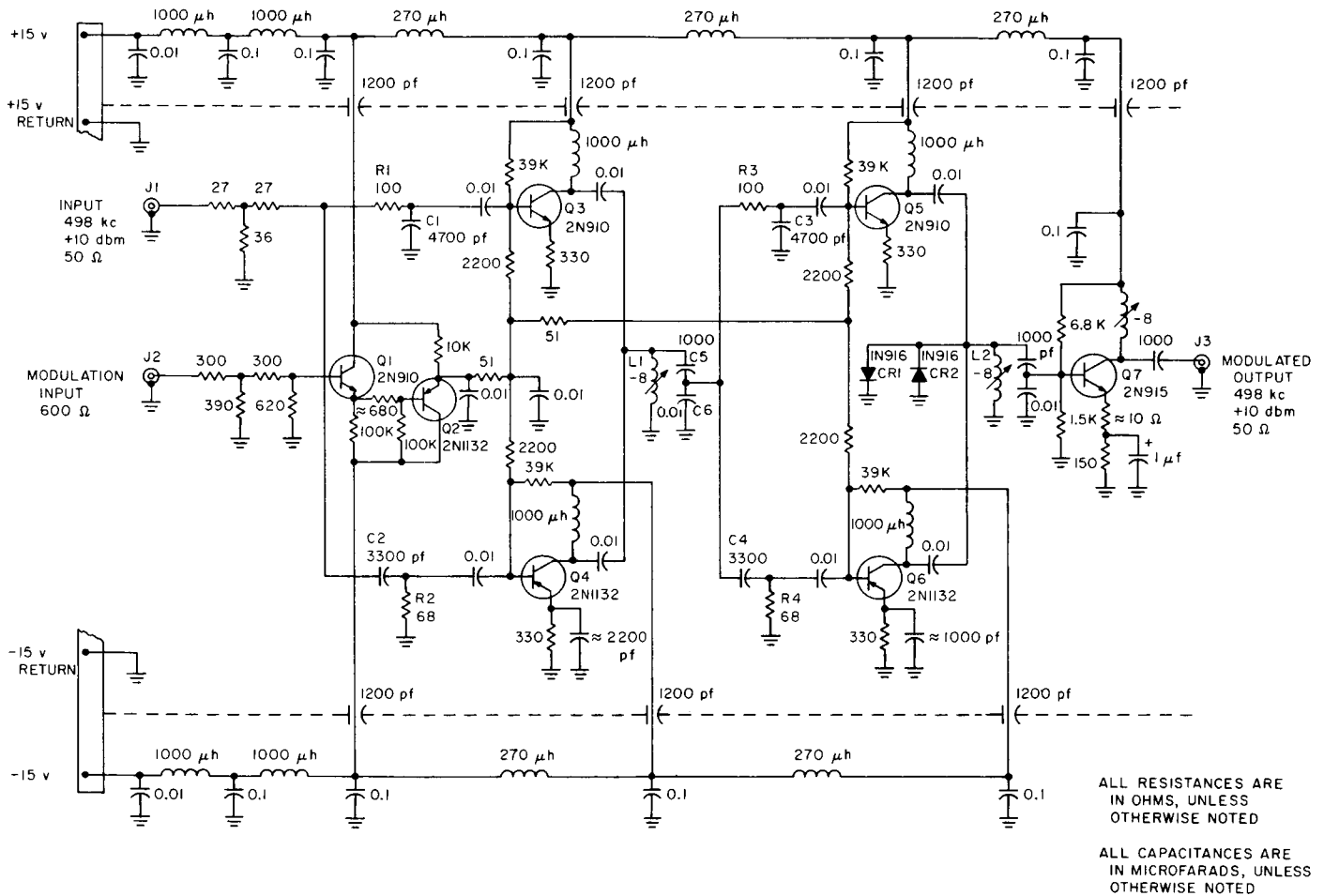


Fig. 17. 498-kc wide-angle phase modulator

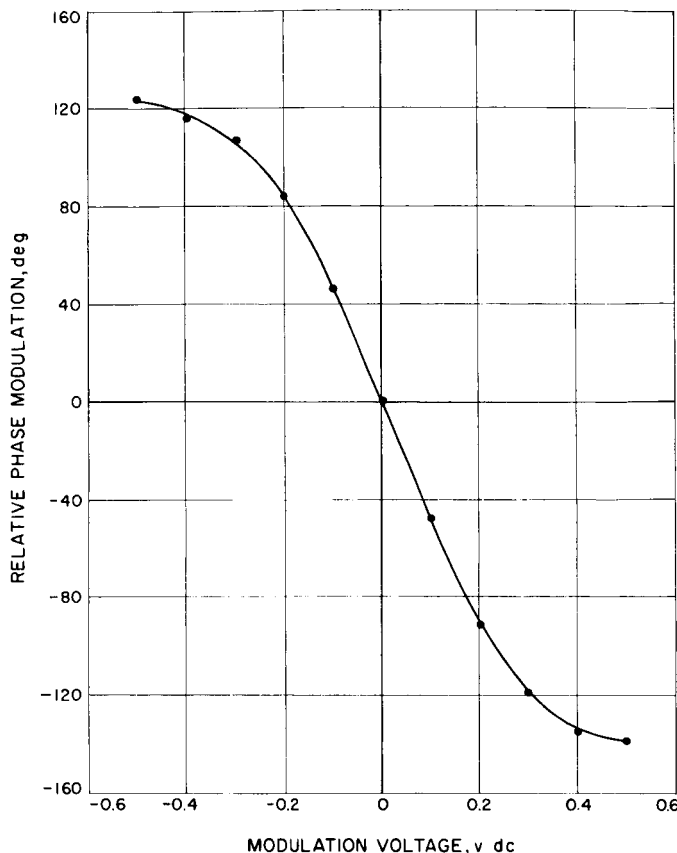


Fig. 18. Phase versus modulation voltage

G. Amplitude Stabilized Signal Source

1. Summary

A signal amplitude leveling system is being developed for use during antenna gain and pattern measurements. Operating in conjunction with a signal generator and a traveling wave tube (TWT), the system is expected to (1) reduce the difficulty in making gain and pattern measurements, and (2) reduce power drifts which lead to measurement errors. The design goal is an amplitude stability of ± 0.05 db. A description of the system is given here, as well as testing results to date.

2. Background

One technique used for measuring antenna gain is the direct measurement of power input to the collimation tower antenna and the power output at the terminals of

the receiving antenna. If the space loss between the antennas and the gain of the collimation tower dish are known, the receiving antenna gain is determined from the power measurements as:

$$Gr = Pr - Px + \alpha - Gx \quad (1)$$

where

Gr = receiving antenna gain, db

Pr = power received, dbm

Px = power radiated, dbm

Gx = transmitting antenna gain, db

α = space loss, db

Eq. (1) indicates that an error in measuring the magnitude of Px will result in an equal error in the measured value of Gr . Drifts in radiated power have been as much as 0.5 db during gain measurements made in the field using a signal generator and a 10-w TWT. Because these drifts sometimes occur rapidly and thus cause difficulty in the simultaneous determination of radiated and received power, the stable source is being developed. The system will level the signal at the input of the collimation tower standard gain dish.

3. Configuration

A block diagram of the stable source is shown in Fig. 19. During operation, the signal fed into the radiating dish is sampled by means of a directional coupler, and the coupled portion is converted into DC by a crystal video detector. The detector output is then proportional to the radiated power. A summing junction is used to compare the detector output and a DC reference voltage, and any resulting error voltage is integrated and used to drive the voltage-controlled attenuator which then makes corrections for the error. The switch selectable filters allow operation at either 2285 ± 15 Mc or 2110 ± 10 Mc.

4. Testing

The expression for signal output of the system as a function of time, $C(t)$, for a step change in the reference voltage R is:

$$C(t) = \frac{R}{K'} \left[1 - e^{-Kt} \right] \quad (2)$$

where

K' = the slope of the detector, v/db

K = product of all the system gain constants

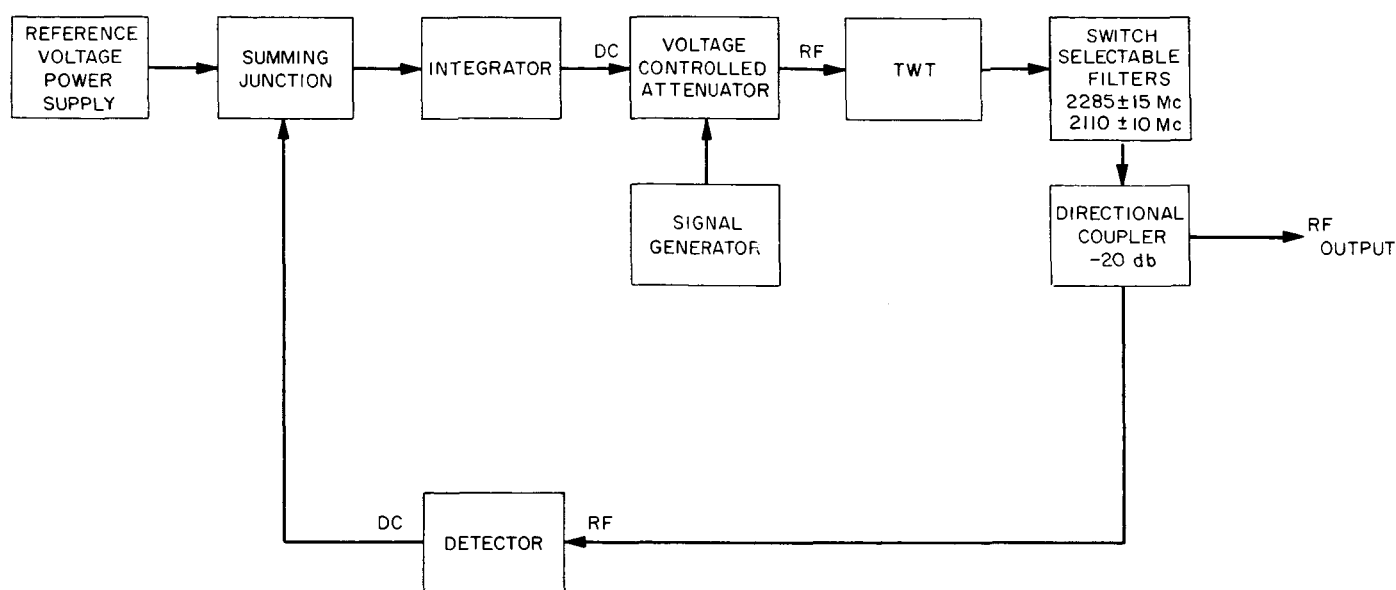


Fig. 19. Stable signal source

From Eq. (2) it can be seen that the steady state transfer function is $C/R = 1/K'$. The value of K' determined in test is 0.28 v/db. The maximum allowable drift in R is the product of the desired stability and K' . It is $\pm(0.05)(0.28)$ or ± 14 mv. Tests run on the reference power supply, over a temperature range of -25 to $+82^\circ\text{C}$ and a $\pm 10\%$ line voltage change, resulted in drifts < 1 mv. The stability requirement of ± 14 mv also applies to the integrator input drift and the detector output drift. Although the integrator and its power supply were found to drift < 3 mv over $\pm 10\%$ line voltage change, temperature drift of the integrator was $\sim \pm 30$ mv; therefore, temperature control is necessary. Since further temperature testing of the integrator power supply alone resulted in integrator input drifts < 7 mv, temperature control

of the power supply is considered unnecessary. Final testing has not been completed, but temperature stability of the order of degrees should be adequate. Likewise, the detector will be temperature-controlled, as its drift was ~ 140 mv over a range of -25 to $+75^\circ\text{C}$. The other critical component—the directional coupler—was found to drift approximately 0.2 db over a temperature range of -25 to $+75^\circ\text{C}$, and therefore will also require temperature control.

No further tests are planned until final packaging (now in progress) is completed. However, the system has been operated with no temperature control for a 17-hr period in a laboratory environment, and the total drift, including an H-P 431B power meter, was < 0.03 db.

V. Communications Research and Development

A. Experimental Closed Cycle Refrigerators (CCR) for Masers

A simple compressor system has been designed and built for the refrigerator which has been described heretofore. Fig. 1 shows a front view of the assembly with side and top panels removed.

A Copeland air-conditioning compressor pump forms the base of the system. The two-stage oil lubricated compressor is integrated with heat exchangers and filters to remove effectively all traces of oil from the helium gas. The capacity of the compressor assembly is approximately 17 ft³/min (standard) at intake pressure of 90 psia and exhaust pressure of 300 psia; and approximately 1.5 ft³/min (standard) at intake pressure of 15 psia and exhaust pressure of 300 psia.

A test program is under way to assess the reliability of the complete CCR system.

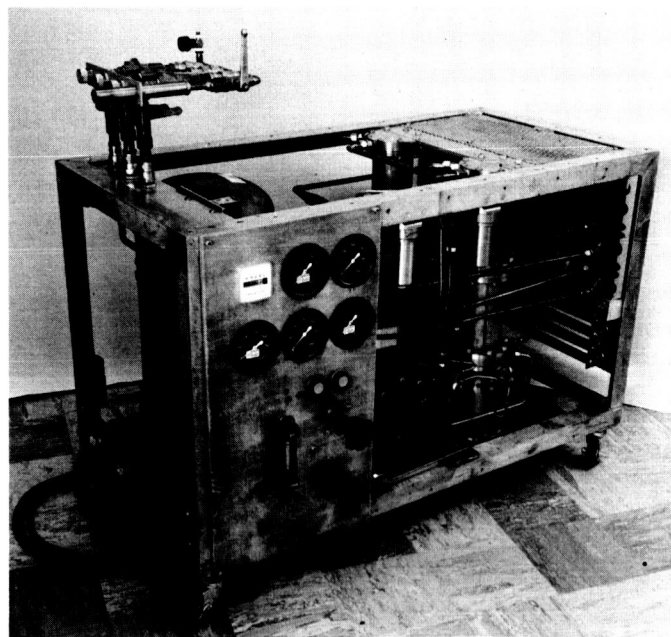


Fig. 1. Front view of compressor for closed cycle refrigerator

B. Experimental X-Band Lunar Planetary Radar Project: X-Band Radar Feed Installation

1. Introduction

Previous issues of the SPS, Vol. III have shown the 30-ft Venus reflector X-band installation. Performance has been discussed in SPS 37-30 and 37-31, Vol. III. During May 1965, the equipment was reinstalled on the antenna with a few minor modifications. This reporting will discuss the modifications made to the paraboloidal surface and waveguides.

2. Microwave Installation

During the 1964 experiment, the waveguide switches were a source of intermittent failures. Prior to the May 1965 installation, the switches were modified to increase reliability. In terms of RF performance the principal modification was to decrease the rotor diameter 0.001 in. to preempt galling of the rotor/stator interface. While the original switches provided greater than 60-db isolation, the reworked units have deteriorated to between 50 and 60 db. Preliminary laboratory cycling and antenna-mounted service indicates the reliability problem has been solved.

A two-stage regulator has been installed in the dry nitrogen waveguide pressurizing system. The new regulator provides a nominal 5 oz/in.² gage pressure. All waveguide flanges have been sealed using a silicone rubber compound¹. The sealing is done around the outside faces of a coupled flange and includes the flange hardware. This method of sealing has been successfully used on the S-Band DSIF outdoor waveguide runs to preclude entrance of water films and dust in flange inclusions.

A problem of antenna pointing has arisen. This is because the reflector was changed from a zenith-attitude-aligned system (hyperboloid and paraboloid) to a horizon-attitude-aligned system. The horizon-attitude alignment was done in an attempt to match theoretical and experimental pattern and gain data at a higher frequency. The expected zenith pattern and gain deterioration at X-band is essentially negligible; however, antenna pointing is affected to the order of 0.1 deg. It is expected that radio-

metric star tracking will allow suitable correction terms to be generated and included in the tape command drive system.

C. 22 Gc/sec Gain Calibration

1. Summary

During June 1964, the Goldstone Venus 30-ft reflector was utilized as a focal-point-fed large aperture for sweep frequency radiometric observations of Venus. Antenna radiation patterns taken during the period have been reported (SPS 37-29, Vol. IV, pp. 122-126).

Basically the same equipment was used during January 1965, for radiometric observations of Jupiter. Antenna radiation patterns taken during this latter period have also been reported (SPS 37-33, Vol. IV, pp. 192-195). In this reporting, experimental radiation patterns obtained during the Jupiter period are shown for 21.0 and 24.0 Gc/sec. The experimental patterns have been reduced to a log amplitude scale and are compared with patterns predicted using the JPL IBM 7094 Radiation Pattern Program (SPS 37-23, Vol. III, pp. 34-38). Evidence of feedhorn defocusing is discussed.

2. Computed and Measured Results

As described in SPS 37-33, Vol. III, pp. 69-81, considerable effort has been extended to achieve an accurate calibration of the aperture efficiency for the 30-ft reflector over the frequency band 20.6 to 24.0 Gc/sec. Two distinct efforts, one attempting to predict and the second attempting to measure aperture efficiency, have given dissimilar results. Specifically, the discrepancy is most notable in the slope of aperture efficiency versus frequency. As reported in the above reference, the measured slope is -0.70 to -0.84 db/Gc, including probable error; while the predicted slope is -0.37 db/Gc, with a probable error in the order of 0.01 db/Gc.

Because of this discrepancy, a short study was conducted to place upper limits on the change rate of gain loss due to aperture phase errors with respect to frequency (SPS 37-33, Vol. IV, pp. 258-261). In that study it was shown that a minimum path length error in the aperture of 0.41 in. must exist to yield the measured slope.

¹Dow Corning Silastic RTV 732

In order to investigate the possibility of a phasing error in the aperture in addition to the error present due to the reflector surface perturbations, the JPL IBM 7094 radiation pattern program was used. A series of cases were run for 21.0 and 24.0 Gc/sec with input describing experimentally determined feedhorn radiation patterns and experimentally determined paraboloidal surface deflections. The series of cases were parametric in the physical placement of the feedhorn about the focal

point. Three feed points corresponding to $\delta = 0$ and $\delta = \pm 0.27$ in., where δ is the deviation along the Z axis from the focal point, were tried. For $\delta = +0.27$ and $\delta = 0$ in., the results disagreed with experimental patterns. For $\delta = -0.27$ in. (feed too close to the reflector), the agreement was fair, as shown in Figs. 2 through 5. Figs. 2 and 3 show 21.0 Gc measured and machine-computed radiation patterns for the azimuth and elevation planes, while Figs. 4 and 5 show 24.0-Gc performance.

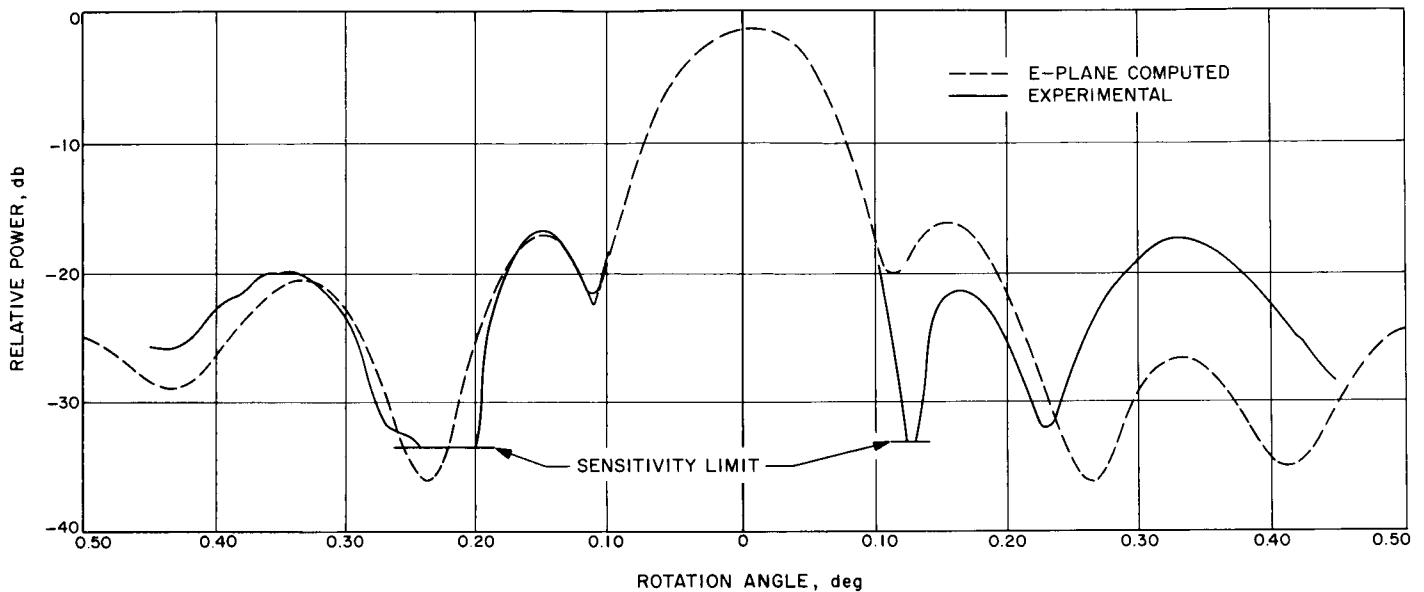


Fig. 2. 30-Ft reflector azimuth patterns, 21.0 Gc/sec

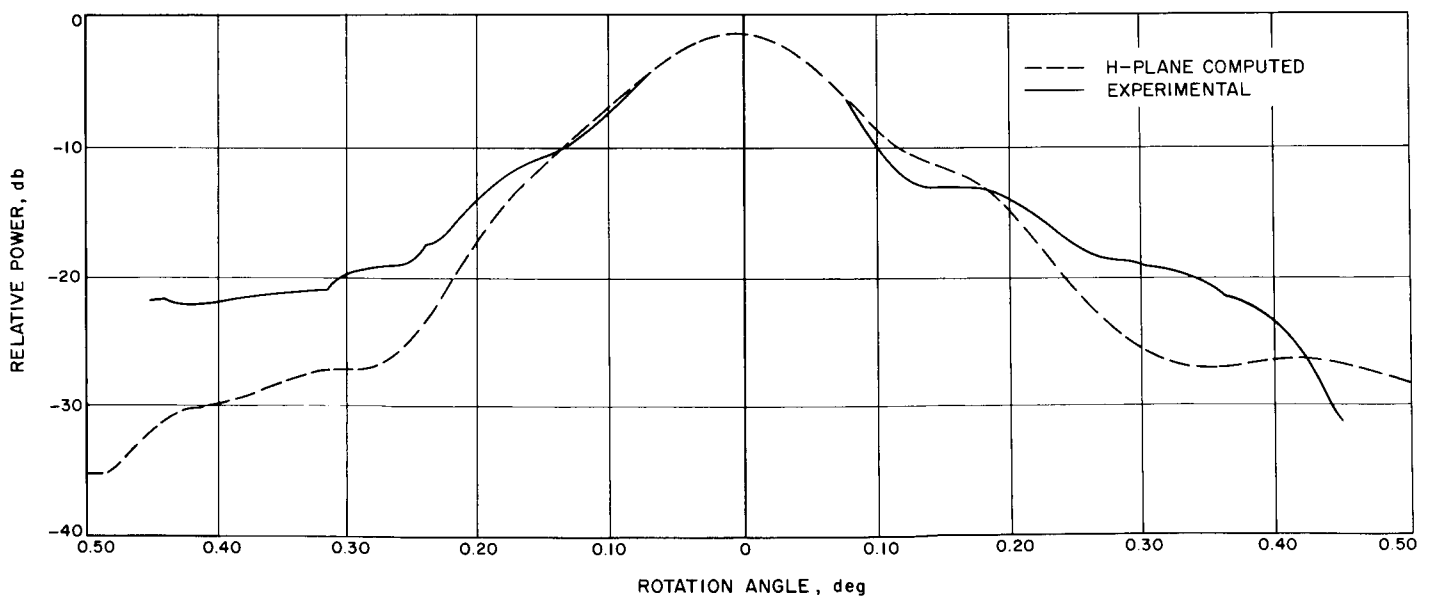


Fig. 3. 30-Ft reflector elevation patterns, 21.0 Gc/sec

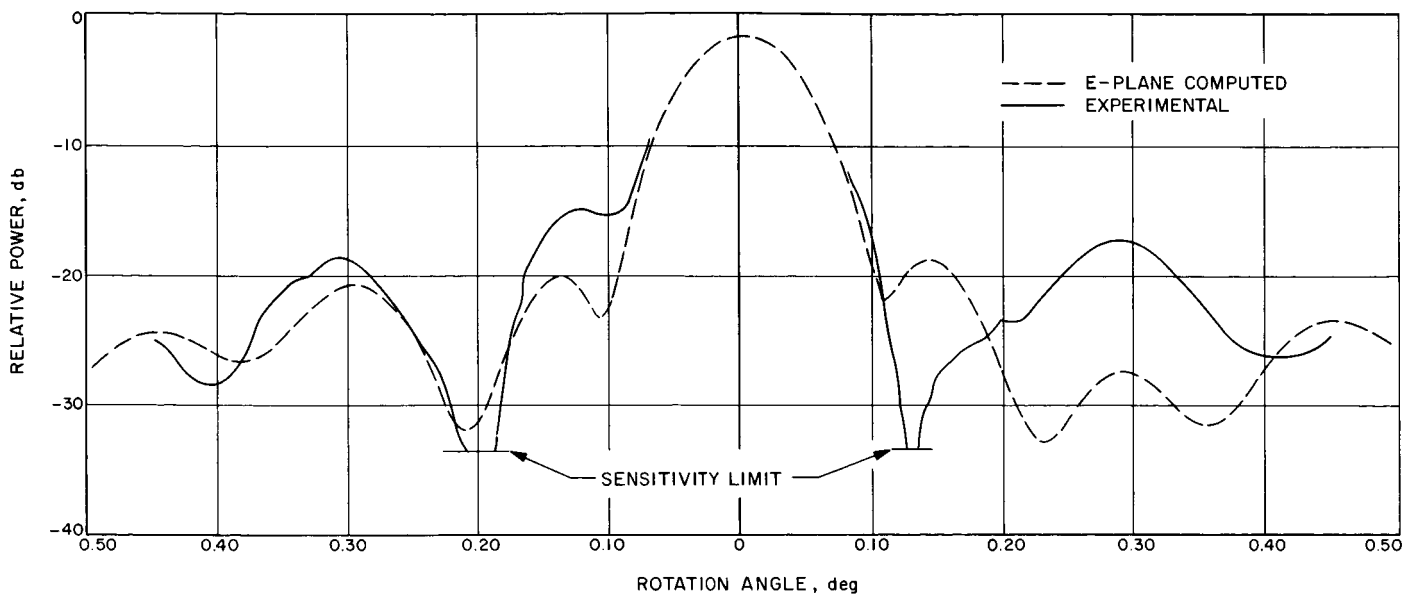


Fig. 4. 30-Ft reflector azimuth patterns, 24.0 Gc/sec

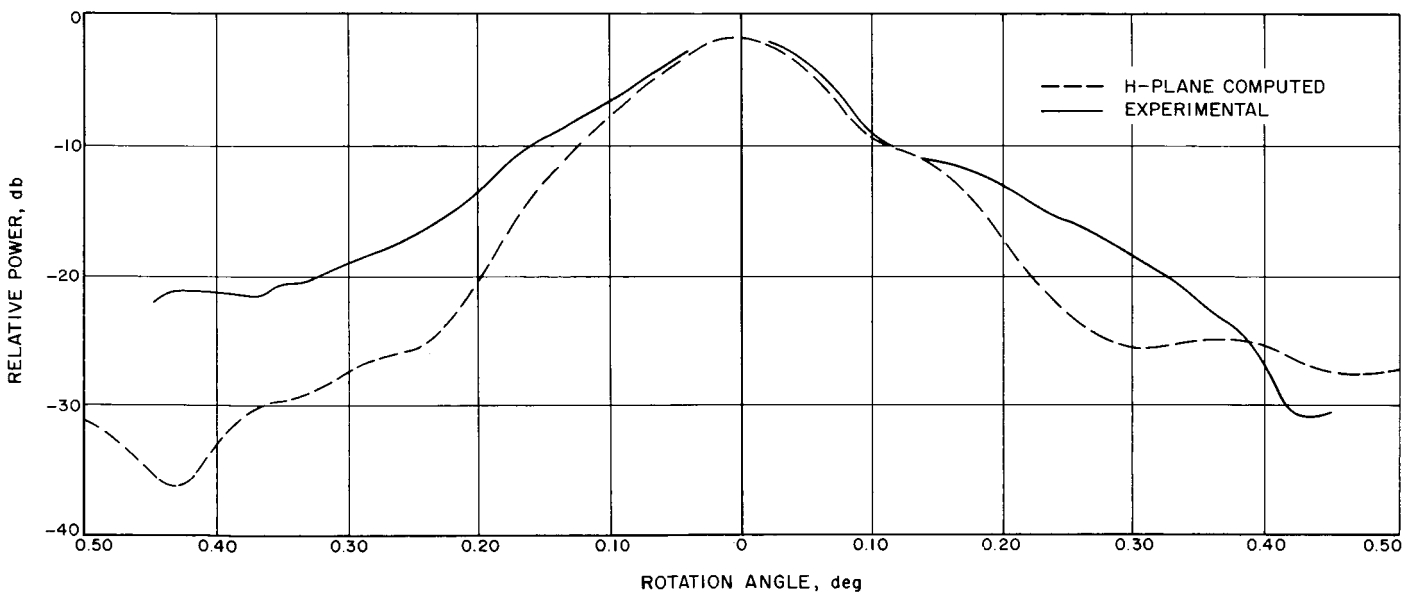


Fig. 5. 30-Ft reflector elevation patterns, 24.0 Gc/sec

Initially, $\delta = \pm 0.27$ in. was arbitrarily selected to cause an aperture edge phase error of ± 90 deg at the center frequency of interest. It is apparent from trends observed in the parametric series that $\delta > -0.27$ in. would cause better agreement; however, this case has not yet been tried.

In summary, it appears the experimentally determined slope of aperture efficiency versus frequency for the

30-ft reflector in the 22-Gc band is more reliable (for use in reducing experimental data obtained at that time) than the initially predicted slope, which assumed perfect focusing. Based on a series of machine-computed patterns compared to experimental data, the discrepancy between experimental and predicted data can be explained if the feed was placed too close to the paraboloid; trends observed in the computed data indicate the distance was in excess of 0.27 in.

D. CW Signal Power Calibration With Thermal Noise Standards

1. Introduction

An attempt to improve the accuracy of the calibration of the CW received signal power in the DSN is presently under way. A convenient measure of a spacecraft received power level is the receiver AGC voltage which is calibrated for absolute received power, defined at the receiver input, with a calibrated test transmitter. The receiving system equivalent noise temperature is determined accurately with the use of calibrated microwave thermal terminations. The test transmitter CW signal power level is then calibrated directly at the receiver input by comparison with the known receiver input equivalent noise power. A CW signal power calibration by the Y-factor method, normally used in noise-temperature calibrations, is used to calibrate the test transmitter. Calibrations were initiated on June 29 and have been extended in time past *Mariner IV* encounter.

2. Theory

The Y-factor method consists of accurately measuring the ratio, at the output of the receiving system, of the

CW signal power P_s plus the system noise power P_n to the system noise power.

$$Y = \frac{P_s + P_n}{P_n} \quad (1)$$

A precision IF attenuator is adjusted for equal power levels with the CW signal on and off. It may be shown (SPS 37-32, Vol. IV, p. 244 and SPS 37-33, Vol. III, p. 81) that Eq. (1) may be written in the form

$$P_{si} = (Y - 1) \frac{kT_s B}{g(f_s)} \quad (2)$$

where

P_{si} = input signal power (Fig. 6)

k = Boltzmann's constant

T_s = equivalent input noise temperature of the receiving system

B = system bandwidth

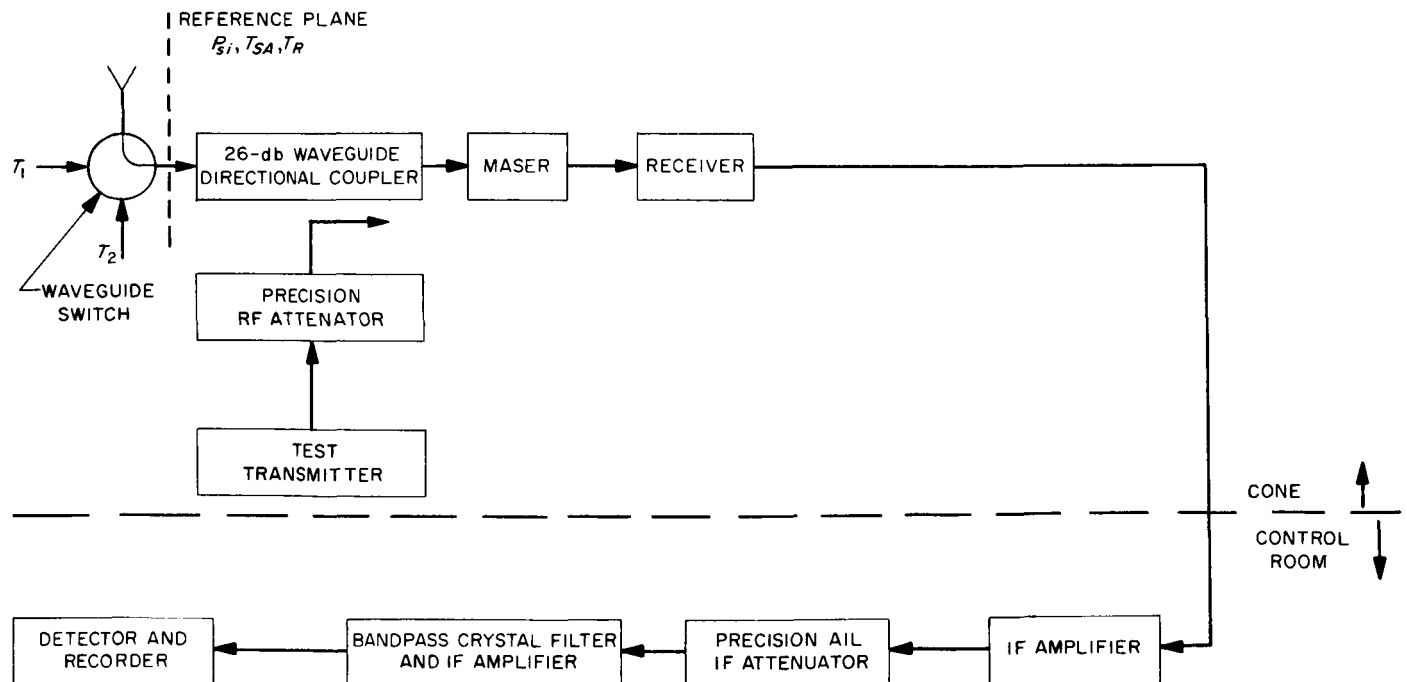


Fig. 6. Block diagram of calibration system

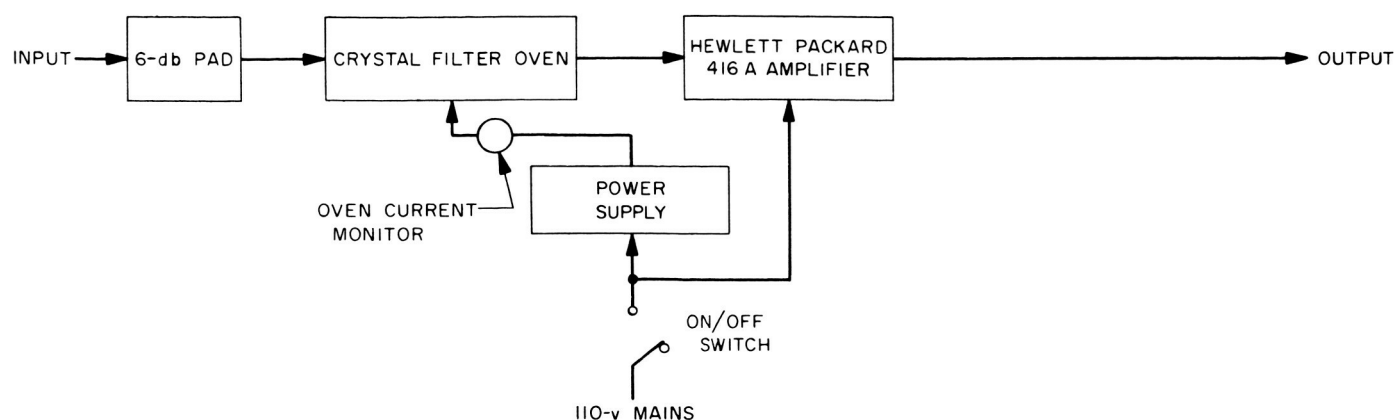


Fig. 7. Filter and amplifier schematic diagram

and

$$B = \int_0^{\infty} g(f) df \quad (3)$$

where

$$g(f) = \frac{G(f)}{G(f_0)}$$

= normalized gain response (usually f_0 is the frequency of the maximum response)

$$g(f_s) = \frac{G(f_s)}{G(f_0)}$$

= normalized gain at the signal frequency f_s .

3. Equipment

Fig. 6 shows a block diagram of the system. The band pass filter is a narrow-band, temperature-controlled crystal filter. Fig. 7 is a schematic diagram of the filter unit. The filter, amplifier and power supplies have been mounted in a $3\frac{1}{2} \times 19$ in. standard rack (Fig. 8). Oven current, which is a function of oven temperature, is monitored with a milliammeter on the panel.

Three units have been constructed and one installed at each of the following DSIF stations: 11, 12, 13. This panel is mounted in back of the existing DSIF maser

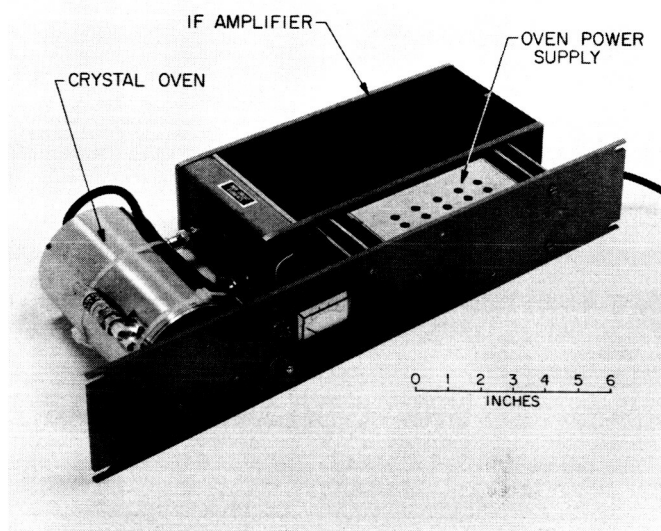


Fig. 8. Photograph of filter and amplifier unit

instrumentation rack and can be inserted into and removed from the DSIF system simply by connecting or disconnecting the input and output.

Typical filter specifications are:

Oven temperature	50°C
Center frequency	50-Mc, DSIF 11 (Pioneer) and DSIF 12 (Echo)
Center frequency	30-Mc, DSIF 13 (Venus)
3-db BW	±5 kc
50-db BW	±25 kc

All responses outside 50-db BW, 50 db down or more

Overall dimensions: 1½ in. diameter × 2½ in. height

Filter bandwidth, as defined in Eq. (3), was evaluated by measuring the gain as a function of frequency over a sufficient number of data points. This curve was inte-

grated on an IBM 1620 computer by trapezoidal integration. Several sets of curves were taken, and an average was found for each filter. After some 3 or 4 wk of operation the filter bandwidths were evaluated again as a check. Typical results are shown in Table 1.

4. Operation

Table 2 shows the form used to record the daily information at each station. Data taken by the DSIF 11 site on July 2 are presented. The maser gain and signal frequency is recorded as well as the temperature of the ambient load. The latter is read on a thermometer installed in a good heat sink mounted on the ambient load in the antenna cone. An accurate reading of ambient load temperature is required for the system temperature measurement by the Y-factor method of switching between the cold sky and the ambient load giving Y_{A0} as

Table 1. Filter characteristics

Filter location	Center frequency (nominal), Mc	Average bandwidth by trapezoidal integration from Eq. (3), kc
DSIF 11	50	11.264
DSIF 12	50	9.721
DSIF 13	30	9.858

Table 2. AGC calibration data

Site: DSIF 11				Pre- Y_A reference: 10.00 db			
Date: July 2, 1965				Post- Y_A reference: 9.86 db			
Time: 20:05 Z.				System temperature: Y_{A0} , db = 8.30, 8.28, 8.27, 8.30, 8.29			
Maser gain: 37 db				Ambient temperature: 21.0°C			
Spacecraft AGC volts: 2.72				Signal frequency: 2297.489408 Mc			
AGC, v	P_{xi} (nominal), dbm	AIL Attenuation, db	Y , db	Y , ratio	$Y - 1$, ratio	$Y - 1$, db	P_{xi} dbm
-6.77	-110	41.66	31.78	1507	1506	31.78	-109.74
-6.42	-115	36.82	26.89	488.7	487.7	26.88	-114.64
-6.05	-120	31.77	21.84	152.7	151.7	21.81	-119.71
-5.64	-125	26.45	16.52	44.88	43.88	16.42	-125.10
-5.26	-130	21.77	11.84	15.28	14.28	11.55	-129.97
-3.62	-149						
-3.26	-153						
-2.87	-157						
-2.49	-161						
-2.12	-165						
-2.01	-166						
-1.93	-167						
-1.78	-168						
-1.65	-169						
-1.55	-170						

Average Y_{A0} (db) = 8.288 = 6.742 ratio

$$\frac{T_0 + T_R}{T_{SA}} = 6.742 = \frac{273.18 + 21.0 + 10.5}{T_{SA}}$$

$T_{SA} = 45.19^\circ\text{K}$

shown in Table 2. This system temperature T_{SA} is that measured with the maser input connected to the antenna. The same value for the receiver temperature T_R , which is composed of the maser temperature and the follow-up receiver contribution (obtained from the original noise evaluation) was used throughout the test. The individual Y-factor readings shown in Table 2 are obtained by subtracting the average of the pre- and post- Y_A reference from the individual Airborne Instrument Laboratories (AIL) attenuator readings. The data taken at the site are those shown in the upper portion and the first three columns of the table. Table 2 also shows the solution of Eq. (2) for the first five nominal input power levels. The remaining nominal input power levels and

the corresponding AGC voltages form the standard station AGC curve.

Figs. 9, 10, and 11 are derived from data from Table 2. Fig. 9 plots the precision IF attenuation against nominal test transmitter power level and checks the linearity of the system. Fig. 10 is a graph of receiver AGC voltage against nominal and calibrated test transmitter power level. Fig. 11 shows the standard (nominal) station AGC curve and a synthetic AGC curve extrapolated from the experimental curve shown in Fig. 10. The calibrated spacecraft power level is taken from this synthetic curve, using receiver AGC voltage readings.

5. Results

The received CW signal power from the *Mariner IV* spacecraft is being calibrated. Figs. 9 to 11 are typical of the results for one site on one day. The agreement between nominal and calibrated power levels is not always as good as shown in these figures. Table 3 shows

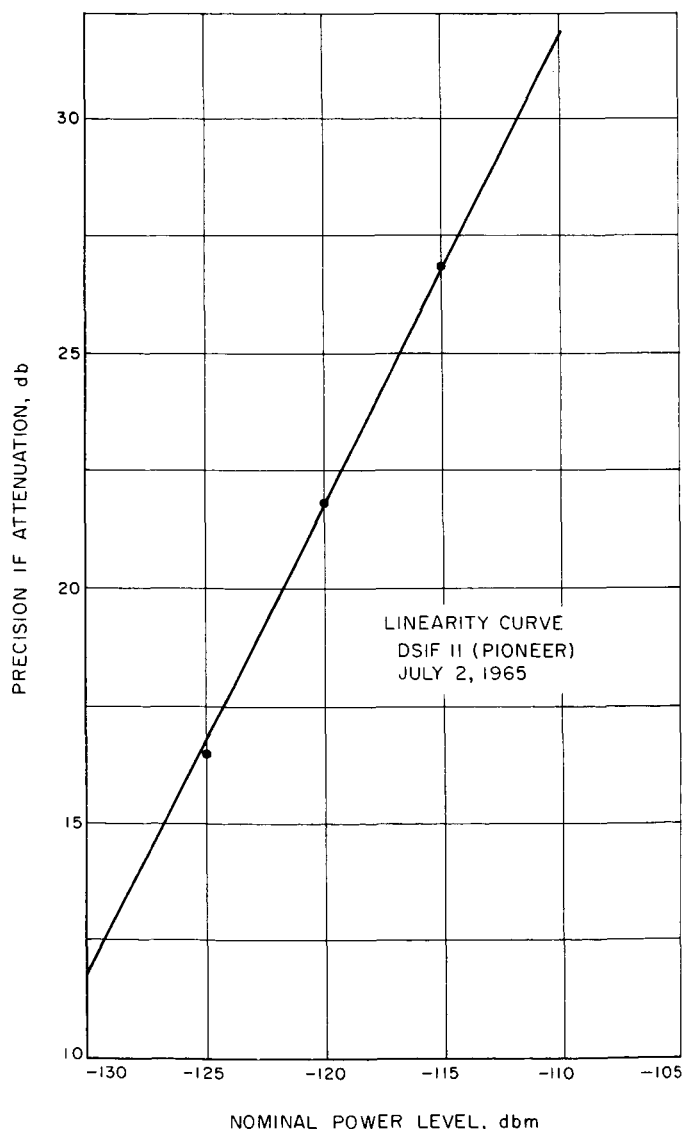


Fig. 9. Linearity curve

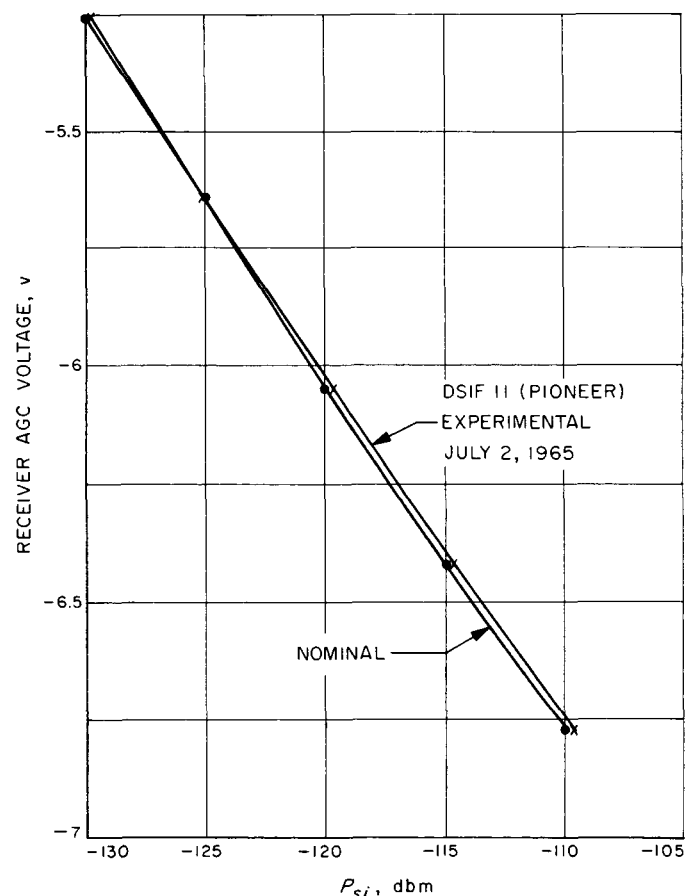


Fig. 10. Nominal and experimental AGC curves

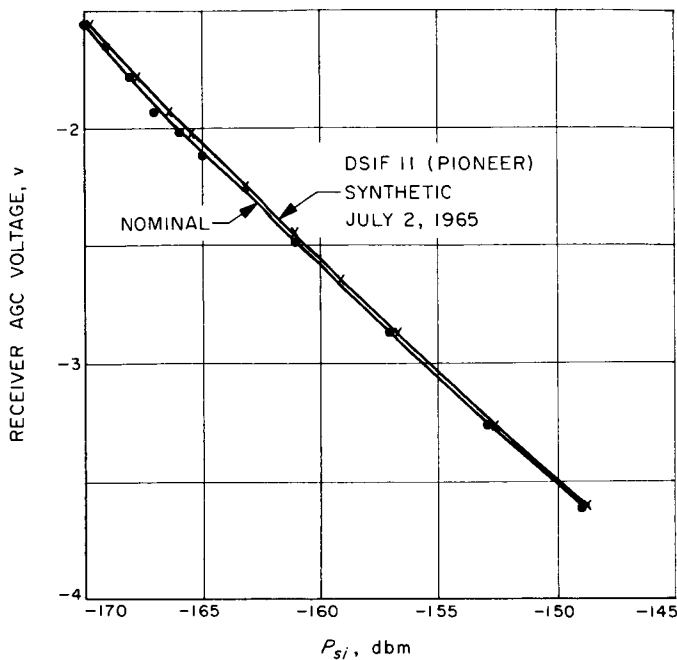


Fig. 11. Nominal and synthetic AGC curves

the receiver AGC voltage when tracking the spacecraft with the times of measurement and the nominal and calibrated received spacecraft power level.

The results may be presented in a number of ways. The following considerations will be taken into account:

- (1) Measurements on a single day are not sufficient. The results shown in these figures and tables are

Table 3. Nominal and calibrated received spacecraft power level

Date	Time (GMT)	Receiver AGC voltage, v	Nominal spacecraft power level, dbm	Calibrated spacecraft power level, dbm
July 2, 1965	2000	-2.70	-158.8	-158.6
	2100	-2.725	-158.5	-158.3
	2200	-2.725	-158.5	-158.3
	2300	-2.72	-158.6	-158.4
July 3, 1965	0000	-2.70	-158.8	-158.6
	0100	-2.69	-158.9	-158.7
	0200	-2.725	-158.5	-158.3
	0300	-2.725	-158.5	-158.3
	0400	-2.725	-158.5	-158.3

typical for one day of those days on which measurements have been taken. Every effort is being made to continue the experiment for more than a month.

- (2) Although a daily plot of calibrated and nominal spacecraft received power can be drawn for each station, no comparisons can be made between stations until the antenna gain of each station has been accounted for.

The antenna gain of each station is being measured using radio star tracks over an extended period of time, typically 3 or 4 wk.

E. Venus Station Operations

1. Experimental Activities

a. Summary. The main station activities during the reporting period were *Mariner* 1964 spacecraft support, lunar radar, and star tracking. Table 4 is a summary of activities at the Venus Station during this period.

2. Subsystem Performance

a. 100-kw transmitter (operation). The R&D transmitter for this reporting period has not been in operation due to the *Mariner* standby condition of the station.

Table 4. Summary of Venus Station experimental activity (June 17, 1965 through August 10, 1965)

Activity	Hours	Percent
Primary experiments		
Lunar radar	142	10.8
Star tracks	238	18.0
Mariner support		
Transmission, reception and testing	305.4	23.1
Testing, calibration, construction, and scheduled maintenance	634.6	48.1
Total	1320	100.0

b. Mariner 100-kw transmitters. During this reporting period the *Mariner* transmitters have operated on the spacecraft and in the water load for testing a total of 269.2 filament hours and 125.5 beam hours on Amplifier 1 and 524.2 filament hours and 179.9 beam hours on Amplifier 2. The transmitters have operated on the spacecraft for a total of 37 hr and 53 min. Approximately 1 hr and 25 min of scheduled track time was lost because of equipment failures with a total off-time, including standby periods, of 5 hr and 56 min.

Area of failure	Hours	Minutes	Operation
Reflected power trip	1	10	Test
Body current instrumentation	2	13	Test
Reflected power amplifier	1	08	Test
Reflected power amplifier adjustment		12	Track
Station power		13	Pretrack
Waveguide switches in wrong position	1	—	Track

The causes of these failures are now under investigation, and the equipment will be redesigned to eliminate these problems in future operation.

c. System improvements and modifications. Some of the low water flow trips for the interlocks of the transmitter have been changed to insure a more reliable system without endangering the safety of the klystron amplifier or the system.

Mod. IV receiver. During this period the Mod. IV receiver operated normally with no lost time due to equipment failures. The receiver still maintains its operational capability on both X- and S-band. The X-band portion has been used in lunar experiments, and the S-band portion was kept on standby during the *Mariner* fly-by.

It has been noted that during periods of particularly humid weather, condensation forms on the receiver cold plates. Thus far, the moisture has been found only on the exposed areas of the cold plates and not under or

in the receiver modules. This condensation has not affected the normal operation of the receiver so far, but work is under way to improve the operation of the cold plate water-cooling equipment.

Various changes and modifications were made during this period:

- (1) X-band portion. RF leakage-suppression-type gaskets were installed in the X-band signal generator in an effort to reduce signal leakage noted earlier. Tests will be conducted to determine their effectiveness. Also, the 35.2-Mc VCO was reinstalled in the signal generator after having been repaired at JPL. This will allow operation of the generator from either a free-running internal oscillator or a coherent external signal source.
- (2) S-band portion. The new cold plate power supply for Cabinet 5 was tested and found to have internal wiring faults. The power supply was returned to JPL for correction of these faults.

Programmed local oscillator. In the RF portion, the Montronics frequency synthesizer was reinstalled in the local oscillator, and normal operation could not be obtained. Operation with an HP synthesizer was normal. It was found that the slightly higher spurious signal output of the Montronics produced a distorted output from the divide-by-75 module in the bias up loop. Retuning of the module solved the problem, and operation is now normal on either synthesizer.

The digital portion of the local oscillator failed during pre-flyby lunar experiments. A general system checkout was performed by the laboratory project engineer. Since the fault is intermittent in nature, the exact cause could not be located, but it seemed to be in the tape reader portion of the equipment. Readjustment and realignment of the tape reader and replacement of marginal digital cards has cured the problem. Operation is now normal.

Central frequency synthesizer (CFS). During this period, various modifications were made to the CFS by the laboratory project engineer. This work was done primarily to maintain the equipment in its optimum operating condition. Most of the work was directed at reducing the dynamic phase error in the various reference loops. Work is continuing. A faulty divide-by-100 module has been returned to JPL for repair. Removal of this module produces an out-of-lock condition in the 31.44 and the 31.84 Mc reference loops.

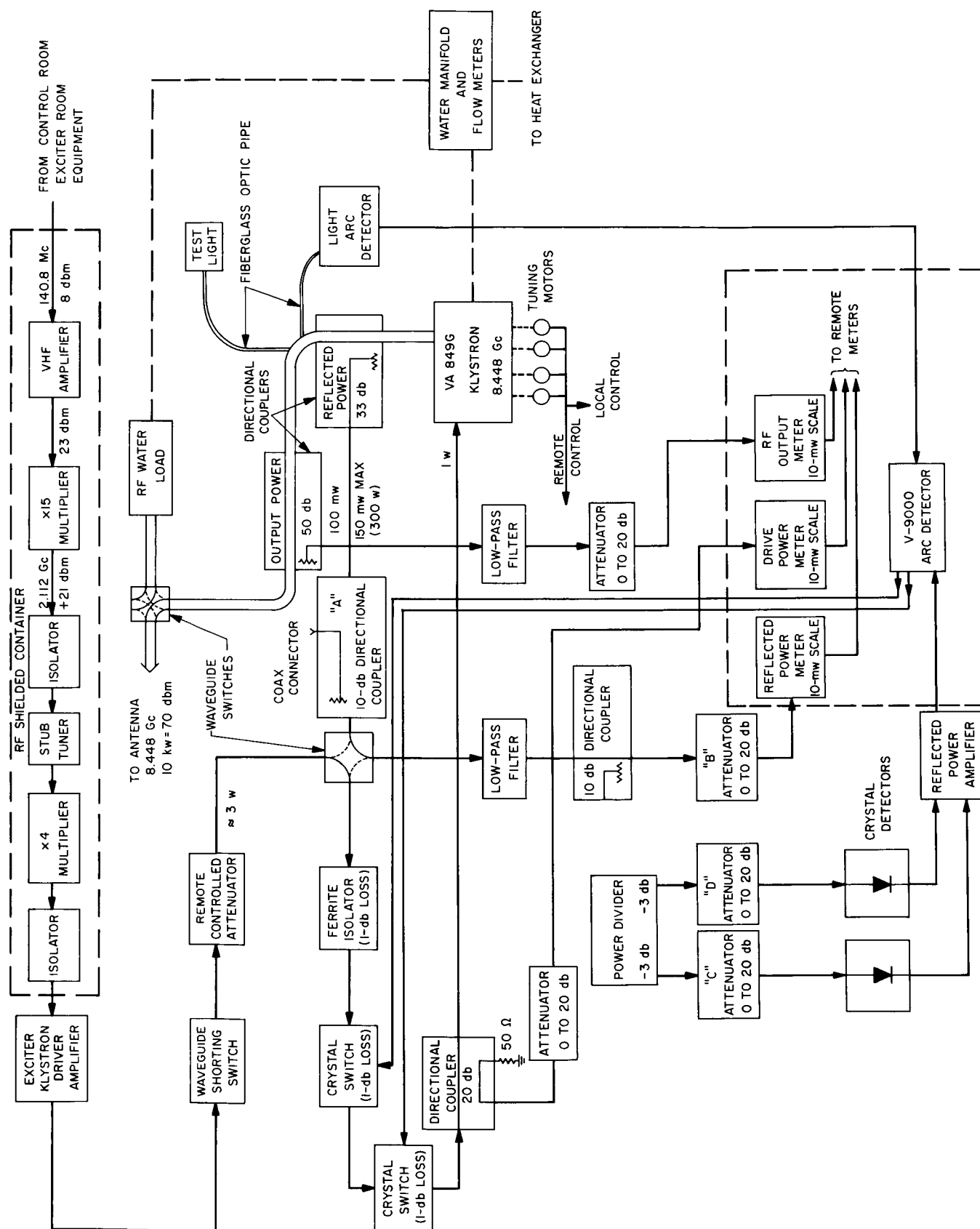


Fig. 12. RF section of X-band transmitter

F. Lunar Radar X-Band Transmitter

1. Introduction

Immediately preceding the *Mariner* Mars encounter, the X-band lunar radar experiment was stopped temporarily. During this shutdown period, the X-band 8.448 Gc transmitter was tested and modified to permit more reliable operation and easier maintenance. The transmitter output power was increased from 9.5 Kw to 10 Kw by raising the output voltage of the motor generator supplying the high-voltage transformer-rectifier from 122 to 124 v. A discussion of the recent changes in the block diagram (Fig. 12) is included in this report.

2. Antenna Exciter Chain

An isolator was installed at the output of the $\times 4$ Varactor multiplier module to insure consistent wide bandpass characteristics independent of its load VSWR. The overall bandpass of the exciter chain measured at the output of the $\times 4$ multiplier was measured to be 50 Mc at the 1-db points with the isolator installed.

3. Exciter Klystron Driver Amplifier

The exciter klystron amplifier as described in SPS 37-34, Vol. III, pp. 57-58 has accumulated approximately 400 hr of reliable operation. The VA 401J klystron was found to be tuned 3 Mc too high. The erroneous tuning was determined as being due to factory tuning at beam potential of 1300 v while normal operation at the Venus Station is 1000 v. The klystron was subsequently retuned at the lower voltage, and the bandpass response curve is shown in Fig. 13.

4. Waveguide Shorting Switch

The purpose of the solenoid-operated waveguide shorting switch mounted in the RF drive line is to insure RF drive cutoff during the receive mode. It is redundant in operation with a solenoid-operated coax switch installed at the 35.2-Mc input of the exciter chain in the control room and decreases the possibility of waveguide arcs in case of failure of the coax switch.

5. Reflected Power Calibration

A 10-db directional coupler "A" has been installed in the reflected power monitoring line to facilitate making rapid and accurate reflected power calibrations for the reflected power meter and the arc detector's reflected power amplifier. The monitoring system is calibrated by

inserting a 1.35-w signal at the coax connector of the 20-db directional coupler "A". This injects 135 Mw (equivalent to 300 w of reflected power in the output waveguide of the transmitter) into the reflected power line feeding the power meter and arc detector system. Attenuators B, C, and D are then adjusted for their proper output levels.

Prior to the installation of the 10-db directional coupler, it was necessary to disconnect manually the waveguide attached to the transmitter's output waveguide 33-db directional coupler and attach a coax to waveguide adaptor to the waveguide. The procedure was time-consuming and introduced the possibility of waveguide contamination and flange damage.

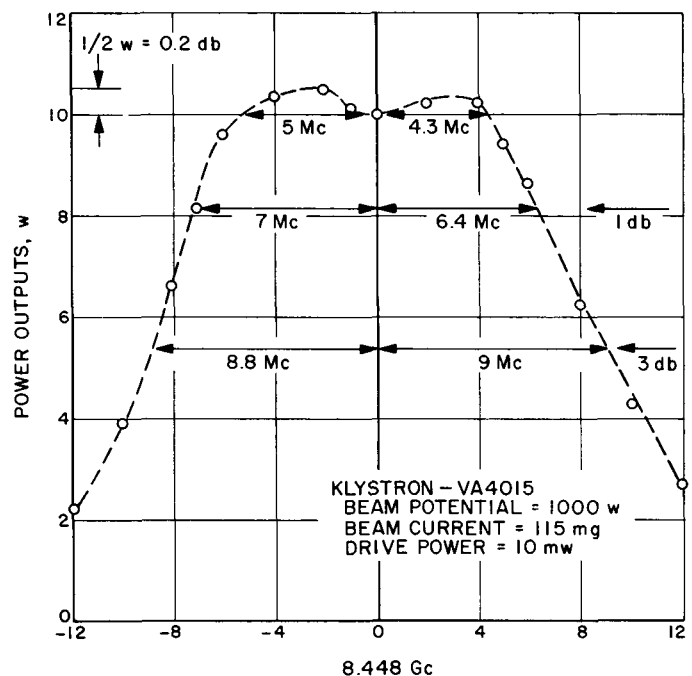


Fig. 13. Bandpass characteristics of exciter klystron driver amplifier

G. 100-kw S-Band Final Amplifier

1. Introduction

Current work designed to upgrade the performance and reliability of the 100-kw final amplifier includes:

- (1) Mounting and housing modifications to accommodate the Eimac 100-kw klystron (SPS 37-33, Vol. III, p. 88), and
- (2) Design and testing of a final amplifier power output measurement system.

2. Eimac Klystron Mounting and Housing

Since the Eimac 100-kw klystron is larger and heavier than the Varian klystron it will replace, it is necessary to provide a stronger mounting and a larger housing. The new mounting is designed to:

- (1) Support the weight and bending moment of the tube and focus magnet in any antenna position, and
- (2) Allow easy and accurate positioning of the klystron for mating to the output waveguide.

Permanent installation of handling equipment (hoist, etc.) will also be required for installing and removing the klystron in the cramped quarters of the cone.

The focus magnet of the Eimac klystron will require about twice as much current as that of the Varian tube. A suitable power supply is currently under construction.

Although the Eimac klystron will operate at approximately the same beam voltage as the Varian tube, the existing doubly shielded coaxial cable used to carry beam power from the ground level power supply up to the klystron in the antenna feed cone is being replaced as part of the upgrading program. Breakdown in the existing type of cable has resulted in system outages twice within a 3-yr period. It is expected that the larger diameter cable now being fabricated will perform more reliably. The failure mechanism in the cable probably consists of gradual deterioration of the insulating material from corona-induced chemical reactions followed by complete voltage breakdown. A corona testing procedure may be required for the evaluation of all high-voltage components, including cables.

3. Final Amplifier Power Output Measurements

The 100-kw klystron power output is presently measured by a water-load calorimeter, together with an "in line" system consisting of directional couplers and low-level (10-mw) RF power meters (Fig. 14). The water load calorimeter is primarily used to calibrate the inherently less accurate directional coupler RF power meter system immediately before and after each transmitter run. Since a run may last up to 10 hr, the stability of the

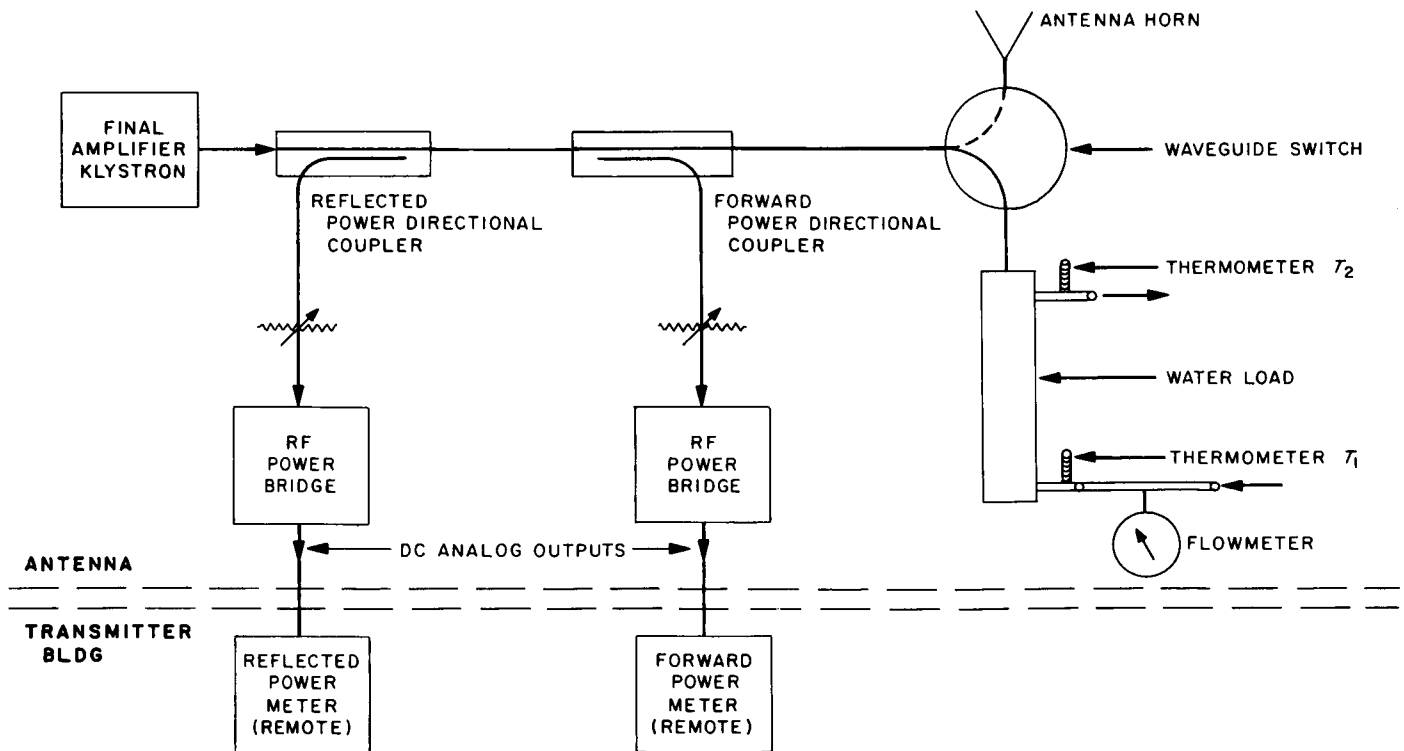


Fig. 14. 100-kw S-band final amplifier output power measurement system

in-line system is important. The present system has several defects, the principal shortcomings and their remedies being:

- (1) The questionable stability of the in-line power measurement system. Temperature cycling of components and of the system, simulating runs of several hours' duration, will determine the stability of the system.
- (2) The water load presently used consists of a glass vessel filled with water into which RF power is coupled from the waveguide. The glass vessel is easily broken, and the large mismatch which results is potentially fatal to the klystron. The water load now being built for JPL by Litton Industries Tube Division eliminates this type of failure by use of a teflon water tube.
- (3) The instrumentation of the present water load consists of a conventional orifice plate flow meter and two mercury thermometers which measure inlet and outlet water temperatures. These are situated in the cone and cannot be remotely read. The inconvenience of raising the antenna to the zenith position and climbing into the cone to read the instruments reduces the effectiveness of the system. Therefore, a remote reading system has been designed (Fig. 15). The system is essentially an analog computer for the equation

$$P = K(T_2 - T_1) F \rho C \quad (1)$$

where

P = RF power absorbed by water flowing through load

T_1, T_2 = inlet and outlet water temperature, respectively

F = volumetric flow rate

ρ = density of water

C = specific heat of water

K = a constant depending upon the units used

The analog computation assumes that ρ and C are constants which are subsumed, together with K , in the scale factors K_1, K_2 of Fig. 15.

In order to evaluate the overall error of the system, we rewrite Eq. (1) as

$$P_w = e P_N = K(T_2 - T_1) F \rho C (1 + h) \quad (2)$$

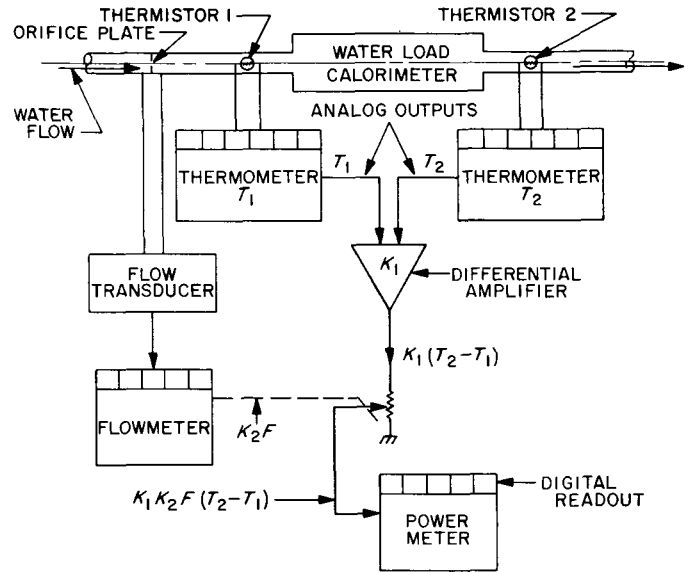


Fig. 15. Water load calorimeter instrumentation

where

P_N = the net power entering the terminals of the load, and

P_w = that part of P_N which is absorbed by the water flowing through the load, so that

e = the efficiency of the load and $(1 - e)P_N$ is the sum of all the heat losses to sinks other than the water flow.

h = the relative error of the analog multiplication process itself.

Eq. (2) shows that the analog multiplier output must be corrected for $e \neq 1.0$ and for variation of ρ and C . These corrections are:

e : rough calculations indicate that with proper thermal insulation of the load, $1 - e < 0.2\%$. This, as we shall see below, is swamped by the expected random measurement errors and can be neglected in the remainder of the discussion.

ρ : decreases from 1.00 g/cm³ at 4°C to 0.975 g/cm³ at 75°C.

C : differs from 1.0 cal/g only in the neighborhood of 0°C, where it is about 1.01.

The random errors are:

- (1) The measurements of T_1 and T_2 , contributing each a relative error of $\Delta T_1/(T_2 - T_1)$ and $\Delta T_2/(T_2 - T_1)$. Since $|\Delta T_K| < 0.25^\circ\text{C}$, $K = 1, 2$, and $T_2 - T_1 \cong 15^\circ\text{C}$, each of the relative errors is less than 1.7%.
- (2) The measurement of F , contributing at most 1%.
- (3) The analog multiplication process error h ; less than 1%.

By the rule

$$\frac{|\Delta P|}{P} \leq \frac{|\Delta T_1|}{T_2 - T_1} + \frac{|\Delta T_2|}{T_2 - T_1} + \frac{|\Delta F|}{F} + |h|,$$

which applies when the errors are uncorrelated, we have

$$\frac{|\Delta P|}{P} < 2 \times 1.7\% + 1\% + 1\% = 5.4\%$$

These error estimates are based upon data supplied by the manufacturers of the transducers of Fig. 15 and may include systematic errors. These can, in principle, be measured, but a better procedure is to calibrate the instrumentation system by use of a water load designed to absorb DC power. Since DC power can be measured with an accuracy of about $\pm 1/2\%$, any systematic error greater than 1% would be detectable. Fortunately, such a DC load does exist at Goldstone and will be used for calibration.

H. Frequency Generation and Control

1. S/X Band Central Frequency Synthesizer

a. Introduction. A frequency divider (1.0 Mc to 200 kc) has been developed to meet the input requirements for the 31.84-Mc phase lock loop, the 35.2-Mc phase lock loop and the generation of 455 kc. (See SPS 37-33, Vol. III, Fig. 27, p. 92.)

Seven distribution amplifiers have been procured from a local vendor to fully implement the low-frequency amplifier requirements. Refer to SPS 37-33, Vol. III, Fig. 29, p. 94.

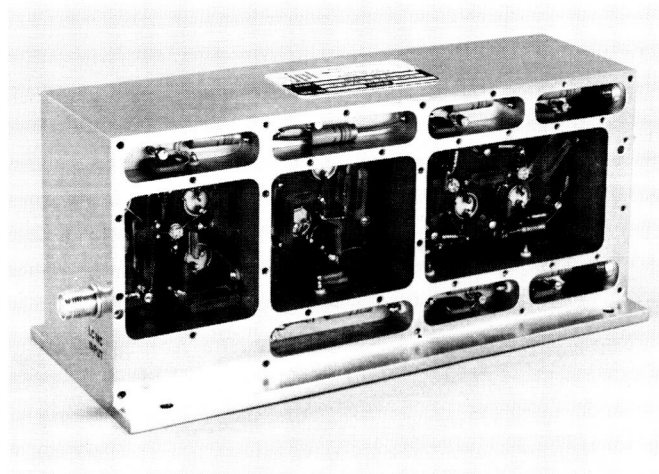


Fig. 16. Frequency divider, 1.0 to 0.20 Mc

b. Frequency divider. This module consists of solid-state circuitry in a machined and gold-plated cavity-type chassis. Frequency reduction is accomplished by the use of a limiter, synchronous oscillator, crystal filter, and isolation amplifiers (Figs. 16 and 17).

The frequency divider has met a series of stringent tests that include an input impedance measurement, power supply variations, limiting characteristics, stability, isolation and noise tests, harmonic distortion, spurious signals, RFI leakage, environmental test, and a bandwidth measurement.

The input impedance measurement determined the VSWR over an input range of ± 3 db at the +10 dbm level (Fig. 18).

A power supply reduction of 17% reduces the usable 200-kc output only 1 db. This can be seen on Fig. 19.

The limiting curve of Fig. 20 demonstrates the high 200-kc output level even when 30 db of input signal is lost. Removal of the 1.0-Mc input signal results in total loss of 200-kc output signal.

No extraneous oscillations are induced by any combinations of opens, loads, or shorts on the input and output terminals; thus stability is maintained.

Isolation from output-to-input terminal is > 65 db for all frequencies between 10 kc and 2.0 Mc.

The noise measurement consisted of shorting and opening the 1.0-Mc input terminal and observing

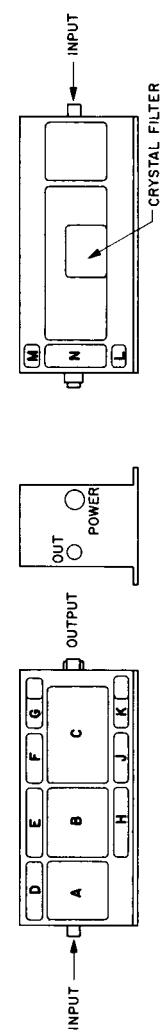


Fig. 17. Central frequency synthesizer, 1 Mc to 200 kc

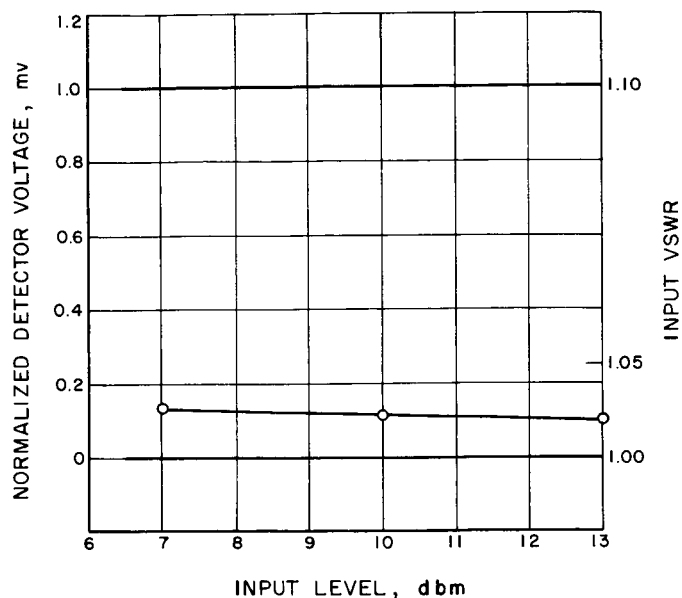


Fig. 18. Input impedance versus input level

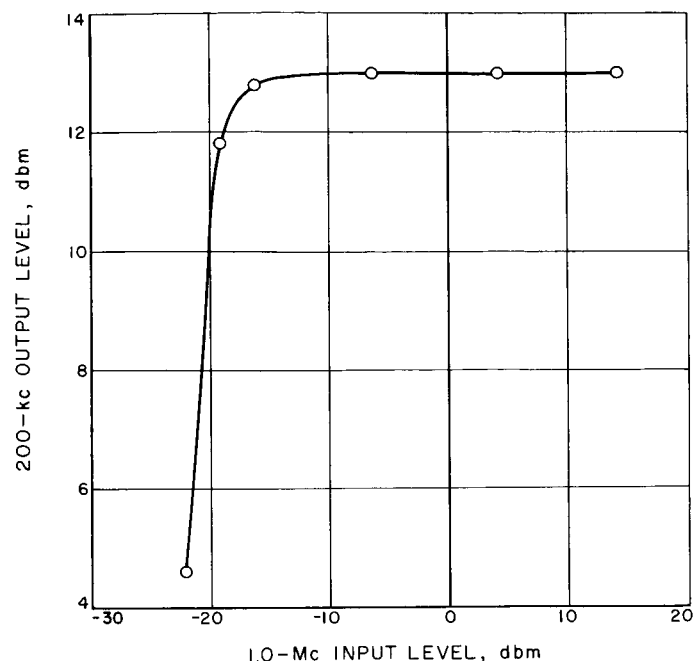


Fig. 20. Limiting characteristics

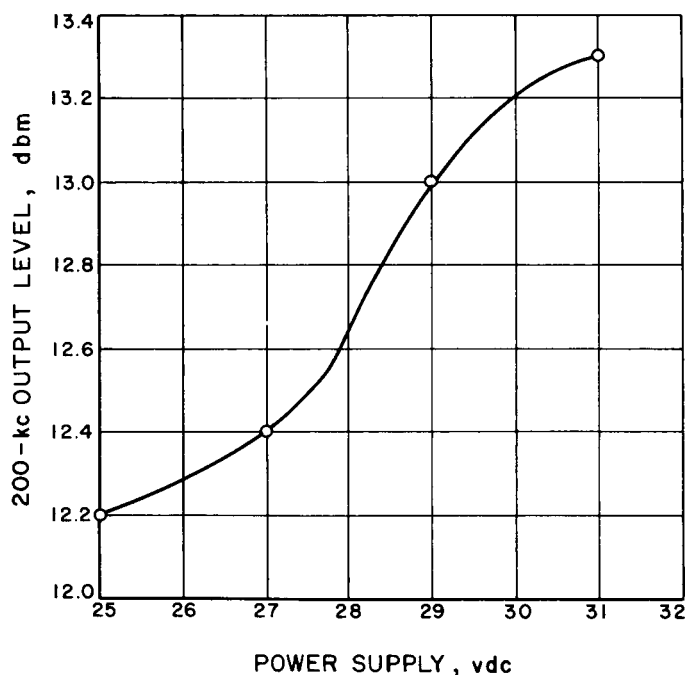


Fig. 19. Power supply variations versus 200-kc output level

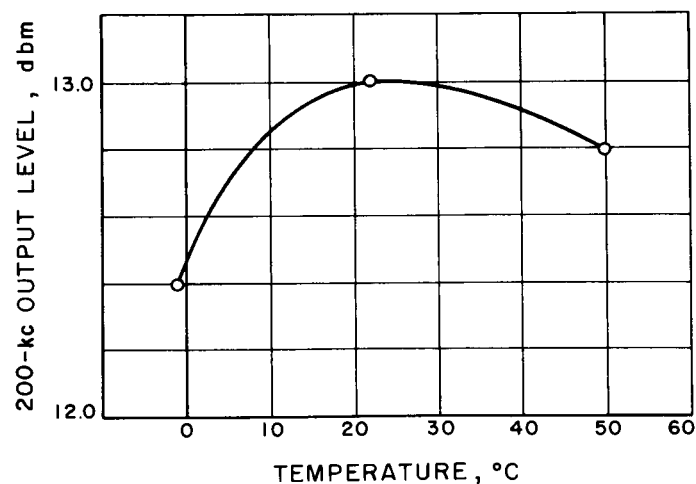


Fig. 21. Environmental conditions

the 200-kc noise on the output terminal. In either case, the output noise was never $> 17 \mu\text{v}$. The harmonic distortion was measured and found to be 3.2%. There are no spurious signals between 1 cycle and 1.5 Mc. System frequencies of 455 kc, 30 Mc, and 30.455 Mc were immeasurable.

The RFI leakage was checked at the input and output terminals, the power line, and all external mechanical junctions. In no case were the 1.0-Mc and the 200-kc leakage signals $> 0.5 \mu\text{v}$.

The frequency divider was subjected to a temperature environment from 0 to 50°C. Fig. 21 depicts a $+0.5 \text{ db}$, -0.25 db output signal variation over a temperature range of $\pm 25^\circ\text{C}$ at 25°C.

Table 5. Performance data for distribution amplifiers

Amplifier, Mc		Isolation		Output noise (input terminated), μv	Dynamic range of input for constant output, db	RF leakage (all frequencies), μv	Bandwidth at 3 db, kc/sec	Power supply variations of 10% versus output, db	Power drain, w
Serial No.	Frequency, Mc	Output to input, db	Output to output, db						
1	0.125	137	35.5	85	20	<1.0	20	-0.92	1.08
2	0.200	134	35.0	25	30	<1.0	46	-1.02	1.14
3	0.400	149	33.0	30	25	<1.0	90	-0.96	0.99
4	1.000	104	35.0	17	25	<0.5	140	-0.90	1.02
5	1.000	120	32.5	7.8	20	<0.5	135	-0.90	1.08
6	1.000	120	31.0	12	20	<0.5	150	-0.90	1.08
7	1.000	120	31.0	9	20	<1.0	155	-1.06	1.08

The bandwidth of the divider is determined by the crystal bandpass filter and is 168 cycles wide at 200 kc. The bandpass variation is 0.5 db over the bandwidth range.

Other performance features are output level of +13 dbm, (-0 db, +3 db), into 51Ω and a power drain of 0.41 w from a +30 vdc supply.

c. Distribution amplifiers. The seven procured modules are: (1) 125 kc, (1) 200 kc, (1) 400 kc and (4) 1.0 Mc distribution amplifiers. They are similar in construction to prior amplifiers; the only difference is that terminal boards are being used in place of printed circuit boards (SPS 37-33, Vol. III, p. 92).

Performance data is presented on Table 5 and is very nearly equal to previous models.

I. Efficient Data Systems

1. Error Control for DSN Teletype Links

a. Summary. This note describes a desirable future configuration for the DSN teletype links. For spacecraft commands going to the DSIF from the SFOF, an extremely low error probability is needed. The system for telemetry data and monitor and status data from the DSIF sites to the SFOF would be essentially the same

as that for the outward command and prediction links, except that the information rate might be higher because a larger error rate can be tolerated in the return direction. A switch controlled by the message header would be available which would allow ordinary uncoded teletype messages to be communicated over the same circuits with ordinary teletype transmitters and receivers. An error-rate monitoring system for this ordinary teletype operation is described.

b. Introduction. Previous SPS's (Refs. 1-4) have described recent work on the inter-DSN teletype channels for the purposes of choosing an error-correcting coding-decoding system for use on the spacecraft command links. These links originate in the SFOF and terminate at the DSIF sites. The spacecraft commands which they carry are so vital to mission success that an extremely low error probability must be achieved. The same reliability is needed for orbit predictions sent to the DSIF sites.

Recent experiments (Ref. 3) show that the teletype character error probability does not get above 0.01, even on transoceanic links to Australia and South Africa. One code suggested for the outward links (allowing repeat requests) would have an output bit error probability in such worst case of only 4×10^{-9} . For the inward links, a similar bit error probability of 5×10^{-6} is achieved by a related code, not having repeat requests. This higher error probability is regarded as acceptable for the inward links. The outward link code suggested is triple-character-error correcting in a word of length 15 characters. A double-character-error-correcting code used for the inward links results in the worst-case output bit error

probability going up to the higher value of 5×10^{-6} . This increase is, however, acceptable for the inward link, where higher error probabilities can be tolerated. The information rates are 0.43 for the outward link and 0.53 for the inward link. A double-character-error-detecting code for error-rate monitoring on otherwise uncoded links is also described, which adds about 0.06 redundancy to an uncoded channel.

c. Format. In this section the common format of both the outward (SFOF to DSIF) link and the inward (DSIF to SFOF) link will be described. As in Ref. 3, the messages to be considered must go through the communications processor at NASCOM, Goddard Space Flight Center. Due to the programming of the processor for ordinary linguistic teletype, the "end of message" triple of 5-level characters "Figures-H-Letters" must be avoided, since the processor stops the transmission if such a triple occurs in the message. Similarly, "blanks" are deleted in the present NASCOM communications processor, as experiments have verified.

To protect against code words that cause either this "end of message" triple or blanks to appear, the following is done: a binary system is used in which the first four channels represent information and the fifth is an odd parity on the first four. This choice accomplishes three things simultaneously:

- (1) "Figures" and "H" are even-parity characters, hence a specific double bit error would have to occur for the forbidden triple to appear.
- (2) Blanks cannot occur in the sent messages, for if the first 4 bits of a 5-tuple are "0," the fifth is then a "1."
- (3) The fifth channel tends to be the noisiest of the five teletype channels (Ref. 3), so that the remaining four channels exhibit a somewhat decreased error probability.

It should be noted that the fifth channel is not to be used as part of the error-correcting code; decisions on detection and correction are based on the first four channels of check symbols to be added (but a decision to reject an entire received word can be based on the number of odd parity check bits failing).

The check symbols are added in the encoding process. Blocks of 4 bits are regarded as elements of the $16 (=2^4)$ element field, and check symbols over this field are added onto the message by the encoder. For the command circuit, there are 8 information symbols and

6 check symbols. For the status circuit, 10 information symbols and 4 check symbols are to be used.

A fifteenth synchronization symbol, which would be put in front of the code word, has been chosen according to criteria in Ref. 3 (actually the 5-tuple 10001). The 4-bit check symbols then are augmented by the fifth channel, added as odd parity. The entire word is now of length 15 teletype characters (Fig. 22). All symbols (except the synchronization symbol) have odd parity. Since of the 75 bits only 8×4 in the outward link and 10×4 in the inward link are available for information, the actual information rates are 0.43 and 0.53, respectively.

d. Operation. The operation of this system will now be described according to the block diagram of Fig. 23. Data is generated by a data source; some of these sources were described in the introduction of this section. The data is converted to binary format in blocks of 40 bits for the inward link, and 32 bits for the outward link. The message encoder then encodes the message.

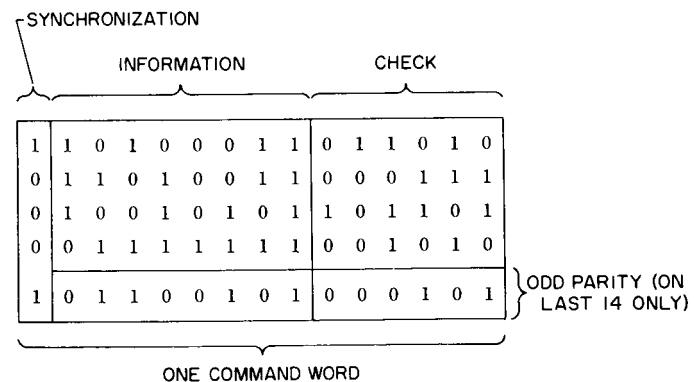


Fig. 22. Encoded word of length 15

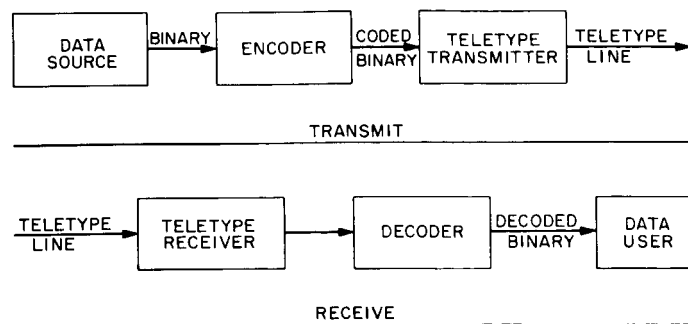


Fig. 23. Block diagram of coded teletype

First, the first 4 bits of the synchronization symbol are added, and the resulting 9 or 11 4-bit characters are encoded (the fifth bit of the synchronization symbol is added on at the end of the encoding process). Then the (4 or 6) 4-bit check symbols are added onto the end of the word. There are now 15 4-bit symbols. The fifth bits of the teletype characters are added to each 4-bit character as odd parity (except that the first, or synchronization, symbol has a "1" added instead of a "0" as its fifth bit). The length 15 word is then sent over the teletype lines. At the domestic rate of 6 characters/sec, an encoded word takes 2.5 sec to send. Information as to whether the message is ordinary teletype or encoded teletype would be put in the message header, rather than into the text itself. An encoding program has been written; it takes only milliseconds to run on a typical DSN machine (SDS 910).

Note that at this point no teletype tape has been used, the messages being generated and sent directly by machine. This will be the goal of the receiver portion of the system, too. For commands, for example, the message can go directly to the spacecraft (after perhaps a round-trip verification procedure).

Not only will such a system allow real-time control of *Surveyor*-type missions with short delay times (seconds instead of minutes), but there is another advantage. It is thought that more than half the errors observed in Ref. 3 are due to teletype reader or punch errors. With these "noisy" machines out of the system, the input character error rate would be even lower than a worst-case "0.01." But since such experiments have not been performed yet, the conservative "0.01" figure has been used in the calculations.

The encoded message (for an outward-bound link) goes over domestic teletype circuits from JPL to Goddard Space Flight Center, through the NASCOM communications processor for switching, then over more domestic lines to San Francisco, and then (normally) cable for Pacific service, always via HF radio from New York for Atlantic service. For Pacific service, cable is normally used to Hawaii and then HF to Australia, although the routes can vary at the discretion of the teletype common carrier. On the HF links, the message is subject to a repeat request ("ARQ", Ref. 2) system, which is not under JPL control. By similar routes the message finally gets to its destination, a DSIF communications center.

Here the message is detected by a teletype receiver and fed directly without tape intervention into the decoder. This machine is similar to the encoder, but has a

bigger job to do—decoding is always harder than encoding. However, a decoding program has already been written. The teletype-computer interface reads the message into the decoder: fifth channel, information, check, and synchronization. The header is first stripped. Then the synchronization is found by a process of detecting for the chosen sync symbol; the program is capable of restoring mutilated synchronization, and correcting for inserted or deleted symbols, even in the presence of a single character error (Refs. 1, 2). After synchronization is found, the decoder determines whether or not it has a code word. If so, the information bits are put into a buffer for transmission to the station equipment for which the message is intended, either automatically or else when a full message is received and verified.

If errors are detected, the machine embarks on an error-correction procedure, the most difficult part of the entire operation. But even for the outward link using full triple-error correction, the decoding takes less than 1/5 sec; in the simpler inward link, 1/40 sec is the maximum. Furthermore, the average time to decode is only a few milliseconds. Some errors will not decode at all. However, a retransmission channel for verification will be available, so that a retransmission would be asked for if the message cannot be decoded. In fact, it may be better to ask for repeats even if the code is theoretically capable of unique decoding.

e. Performance. If it is decided to have a return verification channel, it will be better in the outward case to only double-error correct and to *quadruple*-error detect (the code is capable of this mode of operation). In return for a slightly higher but still very low probability of having a retransmission needed (4×10^{-4} instead of 6×10^{-6}), one gains a remarkably low output bit error probability (less than 10^{-8}) even in the ultraconservative worst case.

Table 6 gives the output bit error probabilities and retransmission probabilities for the various modes of operation. The decoding programs vary from about 100 instructions (detection only) to about 1000 instructions (full triple-error correction), for use with typical DSN general-purpose machines.

Using the code in the double-error correcting, quadruple-error detecting mode allows the decoding program to become simpler to write and to store, as well as faster to run, than the program for full triple-error correction. Furthermore, the final error probability is lower. Thus, this mode is the recommended one for the outward link.

Table 6. Output bit error probabilities and retransmission probabilities

Input uncoded character error probability	(15, 9) Code (minimum distance 7)										(15, 11) Code (minimum distance 5)					
	Correct 3		Correct 2, Detect 4		Correct 1, Detect 5		Correct 0, Detect 6		Correct 2		Correct 1, Detect 3		Correct 0, Detect 4			
	Error	Repeat	Error	Repeat	Error	Repeat	Error	Repeat	Error	Repeat	Error	Repeat	Error	Repeat	Error	Repeat
0.01	2×10^{-7}	6×10^{-6}	4×10^{-9} ^a	4×10^{-4}	$< 10^{-10}$	1×10^{-2}	$< 10^{-10}$	1×10^{-1}	5×10^{-6} ^a	2×10^{-4}	2×10^{-7}	1×10^{-2}	4×10^{-9}	1×10^{-1}		
0.005	1×10^{-8}	4×10^{-7}	1×10^{-10}	5×10^{-5}	$< 10^{-10}$	3×10^{-3}	$< 10^{-10}$	7×10^{-2}	7×10^{-7}	3×10^{-5}	1×10^{-9}	3×10^{-3}	$< 10^{-10}$	7×10^{-2}		
0.001	$< 10^{-10}$	7×10^{-10}	$< 10^{-10}$	5×10^{-7}	$< 10^{-10}$	1×10^{-4}	$< 10^{-10}$	2×10^{-2}	6×10^{-9}	2×10^{-7}	$< 10^{-10}$	1×10^{-4}	$< 10^{-10}$	2×10^{-2}		
0.0005	$< 10^{-10}$	5×10^{-11}	$< 10^{-10}$	6×10^{-8}	$< 10^{-10}$	3×10^{-5}	$< 10^{-10}$	8×10^{-3}	7×10^{-10}	3×10^{-8}	$< 10^{-10}$	3×10^{-5}	$< 10^{-10}$	8×10^{-3}		

^a Denotes preferred options for 0.01 input character error probability.

The 20 check bits for two length 29 information words are written horizontally instead of vertically, using only the first four teletype levels. Thus, five teletype characters are needed for checks, the fifth level being odd parity on the first four levels in all check characters, for the same reason as in the case of coded teletype. We now have a message of $(2 \times 29) + 5 + 2 = 65$ teletype characters.

Table 7 gives the number of minutes (at the transmission rate of 5 characters/sec) necessary to estimate the character error rate within 50% and 100% accuracy with probabilities 0.9 and 0.95 at true character error rates of 0.01 and 0.001. For example, if 50% tolerance is wanted with confidence 0.95 at 0.01 character error probability, 5 min of transmission must be observed. This is an entirely reasonable requirement.

References

1. "Error Statistics on Inter-DSN Teletype Channels," *SPS 37-31*, Vol. III, pp. 76-78.
2. "Teletype Coding Experiment," *SPS 37-32*, Vol. III, pp. 51-54.
3. "A New Look at the Inter-DSN Teletype Channel," *SPS 37-33*, Vol. III, pp. 109-110.
4. "Evaluation of the DSN Teletype Communications System," *SPS 37-34*, Vol. III, pp. 64-68.
5. Peterson, W. W., "Error-Correcting Codes," John Wiley and Sons, Inc., New York, N. Y., 1961.